Esta tesis doctoral contiene un índice que enlaza a cada uno de los capítulos de la misma.
Existen asimismo botones de retorno al índice al principio y final de cada uno de los capítulos.

Ir directamente al índice

Para una correcta visualización del texto es necesaria la versión de Adobe Acrobat Reader 7.0 o posteriores

Aquesta tesi doctoral conté un índex que enllaça a cadascun dels capítols. Existeixen així mateix botons de retorn a l'index al principi i final de cadascun deis capítols .

Anar directament a l'index

Per a una correcta visualització del text és necessària la versió d' Adobe Acrobat Reader 7.0 o posteriors.

The interaction of particles with liquid surfaces: a classical study

English translation of the
dissertation
presented to the University of Alacant
in partial fulfillment of the requirements for the degree of
Doctor in Science

by

Mikel-Lorenzo Forcada Zubizarreta

Alacant, May 1991

A Marinela,
pel seu suport,
per la seua fe,
per la seua estima.

Acknowledgements

I would like to thank

Alberto Gras-Martí, for his hospitality and support, without which neither this work nor the continuation of my academic life would have been possible;

Néstor R. Arista, for the time spent at the blackboard and for having given theoretical formulation and conciseness to my raw ideas;

Mario M. Jakas, for the time he shared with me in front of the terminal, and for his advice which helped me to get my feet back on the ground;

Martin Vičánek, for his valuable help, both in physics and text composition, and for his love for classical physics;

Herbert M. Urbassek, for his crucial contributions in the early stages of this work, especially when he invited me to Brunswick;

Rafael Garcia-Molina, for having put forward and formulated the ideas that started this work;

Vicent Esteve, for his efficient preparation of the figures;

all colleagues at the Department of Applied Physics of the University of Alacant, for having offered me an environment that has made my research easy;

and finally, my parents, for their warm support in hopeful anticipation of the day on which I would submit my dissertation.

Contents

Chapter 1

Introduction

1.1 Background and motivation for this work

This work describes a classical theroretical study of some aspects of the static and dynamic interaction between a particle and the surface of a liquid. In all the cases treated, the particle is external to the liquid. As it will be shown in the following, there are a number of systems of physical and technological interest that may be modelled using the theoretical tools that will be described in this work which is divided in two main parts. In the statics part (Chapter 2), I will study the equilibrium shape and the stability of the liquid surface when a particle is held above it, and the potential energy of the system; the results will be applied to various situations of interest. The dynamics part (Chapters 3 and 4) will analyse the transfer of energy from a moving particle to the surface, which results in the excitation of ripple waves, both for an ideal liquid and for viscous liquids.

One of the motivations that led me to start this work was the wish to get a more detailed understanding, in a classical framework, of the interaction of an electron with the surface of a liquid. This problem had already been addressed by Gras-Martí and Ritchie (1985), and later by Barberán, Garcia-Molina and Gras-Martí (1989), using a second-quantization approach, in which the oscillations of the liquid surface (ripples) were modelled as a field of bosons called ripplons. In these papers, the authors studied the self-energy of a stationary charge and the energy loss of a charged particle that moves parallel to the liquid surface. The dynamics part of this thesis includes a classical reformulation and an extension of their theory of energy loss, which allows the treatment of neutral and finite-size particles, as well as finite-depth liquids. The studies that are described in this thesis show that the physical features of the system that were addressed by these authors are of classical nature. The results of the quantum and classical treatments for the inviscid liquid are identical.

The surface of liquid helium, and the interaction phenomena that take place on it, are perhaps one of the piece of physics that has received more interest during the past decades. The interaction of charged particles with this surface has attracted the interest of many researchers, both experimentalists and theorists. Cole (1970, 1974) and Shikin and Monarkha (1974), among others, have studied the interaction of surface electrons with the oscillations of the vapour–liquid interface.

Experimentalists and theorists have studied the stability and formation of dimples (holes) on the surface of liquid helium when electrons are forced against it by an electric field (Shikin and Leiderer 1981; Mel'nikov and Meshkov 1981; Leiderer, Ebner and Shikin 1982; Gianetta

and Ikezi 1982): electrons are localized in depressions of the surface (dimples) that form a lattice when they group together. The theoretical calculations of the sizes of these dimples are similar in nature to some of the calculations that I will report in the statics part of this work: the authors predict and observe lateral dimensions of the order of 1 mm, much like the ones I get for a somewhat different situation: the *bump* induced on the surface of a liquid by the attraction of a single external particle. Note that bumps may also be formed on the surface of an insulating liquid by the divergent electric field due to a pointed electrode held above the surface (Pohl 1978:111).

The statics part of this work is also related to some other theoretical studies in the field of interface science, that address the calculation of the shape of the liquid–vapour interface (meniscus) subject to gravity and surface tension, and to various boundary conditions (see, e.g., Boucher and Jones 1987; Rossolenko and Zhdanov 1990). Other authors address the problem of physical adsorption at corners and pores of solid surfaces (Cheng and Cole 1990), which also involves the calculation of the equilibrium shape of a liquid–vapour interface. A very similar problem, the filling of a cylindrical hole on a solid surface with lubricant, is treated in this work.

Another group of phenomena related to this work, are the scattering and reflection of low-velocity atoms at the surface of liquid helium. The scattering experiments have been addressed by quantum path-integral or related theories (Echenique and Pendry 1976a,b, Swanson and Edwards 1988, Goodman 1989). One of the most spectacular experiments is described by Berkhout et al. (1989), where the focusing of hydrogen atoms using a liquid-helium-coated concave mirror is achieved. The formulation of a theory of slow-atom reflection is currently a subject of interest for various groups (Martin, Bruinsma and Platzman 1988; Tiesinga, Stoof and Verhaar 1990). There are a number of non-linear and discrete atom–atom features (such as the non-linear dynamics of the surface or the atom–atom correlation effects at the interface) that still have to be modelled in an empirical way to get a reasonable description of the experiments. The first part of this thesis adresses some non-linear features of the static interaction of particles with liquid surfaces. However, the complexity of the non-linear response of the liquid at short particle–surface distances has so far prevented the formulation of a simple dynamical theory.

A recent field of experimental research that is closely related to the theory presented in this thesis is atomic-force microscopy. This technique (Binnig, Quate and Gerber 1986) is a powerful tool to measure surface forces (Rugar and Hansma 1990): it consists in measuring the force on a tip that is held at a certain distance from a sample surface. The atomic-force microscope has been used recently to determine the thickness distribution of lubricant films on solid surfaces (Mate, Lorenz and Novotny 1989, 1990; Mate and Novotny 1991). The study of the van der Waals interaction of finite-size particles (such as the tip of an atomic-force microscope) with liquid surfaces is of relevance for the modelling of these experiments; in fact, the experimental work of Mate and coworkers with lubricant films has motivated a fraction of the work that is presented here, both in the dynamics and the statics part. There is a reasonable agreement of the theoretical results reported here with their experiments. One of the most interesting features of the tip–liquid system is related to the non-linear nature of the surface response: the liquid surface becomes unstable when the tip of the microscope approaches the liquid surface at a critical distance. At this point, the surface jumps to contact the tip — an adhesion phenomenon that has also been reported for solid surfaces (Pethica and Sutton 1988; Landman et al. 1989).

The nature of the force sensor used in atomic-force microscopy involves vertical oscillations

of the tip, that may in turn induce oscillations on the liquid surface. A study of this phenomenon and its possible influence in atomic-force microscopy experiments is also reported in the dynamics chapters of the thesis.

In view of the number of potential applications of the theoretical work presented in this thesis, the pertinent basis has been formulated in a fairly general way. This leaves it open for further applications and extensions.

1.2 Sketch of the general model

In this thesis, classical hydrostatics and hydrodynamics will be used to analyse a system that consists of two interacting parts:

1. a liquid body, delimited by an infinite surface (the interface with vacuum), and bound by a force field (such as gravity or adhesion to a solid substrate); and
2. a particle, outside the liquid, that generates a spherically symmetrical field that attracts the liquid towards it. The particle (a point or a sphere) may be at rest or in motion, relative to the reference frame of the field that binds the liquid.

The attractive forces that will be considered in this work are:

1. the electrostatic interaction of charged particle and the dipoles it induces in the liquid, or
2. the van der Waals interaction.

The following restrictions will be imposed to the liquid:

1. it may be described as a continuous medium where atomic structure is neglected; accordingly, the liquid–vacuum interface is assumed to be abrupt;
2. it is bound in such a way that its surface is planar at infinity;
3. it is incompressible; and
4. it does not screen or attenuate appreciably the forces between the external particle and the constituents of the liquid.

If the particle is at rest, I will study the equilibrium shape of the liquid surface, its stability, the equilibrium values of mutual forces as well as their gradients, and the total potential energy for different cases. Special attention will be paid to the non-linear behaviour of the liquid surface at short particle–surface distances. The results will be compared to related quantum-many-body theoretical treatments (Gras-Martí and Ritchie 1985) and experimental results (atomic-force microscopy of liquid films, Mate et al. 1989). These will be the subjects of Chapter 2.

If the particle is in motion, I will study the way it perturbs the liquid surface (exciting its rippling motion), and the transfer of energy from the particle to the liquid (including a more general formulation of the theory of Gras-Martí and Ritchie (1985) for the energy loss of particles that move parallel to the liquid surface). The dynamical response of *ideal* liquids will be considered in Chapter 3. Chapter 4 will describe some aspects of the behaviour of

viscous liquids in the presence of external particles, with a reference to the dynamic aspects of the experiments performed by Mate *et al.* (1989) with the atomic-force microscope.

Finally, in Chapter 5, the results of this work will be summarized and a number of open aspects will be discussed that have not been treated here and that constitute lines of possible interest in future research.

Chapter 2

The static interaction of a particle with a liquid surface

In this chapter, the static behaviour of the system defined in the previous chapter, in which a particle is held fixed at a certain distance from a liquid surface (see Figure 2.1), is described.

When the liquid reaches its equilibrium configuration, the attraction towards the particle is balanced by the force due to the binding field and by the surface tension of the liquid. If the potential generated by the particle is spherically symmetric, the equilibrium configuration of the system is axisymmetrical (has azimuthal symmetry). The liquid *swells* or forms a *bump* on the part of the surface that is nearest to the particle. The liquid body above the unperturbed liquid surface may also be called a *holm* (Boucher & Jones 1987). The liquid is assumed to be incompressible; therefore the bump consists of liquid that comes from elsewhere in the liquid.

The determination of the equilibrium situation of this system is equivalent to the calculation of the equilibrium shape of the liquid surface. The system is axisymmetrical and so, it may be characterized by a *meridian* curve $u(\rho)$ describing the displacement u of the liquid surface, from a reference plane, at a distance ρ from the symmetry axis. The reference plane is defined in such a way that

$$\lim_{\rho \to \infty} u(\rho) = 0. \tag{2.1}$$

The following axis choice is made: the reference plane is the xy plane and the symmetry axis is the z axis. In most of the cases that will be studied in this chapter, the unperturbed surface will coincide with this plane. The outward normal to the liquid surface has always a positive z component.

The equilibrium meridian curve will correspond to a stationary value of the total potential energy of the system (in particular, a situation of stable equilibrium would correspond to a relative minimum of the total potential energy). A stationary potential energy is equivalent to a null balance of all participating forces.

2.1 Total potential energy of the particle–liquid system

The total potential energy of the system will be written here as the sum of the surface energy (V_{st}) and the potential energy of the whole liquid in the fields of the binding force (like gravity or adhesion to a substrate) (V_b) and of the attractive force due to the external particle (V_{int}):

$$V_{tot} = V_{st} + V_b + V_{int}. \tag{2.2}$$

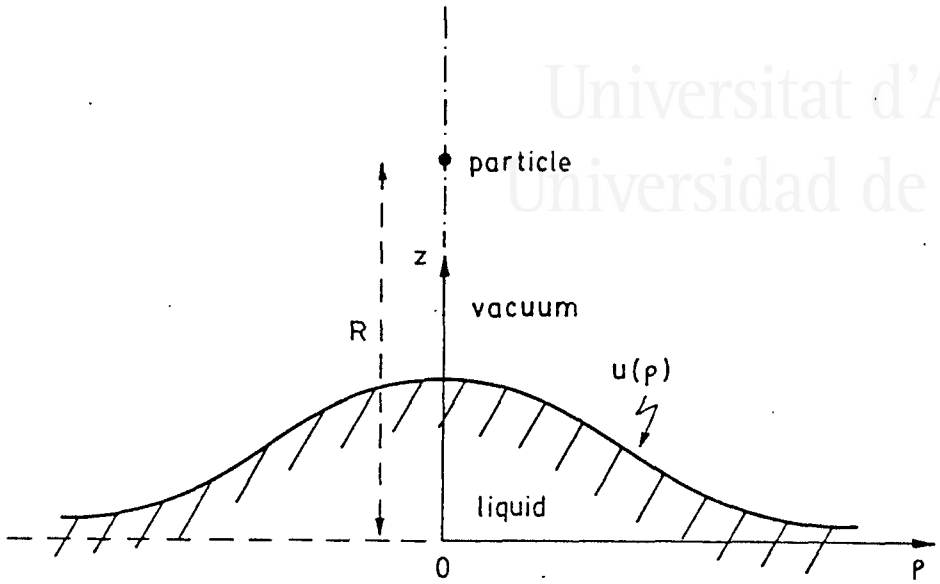

Figure 2.1. Sketch of the static particle–liquid system.

In the next sections, each one of these contributions is described in detail.

I would like to note the fact that the surface energy is added to *potential* energies, to study the equilibrium of the system. In doing so, the microscopical considerations that describe the surface energy as a free energy, which, as a consequence of kinetic-energy contributions, varies with temperature, are neglected. However, for a given temperature and in a macroscopic or *mesoscopic* scale, these contributions may be treated as part of a potential energy.

2.1.1 Surface energy

The increment of the surface energy of the liquid due to a perturbation of its surface (induced, for example, by an external particle) may be written as the product of the surface tension coefficient and the change in the area of the liquid surface. In the case of an axially symmetric fluid body, the increment of the surface energy may then be expressed as a functional of the meridian curve due to the the perturbation $u(\rho)$. The expression also involves $u_0(\rho)$, the meridian curve of the unperturbed system:

$$V_{st} = 2\pi\sigma \int_0^\infty d\rho\, \rho \left\{ \left[1 + \left(\frac{du}{d\rho} \right)^2 \right]^{1/2} - \left[1 + \left(\frac{du_0}{d\rho} \right)^2 \right]^{1/2} \right\}. \tag{2.3}$$

In many of the cases that will be studied here, the surface of the liquid will have a very low curvature, and, in addition, the surface will be initially planar ($u_0 = 0$); therefore, it will be possible to use a simpler expression of the surface energy.

2.1.2 Binding potential energy

Consider now the increment of the potential energy of the liquid in the binding field (which may be a gravitational field or the field of adhesion forces towards a solid substrate), when the liquid surface changes from its unperturbed configuration $u_0(\rho)$ to the perturbed one, $u(\rho)$.

The binding potential energy per unit volume, v_b, will be assumed to be axisymmetrical, that is to say, a function of z and ρ. However, in most cases treated here it will be independent of ρ.

Building a new configuration of the liquid is equivalent to bringing volume elements from the liquid surface very far from the symmetry axis, where the binding energy per unit volume is $v_b(0,\infty)$. The increment of the binding potential energy of the whole liquid is then

$$V_b = 2\pi \int_0^\infty d\rho\, \rho \int_{u_0(\rho)}^{u(\rho)} dz (v_b(z,\rho) - v_b(0,\infty)). \tag{2.4}$$

2.1.3 Interaction energy

The interaction energy between the particle and the liquid will be written as an integral over the whole volume of the liquid. The potential energy per unit volume of a liquid element located at a distance r from the center of the particle will be assumed to be of the form

$$v_{int} = -\frac{B}{(r^2 - a^2)^m}, \tag{2.5}$$

where B is a constant that will depend on properties of the liquid and of the particle and the type of interaction, a is a constant that is related to the size of the particle, and m is an integer exponent that depends on the type of interaction. Throughout all this dissertation, it will be assumed that interactions are not affected by retardation effects.

Retardation is important in the case of van der Waals interactions, and its effect in long-range forces has been experimentally observed (Israelachvili and Tabor 1972a,b, Israelachvili 1985, 1987). Van der Waals dispersion forces between two interacting systems **A** and **B**, the distance between them being r, are due to the interaction of the instantaneous, fluctuating dipole moment of **A** with the dipole moments it induces on the other **B** (and vice versa). Consider how a fluctuation in the charge distribution of **A** is transmitted to **B**. When the charge distribution shakes, it generates an electromagnetic wave which is transmitted towards **B** at the speed of light, c. The charge distribution in **B** shakes in response to the incoming signal, and generates a wave that returns to **A**. The fluctuations on **A** occur with a frequency ω, and if the time interval for the round trip, $2r/c$, is comparable to $1/\omega$, the dipole on **A** will have fluctuated to a new position. Therefore, the interaction is weakened, due to imperfect dipole alignment. Fluctuation frequencies ω for atoms are usually in the ultraviolet range; then, for distances longer than, say, 100 Å, retardation effects may be important, and the power law that approximates the van der Waals interaction goes from r^{-6} to a more rapidly decaying r^{-7} (Atkins 1983:365; see also Spruch 1986).

Eq. (2.5) has been used, only for mathematical convenience, to embed three cases of non-retarded particle–liquid interaction, but is *not* the most general expression. The three cases it comprises are:

1. the interaction of a point charge with the dipoles it induces in a non-polar liquid ($m = 2$, $a = 0$);

2. the van der Waals interaction of a neutral atom with a non-polar liquid ($m = 3$, $a = 0$); and
3. the van der Waals interaction of a solid sphere with a non-polar liquid ($m = 3$, $a =$ radius of the sphere).

Other possibilities for m and a may not have physical meaning.

If the particle is situated on the z axis at a height $z = R$ over the reference plane, the distance r between the particle and a given volume element which is situated at (z, ρ) is

$$r = \sqrt{(R - z)^2 + \rho^2}, \tag{2.6}$$

so v_{int} may be written as a function of ρ and z but the dependence on z enters as $R - z$:

$$v_{int} = v_{int}(R - z, \rho). \tag{2.7}$$

The total interaction energy is then the volume integral of v_{int}:

$$V_{int}(R) = 2\pi \int_0^\infty d\rho\, \rho \int_{-h(\rho)}^{u(\rho)} dz\, v_{int}(R - z, \rho). \tag{2.8}$$

The lower limit of the z integral, $-h(\rho)$, represents the bottom surface of the liquid body. If the liquid lies on a planar substrate, h is a constant; if the liquid is semi-infinite, h is ∞.

2.2 Equilibrium equation

I am interested in obtaining the equilibrium configuration of the liquid, which will be represented by an equilibrium meridian curve. This equilibrium situation corresponds to a stationary value of the total potential energy, this is, the configuration for which all forces acting on the liquid balance. In particular, the *minima* of the total potential energy correspond to *stable* equilibrium configurations. The total potential energy of the particle–liquid system is given in eq. (2.2). It is a functional of the meridian curve $u(\rho)$, $V_{tot} = V_{tot}[u](R)$, and contains the R (the position of the particle) as a parameter.

Let $\tilde{u}(\rho)$ be an equilibrium meridian curve. The potential energy for this curve is a stationary point, so any small increment $\Delta u(\rho)$ around it will, in first order, result in a null change of the total potential energy:

$$V_{tot}[\tilde{u} + \Delta u] - V_{tot}[\tilde{u}] = 0 \tag{2.9}$$

Using expressions (2.2-2.4) and (2.8), one gets, by Taylor expansion, the equation

$$\begin{aligned} 0 \;= 2\pi \textstyle\int_0^\infty d\rho\, \rho \;\Big[& \frac{\sigma\, d\tilde{u}/d\rho}{\sqrt{1 + (d\tilde{u}/d\rho)^2}} \frac{d\Delta u}{d\rho} \\ & + [v_b(\tilde{u}, \rho) - v_b(0, \infty)]\, \Delta u \\ & + v_{int}(R - \tilde{u}, \rho) \Delta u \Big], \end{aligned} \tag{2.10}$$

where the first term of the integrand contains $d\Delta u/d\rho$ instead of Δu. The situation may be easily remedied by integrating this term by parts. One gets

$$0 = 2\pi \int_0^\infty d\rho\, \rho\, \Delta u \left[-\frac{\sigma}{\rho}\frac{d}{d\rho}\frac{\rho\, d\tilde{u}/d\rho}{\sqrt{1+(d\tilde{u}/d\rho)^2}} + [v_b(\tilde{u},\rho) - v_b(0,\infty)] + v_{int}(R-\tilde{u},\rho)\right], \tag{2.11}$$

provided that

$$\lim_{\rho\to\infty} \frac{\rho\, d\tilde{u}/d\rho}{\sqrt{1+(d\tilde{u}/d\rho)^2}}\Delta u = 0, \tag{2.12}$$

a condition that is not too restrictive (a curve that approaches the $z = 0$ plane faster than $1/\rho$ will meet this requirement).

Eq. (2.11) has to hold for *any* small Δu, so the part of the integrand in brackets has to be zero. This yields a second-order, non-linear differential equation for the equilibrium meridian curve $\tilde{u}(\rho)$,

$$-\frac{\sigma}{\rho}\frac{d}{d\rho}\frac{\rho\, d\tilde{u}/d\rho}{\sqrt{1+(d\tilde{u}/d\rho)^2}} + v_b(\tilde{u},\rho) - v_b(0,\infty) + v_{int}(R-\tilde{u},\rho) = 0, \tag{2.13}$$

which I will from now on call the "equilibrium equation". The first term is just $\sigma(1/R_1+1/R_2)$ where R_1 and R_2 are the radii of curvature of the surface defined by $\tilde{u}$ at a given ρ. According to Laplace's formula (Landau and Lifshitz 1987:239), the first term in eq. (2.13) equals the pressure difference across the surface at that point.

Eq. (2.13) has to be solved using two boundary conditions. The first one is eq. (2.1), this is, the surface has to approach the reference plane asymptotically for large ρ. The second one expresses the fact that the surface must have finite curvature at the origin,

$$\left.\frac{d\tilde{u}}{d\rho}\right|_{\rho=0} = 0. \tag{2.14}$$

Solutions $\tilde{u}(\rho)$ satisfying these two boundary conditions are not guaranteed to correspond to minima of the total potential energy (stable equilibrium configurations). The solutions may correspond also to unstable equilibrium.

Equation (2.13), in the general case, has to be solved numerically (see section 2.4). In the following section, however, I will show how this non-linear equation may be reduced to a linear form that has a closed-form solution, which may be applied to some limiting cases.

2.3 Linearized form of the equilibrium equation: linear solutions

2.3.1 Linearization of the equilibrium equation

There are some interesting limiting cases of the particle–liquid system that allow a simpler treatment than the numerical solution of the non-linear equilibrium equation given in the previous section. Equation (2.13) may be reduced to a linear form having closed-form solutions if the following physical conditions are fulfilled:

1. The unperturbed system shows a planar surface: $u(\rho) = 0$ for all ρ. This is the case when the binding potential energy per unit volume v_b is independent of ρ.
2. The displacement of the surface $u(\rho)$ is small compared with the distance between the particle and the originally unperturbed surface, R.
3. The perturbed surface is smooth, that is, the square of the slope of the meridian curve, $(du/d\rho)^2$ is small compared to unity for every ρ.
4. The surface displacement $u(\rho)$ is so small that the the binding potential $v_b(u, \rho)$ may be approximated to vary linearly with u. For gravity binding, this restriction is immaterial.

These approximations hold for cases where the particle is far from the surface and the perturbation induced in the liquid is small. These approximations may be formulated mathematically as:

$$v_b(z, \rho) = v_b(z); \tag{2.15}$$

$$u(\rho) \ll R; \tag{2.16}$$

$$\left(\frac{du}{d\rho}\right)^2 \ll 1; \tag{2.17}$$

$$v_b(u) \approx v_b(0) + Gu, \tag{2.18}$$

where

$$G = \left.\frac{dv_b}{dz}\right|_{z=0}. \tag{2.19}$$

With these approximations, the equilibrium equation (2.13) reduces to the linear form:

$$-\sigma\left(\frac{d^2\tilde{u}}{d\rho^2} + \frac{1}{\rho}\frac{d\tilde{u}}{d\rho}\right) + G\tilde{u} + v_{int}(R, \rho) = 0. \tag{2.20}$$

2.3.2 Solution of the linearized equation

Equation (2.20) may be solved analytically using the Bessel transform technique. Let the meridian curve be expanded accordingly

$$\tilde{u}(\rho) = \int_0^\infty k\,dk\,J_0(k\rho)\,\tilde{u}(k) \tag{2.21}$$

and the interaction potential

$$v_{int}(R, \rho) = \int_0^\infty k\,dk\,J_0(k\rho)\,v_{int}(R, k). \tag{2.22}$$

In these equations J_0 is the Bessel function of the first kind of order zero (Olver 1965). Substituting eq. (2.21) into the linearized equilibrium equation (2.20), one gets, using the properties of Bessel functions,

$$\tilde{u}(k) = -\frac{v_{int}(R, k)}{\sigma k^2 + G}. \tag{2.23}$$

For interaction potentials of the form given in equation (2.5), the Bessel transform is analytical (Luke 1965, eq.(11.4.44)):

$$v_{int}(R, k) = -\frac{B}{(m-1)!}\left(\frac{k}{2\tilde{R}}\right)^{m-1} K_{m-1}(k\tilde{R}), \tag{2.24}$$

where K_n is the modified Bessel function of the second kind (Olver 1965) and order n, and

$$\tilde{R} = \sqrt{R^2 - a^2} \tag{2.25}$$

is a *corrected* particle–liquid distance that accounts for the size of the particle only in the case of van der Waals interactions (see subsection 2.1.3). With this, the general solution of equation (2.20) may be written in terms of a dimensionless integral

$$\tilde{u}(\rho) = \frac{B}{\sigma(m-1)!}\left(\frac{1}{2\tilde{R}^2}\right)^{m-1} \int_0^\infty dt\, t^m \frac{J_0(t\rho/\tilde{R})K_{m-1}(t)}{t^2 + 2\tilde{R}^2/\xi^2}. \tag{2.26}$$

The dimensionless integral depends on two parameters, $\rho/\tilde{R}$ and $2\tilde{R}^2/\xi^2$, where

$$\xi = \sqrt{\frac{2\sigma}{G}} \tag{2.27}$$

is a generalized *capillary constant* (Landau & Lifshitz 1987:240), which measures the lateral size of the bump. The maximum height of the bump may be written as

$$\tilde{u}(0) = \frac{B}{\sigma(m-1)!}\left(\frac{1}{2\tilde{R}^2}\right)^{m-1} i_m(\sqrt{2}\tilde{R}/\xi), \tag{2.28}$$

where

$$i_m(x) = \int_0^\infty dt\, t^m \frac{K_{m-1}(t)}{t^2 + x^2}. \tag{2.29}$$

Figure 2.2 shows values of this function for $m = 2$ and $m = 3$. As was mentioned in subsection 2.1.3, the value $m = 2$ is related to the interaction of a charged point particle with the liquid, whereas the value $m = 3$ is related to the van der Waals interaction between a neutral particle and the liquid.

For small values of x (the relevant case, since, in most cases $\tilde{R} \ll \xi$), the functions $i_m(x)$ may be easily approximated in the following way: if $t^2/(t^2 + x^2)$ is considered to be an approximation of the Heaviside step function $\Theta(t - x)$, then

$$i_2(x) \approx K_0(x) \approx \ln\left(\frac{2}{e^\gamma x}\right), \tag{2.30}$$

and

$$i_3(x) \approx 1 + 2K_0(x) \approx 1 + 2\ln\left(\frac{2}{e^\gamma x}\right), \tag{2.31}$$

where $\gamma = 0.5772\ldots$is Euler's constant. These expressions provide very useful approximations to compute the height of linear meridian curves. The fact that the exact values of eq. (2.29) plotted in Figure 2.2 are almost straight lines reflects the validity of this aproximation. It may be advanced here that, since the capillary constants for most common liquids are of the order of 10^7 a.u., the approximation $\tilde{R} \ll \xi$ is not restrictive at all.

2.3.3 Linearized expression of the total potential energy

The total potential energy, in the linear case, may be easily written by linearizing the expressions of the surface, binding and interaction energies, and evaluating them for the equilibrium meridian curve.

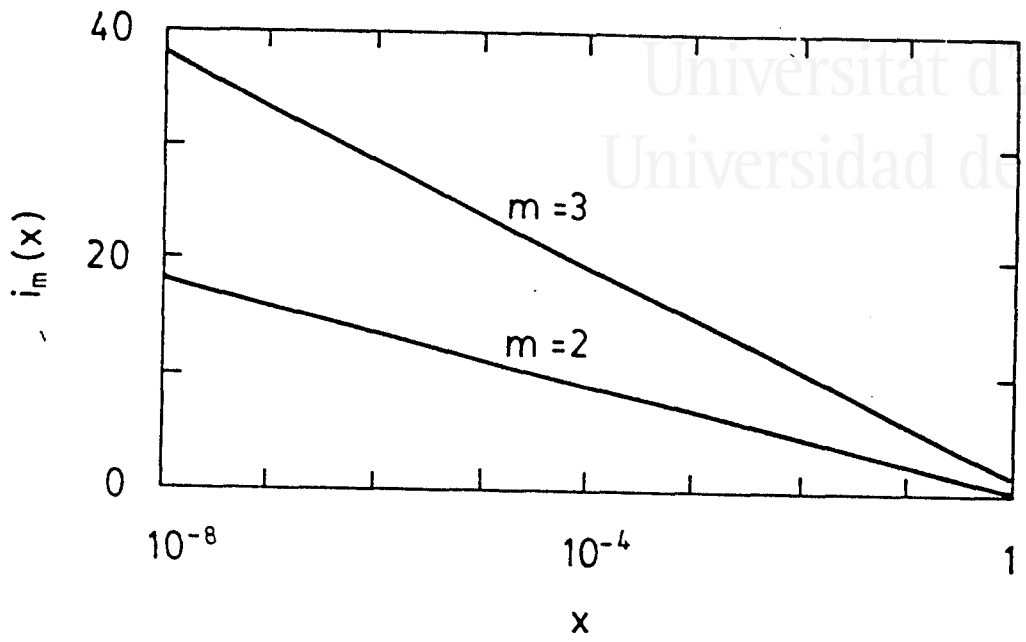

Figure 2.2. The dimensionless functions $i_2(x)$ and $i_3(x)$.

It is important to separate two contributions to the potential energy: one that arises from the interaction of the particle with the unperturbed system and the other arising from the bump that forms on it. It has to be taken into account that the energy contributions may vary with the distance R either directly or through $\tilde{u}(\rho)$.

The *increment* of the surface energy due to the formation of the bump has been given in eq. (2.3). In this section, I am dealing with cases in which the unperturbed surface is the reference plane ($u_0(\rho) = 0$). This is a consequence of the restriction expressed in eq. (2.15). The increment of surface energy is then

$$V_{st} = 2\pi\sigma \int_0^\infty d\rho\, \rho \left[\left[1 + \left(\frac{du}{d\rho} \right)^2 \right]^{1/2} - 1 \right]. \tag{2.32}$$

Taking into account the *smoothness* approximation given in eq. (2.17), V_{st} may be written as

$$V_{st} = \pi\sigma \int_0^\infty d\rho\, \rho \left(\frac{du}{d\rho} \right)^2. \tag{2.33}$$

Next, consider the binding energy. Using eq. (2.15), and the approximation given by eq. (2.18), the increment of binding energy, eq. (2.4) may be written as

$$V_b = \pi G \int_0^\infty d\rho\, \rho\, u^2(\rho). \tag{2.34}$$

Finally, the interaction energy (see eq. (2.8)) has contributions from both the liquid body

under the reference plane,

$$V_{planar} = 2\pi \int_0^\infty d\rho\, \rho \int_{-h}^0 dz\, v_{int}(R-z,\rho), \tag{2.35}$$

which usually simplifies to a closed-form function, and the bump over it,

$$\Delta V_{int} = 2\pi \int_0^\infty d\rho\, \rho \int_0^{u(\rho)} dz\, v_{int}(R-z,\rho); \tag{2.36}$$

using the long-distance approximation, eq. (2.16), the last contribution simplifies to:

$$\Delta V_{int} = 2\pi \int_0^\infty d\rho\, \rho\, u(\rho)\, v_{int}(R,\rho). \tag{2.37}$$

It must be noted here, that these are the contributions to the potential energy of the particle that are due to its interaction with the liquid. If there is, for instance, a solid substrate below the liquid (at $z < -h$) that interacts with the particle, it has to be considered too.

For the calculation of the linearized potential energy, the three contributions that depend on R through the shape of the bump will be considered first: the surface energy, V_{st}, eq. (2.33); the binding energy, V_b, eq. (2.34); and the bump part of the interaction energy, ΔV_{int}, eq. (2.37). After rewriting the Bessel transform of $\tilde{u}(\rho)$, eq. (2.21) as a Fourier transform (Olver 1965, eq. (9.1.18)),

$$\tilde{u}(k) = \frac{1}{2\pi} \int d^2\vec{\rho}\, e^{-i\vec{k}\cdot\vec{\rho}}\, \tilde{u}(\rho), \tag{2.38}$$

it is substituted into the sum of eq. (2.33), (2.34), and (2.37), which I will call ΔV, the potential energy due to the bump. Substitution leads to

$$\Delta V = \frac{1}{2} \int d^2\vec{k}\, \tilde{u}(k) \left[2v_{int}(R,k) + \left(\sigma k^2 + G\right) \tilde{u}(k) \right], \tag{2.39}$$

which, taking eq. (2.23) into account, simplifies to

$$\Delta V = -\pi \int_0^\infty dk\, k\, \frac{v_{int}^2(R,k)}{\sigma k^2 + G}. \tag{2.40}$$

It is interesting to note that this result is exactly half the linear interaction energy, ΔV_{int}. This is consistent with the fact that the response of the liquid, *induced* by the perturbation, is linear. As the particle is brought from infinity to a distance R, the work (surface and binding energy) needed to build the bump is half the final interaction energy, but of opposite sign.

Further substitution of eq. (2.24) yields an explicit expression for the particle-induced contribution to the potential energy of the particle:

$$\Delta V = -\frac{\pi B^2}{\sigma[(m-1)!]^2} \left(\frac{1}{2\tilde{R}^2} \right)^{2m-2} j_m(\sqrt{2}\tilde{R}/\xi), \tag{2.41}$$

where

$$j_m(x) = \int_0^\infty dt\, t^{2m-1}\, \frac{K_{m-1}^2(t)}{t^2 + x^2} \tag{2.42}$$

is a dimensionless function that shows, as i_m, eq. (2.29), a logarithmic dependence on x in the relevant range.

2.3.4 Case study: electron–semiinfinite liquid interaction

Gras-Martí and Ritchie (1985) studied, using a quantum formalism, the linear interaction of an electron with the surface of a semiinfinite body of liquid helium bound by gravity. The classical approach will be used here to study, in the linear approximation, the static properties of this system. The results are in complete agreement with those obtained by Gras-Martí and Ritchie (1985). Here, in addition, results for the shape of the bump, which was not studied by these authors, will be obtained.

First, one has to define the interaction potential v_{int} and the binding potential v_b. The electron induces a dipole in each of the helium atoms. As has been said above, screening of the electric field will be neglected. The interaction energy between the electron and the dipole it induces in each atom is $-\alpha e^2/2r^4$, where α is the polarizability of the atom, r the mutual distance, and e the charge of the electron. The interaction energy per unit volume of liquid may thus be written as

$$v_{int} = -\frac{n\alpha e^2}{2}\frac{1}{r^4}, \tag{2.43}$$

where n is the number of atoms per unit volume in the liquid. Identifying this expression with eq. (2.5), leads to $m = 2$, $a = 0$ (and thus $\tilde{R} = R$, eq. (2.25)), and $B = n\alpha e^2/2$.

The binding energy per unit volume is gravitational in this case:

$$v_b(z) = nMgz, \tag{2.44}$$

where M is the atomic mass of the liquid and g is the gravitational acceleration. With this, G (eq. 2.19) is just nMg and ξ (eq. 2.27) becomes

$$\xi = \sqrt{2\sigma/nMg}, \tag{2.45}$$

the customary capillary constant (Landau and Lifshitz 1987:240). The expression for the shape of the bump formed when the electron is held at a distance R from the reference plane is (see eq. (2.26)):

$$\tilde{u}(\rho) = \frac{\pi n\alpha e^2}{2\sigma R^2}\int_0^\infty dt\, t^2 \frac{J_0(t\rho/R)K_1(t)}{t^2 + 2R^2/\xi^2}. \tag{2.46}$$

Figure 2.3 shows the meridian function that represents the bump induced in liquid helium by an electron at a distance $R = 96$ a.u. from the originally unperturbed surface. This example illustrates the validity of approximations such as eq. (2.16), that allow the use of the linearized equilibrium equation: the height of the bump in this case is ≈ 6 a.u. For shorter distances, it will be necessary to solve numerically the complete, non-linear differential equation for the meridian curve, eq. (2.13). The comparison, in the next section, 2.4, of these results with the complete non-linear results will help to establish the range of applicability of the results of Gras-Martí and Ritchie (1985), since their results are based in the same approximations as this linear, classical treatment.

The linearized meridian curve $\tilde{u}(\rho)$ has the following features:

1. it has a rather flat area around $\rho = 0$;
2. for intermediate of ρ, there is a logarithmic dependence (straight-line portion in the logarithmic plot); and
3. for values of ρ exceeding the capillary constant, ξ, it finally levels off to $\tilde{u} = 0$.

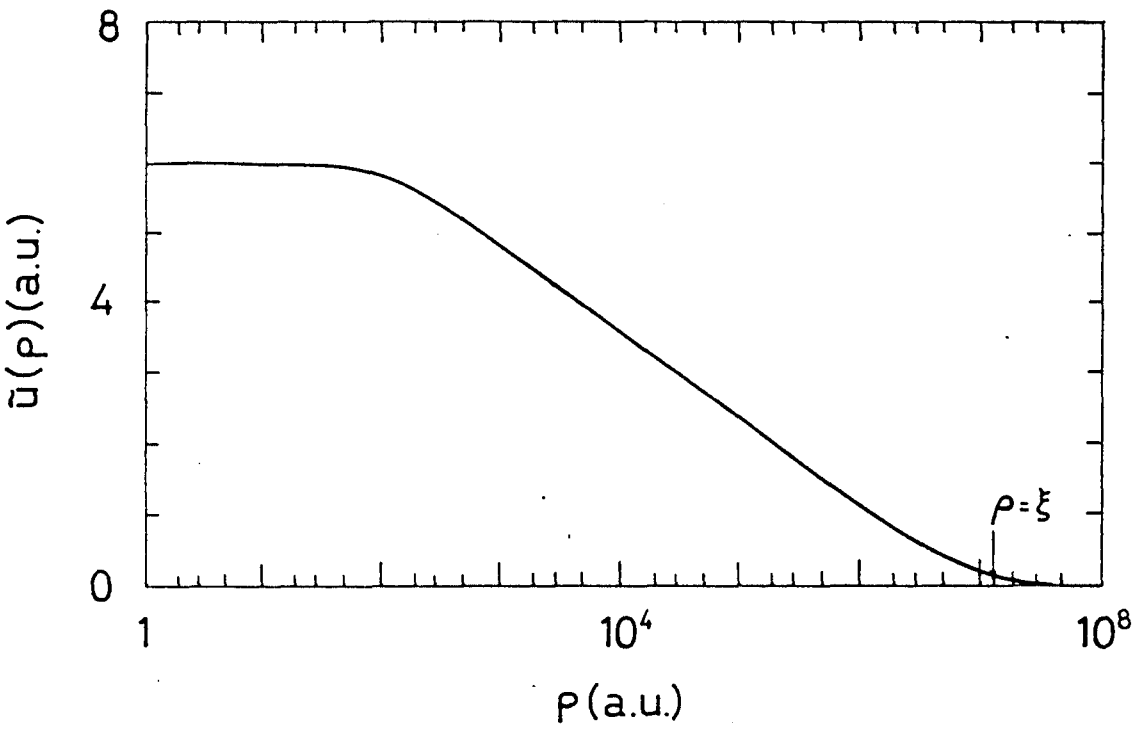

Figure 2.3. Meridian curve of the linear electron-induced bump on a liquid He surface ($R = 96$ a.u.). The point where $\rho=\xi$ is indicated.

Table 2.1. Values, in atomic units, of the material constants (Donnelly 1989; Weast 1982), the capillary constant ξ, and the van der Waals coefficient (Echenique and Pendry 1976a,b; Israelachvili 1985:69), for some noble-gas liquids.

Property	*He* (1.7 K)	*Ne* (25 K)	*Ar* (85 K)
Atomic polarizability, α	1.37	2.63	10.9
Atomic mass, M	$7.30 \cdot 10^{3}$	$3.68 \cdot 10^{4}$	$7.28 \cdot 10^{4}$
Number density, n	$3.12 \cdot 10^{-3}$	$5.34 \cdot 10^{-3}$	$3.13 \cdot 10^{-3}$
Surface tension, σ	$2.25 \cdot 10^{-7}$	$3.53 \cdot 10^{-6}$	$8.48 \cdot 10^{-6}$
Capillary constant, ξ	$1.35 \cdot 10^{7}$	$1.81 \cdot 10^{7}$	$2.62 \cdot 10^{7}$
vdW coefficient (like atoms), Λ	1.7	4.0	47

The small-ρ interval around the origin is the only area where the interaction potential is important; there, the interplay of surface tension and the interaction force yields a certain radius of curvature. Here, the gravity term of the differential eq. (2.20) has a very small weight as compared to the interaction energy and surface tension terms.

The decreasing, straight-line portion of the curve corresponds to an interval where the interaction potential and gravity terms are very small compared to the absolute values of the two surface tension terms in the differential equation, eq. (2.20). Then, the meridian curve corresponds to a minimal surface area. In the linear approximation, the meridian curve in this interval is approximately $c_1 + c_2 \ln(\rho)$, where c_1 and c_2 are constants. This is related to the case of a thin film of liquid supported on two concentric circular frames (Landau and Lifshitz 1987:242). In this case, the meridian curve is $\tilde{u} = c_3 + c_4 \cosh^{-1}(\rho/c_4)$, where the constants are related to the radii and relative position of the frames. This solution reduces to the logarithmic form when the slope of the meridian is small.

Gravity is the most important term is when ρ is somewhat larger than ξ. Here, the solution is simply $\tilde{u} \approx 0$: gravity tends to level off the surface.

Figure 2.4 shows the linear results for the height of bumps induced by an electron above the surface of some non-polar liquids. The "contact" line $\tilde{u}(0) = R$ has been drawn for reference. The linearizing approximations lose their validity as R gets smaller and approaches the intersection with the contact line. The data that have been used to compute these results are given in table 2.1. The dependence of the height $\tilde{u}(0)$ of the bumps on the distance R is very close to an inverse quadratic dependence, this is, $\tilde{u}(0) \sim R^{-2}$. This dependence is due to the prefactor in eq. (2.28), which is only slightly distorted by i_2.

The values of the capillary constants in table 2.1 deserve a comment. Capillary constants give an indication for the lateral sizes of bumps (as it may be seen in Figure 2.3). For liquid helium, ξ is of the order of 1 mm. There are no experimental data about electron-induced bumps; however, considerable data have been collected about dimples or holes formed on the surface of liquid helium when electrons are deposited on it and an electric field is applied (Shikin and Leiderer 1981, Mel'nikov and Meshov 1981, Leiderer, Ebner and Shikin 1982, Gianetta and Ikezi 1982). These authors observe and predict lateral sizes of the order of 1 mm. In fact, the theoretical scheme used by Leiderer *et al.* (1982) has some similarities with the one reported here: these authors also minimize a total potential energy that contains surface tension, gravity and interaction terms. The agreement of their calculations with the

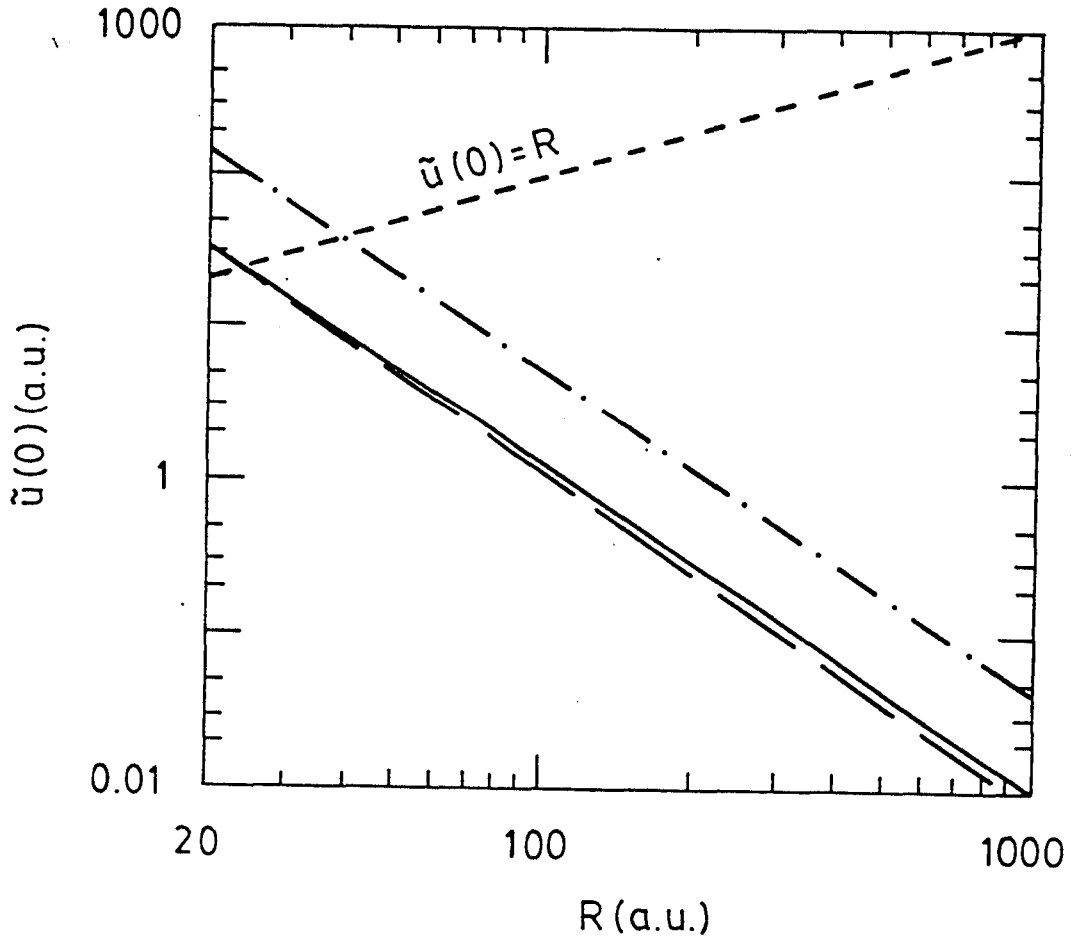

Figure 2.4. Heights, in the linear approximation, of electron-induced bumps on liquid He (dotted-dashed line), Ne (solid line) and Ar (long-dash line). The "contact" line $\tilde{u}(0) = R$ is drawn for reference.

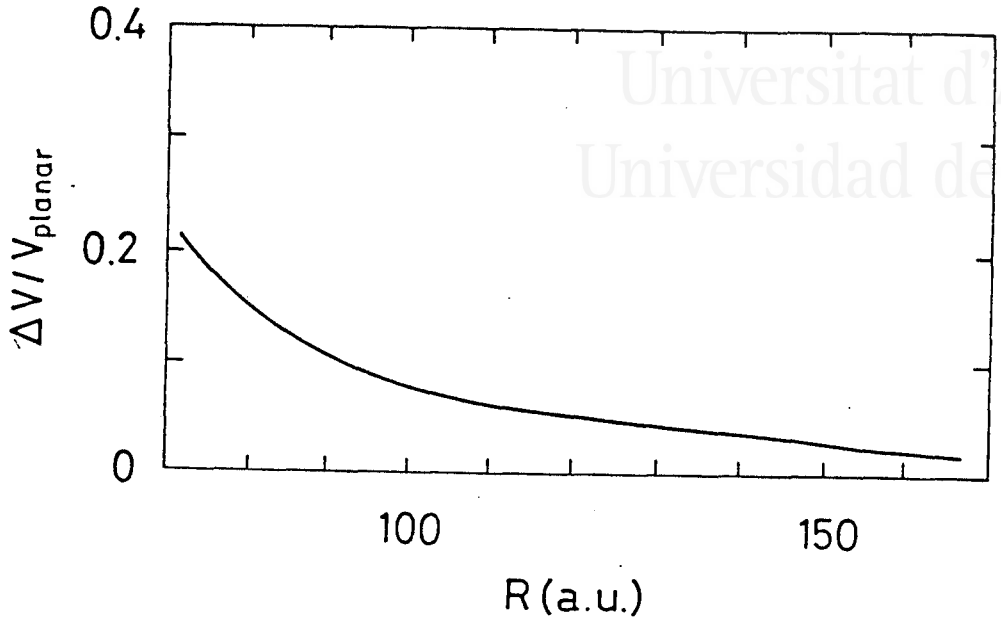

Figure 2.5. Contribution of the bump to the total potential energy of an electron in front of liquid helium, ΔV, compared to the contribution of the unperturbed planar surface, $V_{planar} = -\pi n \alpha e^2/2R$ (from eq. (2.35)).

experiments is remarkable.

The expression for the *self-energy* of the electron in front of the liquid helium (Gras-Martí and Ritchie 1985, eq.(11)) is reproduced with the classical treatment described in this thesis. If the equation for the *induced* potential energy, eq. (2.41) is particularized for the present case, one gets exactly their result:

$$\Delta V = -\frac{\pi n^2 \alpha^2 e^4}{16 \sigma R^4} j_2(\sqrt{2}R/\xi), \tag{2.47}$$

where j_2 is defined in eq. (2.42).

Figure 2.5 shows the contribution of the bump to the total potential energy of the an system formed by an electron and liquid helium, ΔV, relative to the contribution of the unperturbed planar surface, $V_{planar} = -\pi n \alpha e^2/2R$ (from eq. (2.35)). As it may be seen, the contribution of the bump is $\approx$20% at $R \approx 70$ a.u..

In conclusion, this case study serves to state the classical nature of the *self-energy* computed by Gras-Martí and Ritchie (1985) and to give an indication for the range of distances R for which their linear results are valid.

2.4 Non-linear calculations. Case 1: a point charge above a semi-infinite liquid bound by gravity

This section deals with the first of three cases for which I present the results of the numerical solution of the non-linear differential equation (2.13) for the meridian curve: the case of a point

charge in front of a semi-infinite non-polar liquid. This case study will be used to introduce a description of the numerical method, to describe the non-linear features of solutions, and to propose two simple, analytical models that retain the main features of the numerical solutions. The following two sections will be devoted to the remaining two cases, where the methods and techniques described in this section will be applied.

In the previous subsection, the case of a charged particle above the surface of a semi-infinite liquid has been treated within the linear approximation, and here, solutions that are valid also for smaller values of the charge–surface distance R will be described. As has been said above, non-linear solutions show new, interesting features as compared to their linear counterparts.

2.4.1 Description of the numerical method

The complete differential equation (2.13) has been solved using a *shooting* method and the fourth-order Runge-Kutta formulas for second-order differential equations (Davis and Polonsky 1965, eq. (25.5.20)). The integration starts at $\rho = 0$, where two initial conditions are needed. The first one, for the first derivative, is provided by eq. (2.14). The second condition would require the specification of the initial value of the function, $u(0)$, which is unknown. The value of $u(0)$ depends on the charge–surface distance R. Two procedures are possible: one may take a fixed value of R and find the corresponding value of $u(0)$ for the function that satisfies the differential eq. (2.13), or take a fixed value of $u(0)$ and find the corresponding value of R.

The procedure that will be reported here uses the second choice. One takes a fixed $u(0)$ and looks for the corresponding R using the following algorithm: first, a value of R is guessed and the equation is integrated until either of the following two situations, depending on the value of R, is observed:

1. The solution, $u(\rho)$, shows a minimum at some value of ρ and then blows up towards large u as one proceeds with the integration.

2. The solution reaches the value $u = 0$ for a certain finite ρ and sinks towards $-\infty$ as one proceeds with the integration.

The correct value of R may be found, using a bisection technique, at the transition point between the two situations described above. In fact, as the correct value of R is approached from either side, the value of ρ where the solutions start to misbehave approaches infinity. In the limit, the solution would asymptotically approach zero, fulfilling eq. (2.1). In this way, one may obtain the value of R with the desired approximation in an automated way, provided that it has been previously bracketed inside a certain interval.

The program was first tested with the linear equilibrium equation (2.20), the solutions of which are known, eq. (2.26). After this test, the program was ready to be applied to the complete, non-linear differential equation, eq. (2.13).

2.4.2 Non-linear features of solutions: instability

The program was used to calculate equilibrium meridian curves $\tilde{u}(\rho)$ for charge–surface distances R where the use of the linear equilibrium equation, (2.20), was not justified. Nonlinear solutions behaved as expected when higher bumps (larger values of $\tilde{u}(0)$) are considered: the

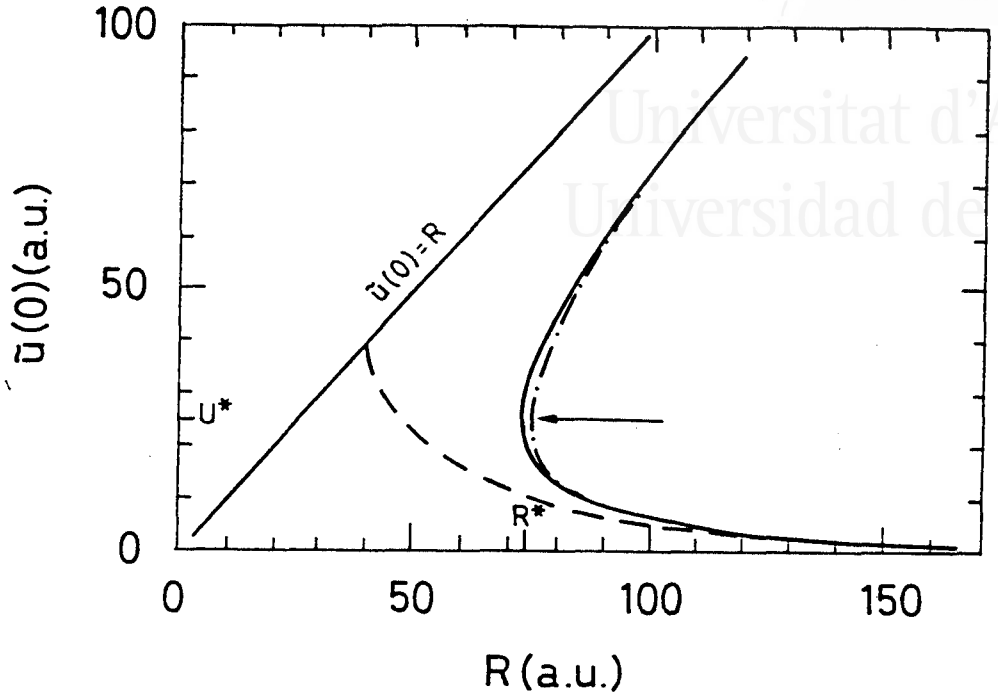

Figure 2.6. Comparison of linear (dashed), full non-linear (solid) and scaled-shape approximation (dotted-dashed) results for the dependence on the charge–surface distance R of the height of the bump $\tilde{u}(0)$ induced by an elementary point charge on the surface of liquid He. The "contact" line $\tilde{u}(0) = R$ has been drawn as a reference. The arrow indicates the maximum $\tilde{u}(0)$ above which solutions $\tilde{u}(\rho)$ of the differential equation do not correspond to stable equilibrium situations.

distances R were larger than the ones calculated from the linear solutions. In other words: for small R, the bumps are higher than their linear counterparts.

But the most interesting feature of the non-linear behaviour is the absence of solutions of the type described in the previous section for values of R below a given value R^*: as one looks for the R's corresponding to increasingly taller bumps, one finds that, at a certain $\tilde{u}(0)$, R starts to increase instead of decreasing. In other words, the function $R(\tilde{u}(0))$ has a minimum value R^*. Figure 2.6 shows the full non-linear results for an electron in front of liquid He. The lower (decreasing) branch of the curve approaches the linear curve for large values of R, whereas the upper (increasing) branch does not show a physically reasonable behaviour: the height of the bump increases as R increases. This last branch may correspond to an extremum of the total potential energy that is not a minimum, but an unstable point.

According to this description, a consequence of the behaviour of the function $R(\tilde{u}(0))$ is the absence of equilibrium solutions for distances $R < R^*$. This may be interpreted as this: at R^* the onset of an instability occurs. For $R < R^*$, surface tension and gravity forces are unable to balance the attractive force on the liquid towards the point charge, and the liquid jumps to contact the point charge.

This kind of instability was observed also by Landman *et al.* (1989) during the molecular

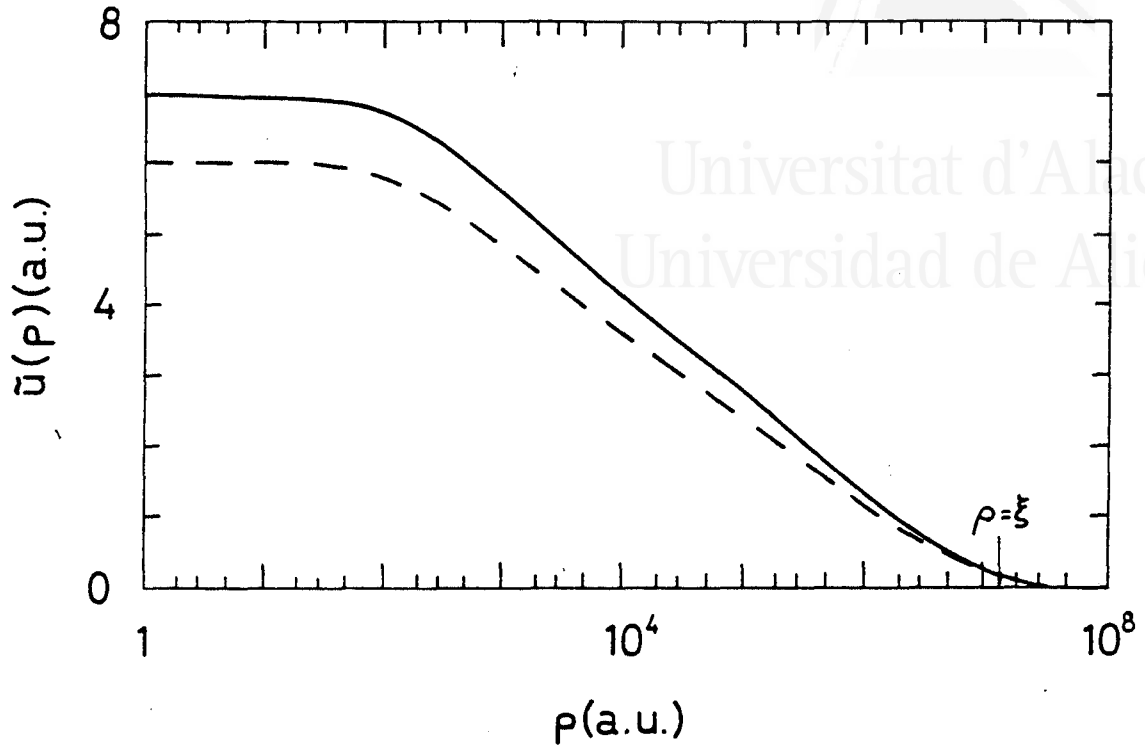

Figure 2.7. Meridian curves of the non-linear (solid) and linearized (dashed) electron-induced bumps on a liquid He surface ($R = 96$ a.u.).

dynamics simulation of the approach of a metallic tip towards a planar metallic surface; these authors call this instability a *jump-to-contact* instability. As it will be shown in the following sections, this instability is a feature that is general to all the static particle–liquid systems studied in this chapter.

Non-linear bumps are strikingly similar in shape to their linear counterparts. This is shown in figure 2.7, where the non-linear and linearized meridian curves of bumps induced on the surface of liquid He by an electron at a height $R = 96$ a.u. are compared. As may be easily seen, the two profiles seem to be just scaled versions of each other. The comments made for the shape linearized bump profile in subsection 2.3.4 apply also here. The decreasing, straight-line portion confirms that, even in the non-linear treatment, the slope is sufficiently small to yield a logarithmic dependence of $\tilde{u}$ on ρ. This is mainly due to the large value of the capillary constant ξ (see figure 2.7).

In addition, it has been found that the non linear solutions for different values of $\tilde{u}(0)$ show a striking similarity of shape, especially around the minimum of the function $R(\tilde{u}(0))$. These features of the meridian curves will be used in the following subsection to construct very simple models of the non-linear solutions.

When one compares the non-linear results for different liquids, some interesting regularities are also observed. If U^* is the maximum height of the profile $\tilde{u}(0)$ for the smallest particle–

liquid distance for which a solution exists, R^*, the following numerical results (in atomic units) have been found for an elementary-charged particle in front of liquid He, Ne and Ar: He, R^*=72.9, U^*=24.1; Ne, R^*=44.2 U^*=14.6; Ar, R^*=44.8, U^*=14.8. The data in table 2.1 have been used in the calculations. This suggests an interesting liquid-independent relation,

$$R^* \approx 3U^* \tag{2.48}$$

which will also be explained in the following subsection by using a simplified model of the charge–liquid interaction.

2.4.3 Simple models that account for the non-linear features of solutions

I propose here two models that account for the most interesting features of the non-linear solutions that are being discussed in this section. These models will also be used in following sections, where different particles and liquid bodies are involved, to obtain approximate results of the pertinent quantities.

The scaled-shape approximation

Here, a liquid-independent model that gives a very good approximation to the numerically computed profile heights, including the relation (2.48), will be described. Profiles computed by numerical solution of eq. (2.13) show shapes that are almost liquid-independent if ρ is measured in units of $\xi/\sqrt{2}$ (ξ being the capillary constant), and they simply scale vertically for all ρ when the height of the particle R is changed. This is a natural scaling when dealing with capillary-gravity problems (Mel'nikov and Meshkov 1981, Boucher and Jones 1987). Taking this into account, profiles may be approximately written in terms of a "universal" function as follows:

$$\tilde{u}^{ssa}(\rho) = \tilde{u}(0)F(\sqrt{2}\rho/\xi). \tag{2.49}$$

Here the superscript *ssa* stands for "scaled-shape approximation". The function $F(x)$ should satisfy the following boundary conditions,

$$F(0) = 1, \quad F'(0) = 0, \tag{2.50}$$

and

$$\lim_{x\to\infty} F(x) = 0. \tag{2.51}$$

In addition, it will be assumed that surface profiles are so smooth that eq. (2.17) holds. This allows to write a simplified expression for the surface tension energy. It will also be assumed that the charge–liquid interaction may be approximated by the interaction of that charge with a planar surface located at a height $\tilde{u}(0)$ (see the flat top of profiles in Figure 2.7). This last approximation will be called the "flat-top approximation" in the following. With these approximations, the bump contribution to the the total potential energy of the system, eq. (2.39), may be written as a function of R and $\tilde{u}(0)$ only:

$$\Delta V \approx \pi\sigma I_F \tilde{u}^2(0) - \frac{n\pi\alpha Q^2}{2}\left(\frac{1}{R-\tilde{u}(0)} - \frac{1}{R}\right), \tag{2.52}$$

where Q is the charge of the particle and

$$I_F = \int_0^\infty dx\, x\left[F^2(x) + \left(\frac{dF}{dx}\right)^2\right]. \tag{2.53}$$

is a constant in this approximation.

Calculation of the minimum of the approximate expression for the total potential energy, eq. (2.52), with respect to $\tilde{u}(0)$, for a given value of R, yields an expression relating R and $\tilde{u}(0)$:

$$R = \tilde{u}(0) + \left[\frac{n\alpha Q^2}{4\sigma I_F \tilde{u}(0)}\right]^{1/2}. \tag{2.54}$$

Further minimization of R in this expression with respect to $\tilde{u}(0)$ yields the liquid-independent equality

$$R^* = 3U^*, \tag{2.55}$$

where

$$R^* = \frac{3}{2}\left[\frac{n\alpha Q^2}{2\sigma I_F}\right]^{1/3}. \tag{2.56}$$

The parameter I_F may be either used as an adjustable parameter to fit the numerical results to a simple expression, or may be computed for each pair of numerical results $(R, \tilde{u}(0))$ to check its small range of variation. Near the minimum distance R^*, I_F has an approximate value of 0.08.

The flat-top model

There is an even simpler approach to the computation of profile heights, based on two of the above approximations: the small-slope approximation, eq. (2.17), and the flat-top approximation. According to this second approximation, one may just substitute $\tilde{u}(0)$ for $\tilde{u}(\rho)$ in the last term of the right-hand side of eq. (2.13) ($\tilde{u}(\rho)$ only starts to depart appreciably from $\tilde{u}(0)$ when ρ is very large, but then the potential is very small) and take the linear form of the surface-tension term to write the simplified equilibrium equation

$$-\sigma\left[\frac{d^2\tilde{u}}{d\rho^2} + \frac{1}{\rho}\frac{d\tilde{u}}{d\rho}\right] + nMg\tilde{u}(\rho) + v(R - \tilde{u}(0), \rho) = 0. \tag{2.57}$$

The solution of this equation may be obtained easily (it is the linear differential equation (2.20) for this case, but with $R_1 = R - \tilde{u}(0)$ instead of R, see eq. (2.26)):

$$\tilde{u}(\rho) = \frac{\pi n\alpha Q^2}{2\sigma R_1^2}\int_0^\infty dt\, t^2 \frac{J_0(t\rho/R_1)K_1(t)}{t^2 + 2R_1^2/\xi^2}. \tag{2.58}$$

This implicit expression has to be used in the following way: by giving values to $R_1 = R - \tilde{u}(0)$ to get the corresponding values of $\tilde{u}(0)$ and therefore R. The agreement of this approximation with the numerical results is remarkable (see Figure 2.6), especially near the minimum distance, R^*, where the linear approximation is not applicable.

By identifying the bump height computed using this treatment, eq. (2.58) with $\rho = 0$, and the one obtained using the scaled-shape approximation, eq. (2.54), it is found that the "constant" I_F in eq. (2.53) depends very smoothly, on R_1:

$$I_F = \frac{1}{2\pi i_2(\sqrt{2}R_1/\xi)}, \tag{2.59}$$

where the function $i_2(x)$ has been defined in eq. (2.29).

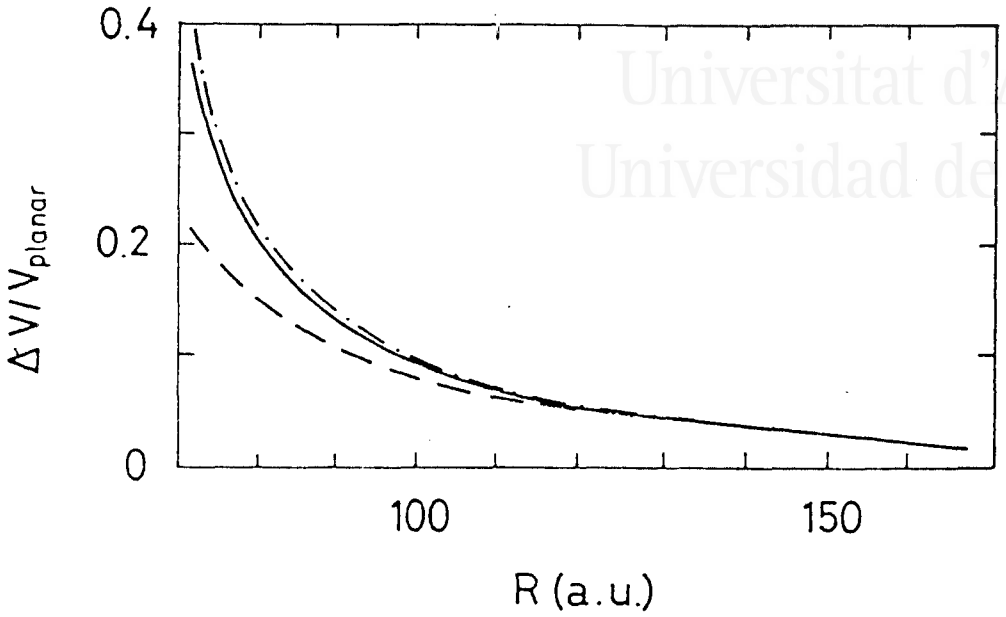

Figure 2.8. Bump contribution to the potential energy of an electron, ΔV, relative to the plane-surface contribution, V_{planar}, as a function of distance, R, for liquid He: full curve, numerical result; dashed curve, linear result, eq. (2.47); dotted-dashed curve, scaled-shape approximation, eq. (2.52).

2.4.4 Potential energy of the charge–surface system

The total potential energy of a charge in front of a liquid surface may be written as the sum of the binding potential energy (2.4), the surface energy (2.32), and the interaction energy (2.8), evaluated for the case of a charge. The interaction energy may be divided in two contributions: the one from the planar, unperturbed surface, eq. (2.35), which in this particular case of charge–liquid interaction may be integrated to yield $-\pi n\alpha Q^2/2R$, and the other from the bump, eq. (2.36).

The potential energy due to the bump has already been approximated in subsection 2.4.3, in order to derive eq. (2.52). The exact expressions have been numerically integrated during the process of solving the non-linear differential equation (2.13). Results for a charged particle in the long-distance limit reproduce the linearized result of Gras-Martí and Ritchie (1985) (eq. (11) in their paper), which have also been obtained classically in this work, eq. (2.47).

Figure 2.8 shows a comparison of potential energies, for an elementary charge in front of liquid He: the full numerical integration result, as well as the scaled-shape approximation, obtained from eq. (2.52), and the linear result, eq. (2.47), are plotted relative to the potential energy for the unperturbed plane. As expected, the non-linear and linear results meet in the long charge–liquid distance limit. These results may be used to estimate the range of R where the linear approximation is applicable. The linear approximation was also used by Gras-Martí and Ritchie (1985) to compute the energy loss of a charged particle moving parallel to the surface of the liquid; in Chapter 3, a classical way of obtaining this energy loss will be described.

2.5 Non-linear calculations. Case 2: a neutral atom above a semi-infinite liquid bound by gravity

The interaction of a neutral atom with a semi-infinite liquid is very similar to the case of a charged particle that has just been described (Case 1). I will simply outline the corresponding results, obtained using the analyses and also the simple methods described in the previous section.

Here, a neutral atom is placed in front of the liquid surface, and the interaction energy here is assumed to have the form of a non-retarded van der Waals interaction:

$$v_{int}(\rho, z) = -\frac{n\Lambda}{[(R-z)^2+\rho^2]^3}, \tag{2.60}$$

that is, eqs. (2.7) and (2.5) with $m = 3$, $a = 0$. Λ is the van der Waals coefficient for the interaction between the external atom and the atoms in the liquid. This case may be also treated in the linear approximation, as has been done for the case of the charged particle, but I will give here only some details of the results of the numerical treatment.

If one substitutes eq. (2.60) in the non-linear differential equation (2.13), and solve it numerically following the procedure explained in section 2.4, one obtains results that are qualitatively very similar to those of a charge in front of the liquid. Numerical results for $\tilde{u}(0)$ as a function of R, obtained for a He atom above liquid He, using the data in table 2.1, are shown in Figure 2.9.

As in Case 1, there is a minimum distance, R^*, below which no stable shape of the liquid surface may be found. Using the data on table 2.1, for a He atom on liquid He, one finds $R^* = 15.85$ a.u.; for a Ne atom on liquid Ne, $R^* = 12.16$ a.u.; for an Ar atom on liquid Ar, $R^* = 15.05$ a.u.

One also finds here an interesting liquid-independent relation that holds at the minimal distance: $R^* \approx 5U^*$ (with U^* the height of the bump at the minimum equilibrium distance R^*; compare this with $R^* \approx 3U^*$, eq. (2.55), obtained for the charge–liquid interaction). Numerical results (in atomic units) for a single atom in front of its corresponding liquid, obtained using the data in table 2.1, are: He, $U^* = 3.16$; Ne, $U^* = 2.47$; Ar, $U^* = 3.03$.

As can be seen, a neutral atom may approach the liquid at a shorter distance than a point charge (the values of R^* are smaller), and the maximum stable heights of the induced bumps (U^*) are smaller. This is mainly due to the shorter range of van der Waals forces as compared to that of the charge–dipole force.

As in the case of the charge–liquid interaction, eq. (2.52), a scaled-shape model, adapted for the new interaction potential, may be used to get an expression for the bump part of the total potential energy:

$$\Delta V \approx \pi\sigma I_F \tilde{u}^2(0) - \frac{n\pi\Lambda}{6}\left(\frac{1}{(R-\tilde{u}(0))^3} - \frac{1}{R^3}\right). \tag{2.61}$$

This reproduces very satisfactorily the numerical results for bump heights, especially around the minimum, and accounts for the liquid-independent relation mentioned above

$$R^* = 5U^*. \tag{2.62}$$

The minimal distance R^* is here

$$R^* = \frac{5}{4}\left[\frac{n\Lambda}{\sigma I_F}\right]^{1/5}. \tag{2.63}$$

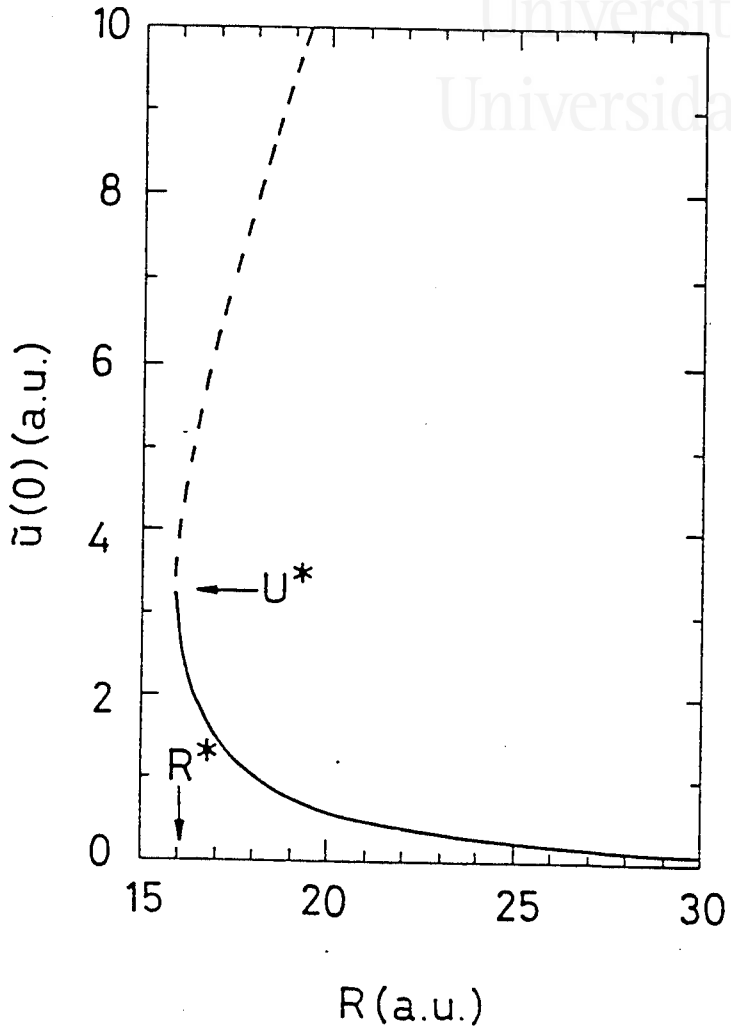

Figure 2.9. Bump height $\tilde{u}(0)$ as a function of the atom–liquid distance R for a He atom on liquid He. The solid part of the curve corresponds to stable equilibrium, whereas the dashed part corresponds to non-stable equilibrium.

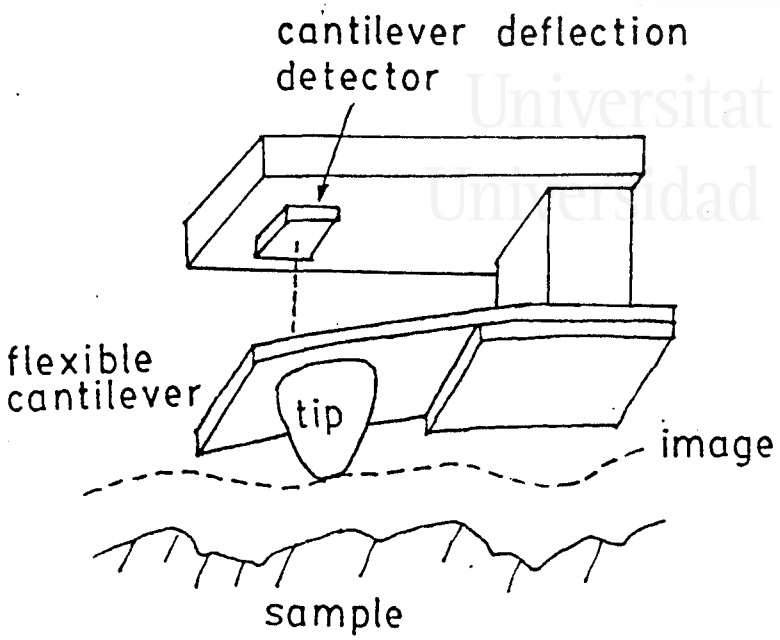

Figure 2.10. A schematic diagram of the atomic-force microscope.

The approximate value of I_F around the minimum distance is 0.07.

The flat-top model that has been used for Case 1 gives, after adaptation to the present situation, a very good approximation to the numerical results (even better than for the charged particle, because the van der Waals potential has a shorter range than the charge–dipole potential). The approximate results for bump heights are almost indistinguishable from the full numerical results, especially around the minimum.

2.6 Non-linear calculations. Case 3: Atomic-force microscopy of thin liquid films

This section will describe the application of the theoretical tools described along this chapter to explain some of the experimental results obtained by Mate, Lorenz and Novotny (1989), when measuring the thickness of thin, solid-supported liquid films using the technique called atomic-force microscopy, by detecting the sudden onset of an attractive force that occurs when the tip of the microscope gets in contact with the liquid.

2.6.1 Brief description of the atomic-force microscope

The atomic-force microscope (Binnig et al. 1986), also called *scanning force microscope* is one of the new scanning probe microscopes that were developed after the invention of the well-known and widely used scanning tunnelling microscope (STM) by Binnig and Rohrer (1982). The principle of operation of the atomic-force microscope (AFM) is very simple

(see Figure 2.10): a sharp tip is mechanically scanned over the surface of the sample. The tip is mounted on a flexible cantilever that bends as a result of the force on the tip. The deflection of the cantilever may be detected, in turn, using different techniques (scanning tunnelling microscopy, capacitive detection, laser-beam deflection, interferometry: see Rugar and Hansma 1990).

Depending on the tip–surface distance, the force may be repulsive or attractive. If the surface is scanned in the constant-force mode, the tip–sample distance has to be continously adjusted as one scans the surface. The result is a topographical image of the constant-force surface, which is closely related to the topography of the surface. In solids, a sharp tip operated in the repulsive, constant-force mode may yield atomic resolution (Rugar and Hansma 1990).

There is another possible mode of operation: the constant-force-gradient mode. The tip is mounted on a cantilever which has a certain force constant. This force constant determines the main frequency of oscillation of the cantilever. If the tip mounted on it is inside the force field of the sample, the gradient of this force field adds to the spring constant of the cantilever. As a result, the free oscillation frequency is shifted. If, on the other hand, the cantilever is forced to oscillate at a given frequency near its free oscillation frequency, a resonance will be observed only when the tip feels the corresponding force gradient. By adjusting the tip height to get resonance, one may scan the surface at a fixed force gradient. This also yields a topographical image of the surface of the sample, usually with smaller resolution than in the constant-force mode.

The most interesting feature of the atomic-force microscope is that, unlike the scanning tunnelling microscope, it may be used to image both conducting and non-conducting samples.

2.6.2 Dipping determinations of liquid film thicknesses

Description of the experiments

Usually, the atomic-force microscope (AFM) is used to study the surfaces of solid samples. In one of the experiments described by Mate et al. (1989), however, the AFM is used to measure the thickness of thin solid-supported lubricant films. In these experiments, there is no horizontal scan of the tip. Rather, the cantilever that holds the tip is moved vertically towards the sample, and the force on the tip is measured by monitoring the deflection of the cantilever.

The sequence of events in such a dipping experiment is shown in Figure 2.11:

(a) When the tip is still outside the liquid, the attractive force due to long-range van der Waals interactions is too small to cause an appreciable deflection of the cantilever that holds the tip. However, as has been described in the previous sections, it has to be expected that the liquid swells and a bump is formed at the surface.

(b) When the tip makes contact with the lubricant film, a new, stronger attractive force appears suddenly, due to the meniscus, and the cantilever bends towards the sample.

(c) With further dipping, the tip reaches the solid substrate, and a strong repulsive force appears: the cantilever bends away, pushed by the solid substrate.

In this manner, one might identify the thickness of the film with the distance the tip has travelled from the point where the sudden onset of an attractive force occurs (the *wetting* point) and the point where the force suddenly becomes strongly repulsive (the *knocking* point).

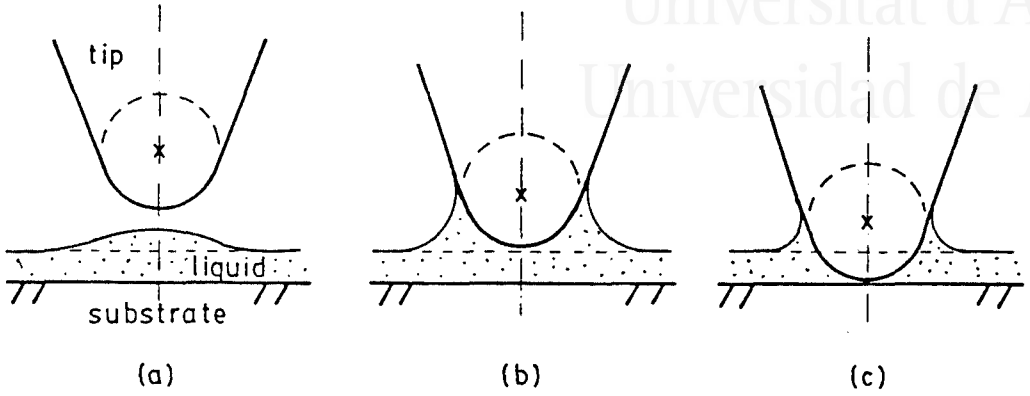

Figure 2.11. Sequence of events in a dipping experiment: (a) the tip is in the air, (b) the tip is wet and (c) the tip knocks on the solid substrate.

When Mate et al. (1989) compare the values of film thicknesses measured using this principle with the values obtained using an interferometric technique known as ellipsometry, they observe a systematic offset: AFM measurements overestimate the thickness of the lubricant films. These authors attribute this offset to the presence of a thin layer of lubricant on the tip itself, due to previous wetting processes, or to the fact that the long tails of lubricant molecules may extend beyond the liquid–air interface under the attraction of the tip. However, the offset seems to depend on the thickness of the film (see Figure 2.12 in page 33). The reasons given by the authors do not explain this dependence.

The offset may also be attributed, in the light of the theoretical results of the previous sections, to the swelling and subsequent instability of the liquid surface in the presence of the attractive force of the tip. In the following section, the minimal distance that the tip can approach the film before wetting is computed in order to compare it with the experimental offset.

Theoretical calculations

In this model of the offset (Forcada, Jakas and Gras-Martí 1991) the differences observed between the thicknesses measured with the force microscope and ellipsometric thicknesses are explained by the appearance of an instability in the liquid film. These calculations also predict the dependence of these differences on the thickness of the film.

The hydrostatic model of particle–liquid interaction described previously in this chapter, represented by eq. (2.13), may be easily applied here. As the tip approaches the sample, the liquid surface becomes non-planar, and a small swelling (a bump) develops. One expects that, in the light of the results of the previous sections (2.4 and 2.5, cases 1 and 2), a minimal distance of tip–sample approach exists, below which there is no equilibrium configuration available for the system formed by the liquid and the external probe. In fact, this has already been discussed extensively for the case of solid surfaces. Both molecular dynamics simulations

(Landman et al. 1989) and continuum calculations (Pethica and Sutton 1988) of tip–solid interactions show a similar instability: a *jump-to-contact* point, after which atoms of the perturbed area of the sample start to vaporize from the surface of the sample to form a neck that joins the tip and the sample. A similar result is also predicted, indeed, for the tip–liquid interaction: a minimal distance is found, below which the bump or swelling of the liquid surface, formed due to the attractive force between the liquid and the AFM tip, is no longer stable: for smaller distances, surface tension and adhesion to the substrate cannot prevent the liquid from *jumping* to contact the tip.

The interaction of a unit volume of the liquid and a unit volume of either the tip or the substrate is modelled as a non-retarded van der Waals interaction of the form

$$\hat{v}(r) = -A\pi^{-2}r^{-6}, \tag{2.64}$$

where A is called the Hamaker constant (Israelachvili 1985:137, Hamaker 1937). This macroscopic formulation of the van der Waals interactions is the most appropriate here, because it does not require an underlying molecular model.

Both the binding and interaction energies per unit volume of liquid are obtained by integration of (2.64) over the volume of either the solid substrate or the tip.

The tip is modelled as a spherical particle of radius a (see figure 2.11). Integration over the volume of the tip yields the following expression for v_{int}:

$$v_{int}(R-z,\rho) = -\frac{4a^3}{3\pi}\frac{A_{int}}{\left[(R-z)^2+\rho^2-a^2\right]^3}, \tag{2.65}$$

which is a particular case of eq. (2.5) with $m = 3$ and a the radius of the tip; A_{int} is the value of the Hamaker constant for the tip–liquid interaction.

Integration of the non-retarded van der Waals interaction, eq. (2.64), over the semi-infinite solid substrate gives an expression for the binding potential energy per unit volume of liquid (see section 2.1.2):

$$v_b(z) = -\frac{A_b}{6\pi(h+z)^3}, \tag{2.66}$$

where h is the thickness of the liquid film, A_b is the Hamaker constant for the liquid–substrate interaction.

For the calculations of this section, the values $\sigma = 1.35 \cdot 10^{-5}$ a.u., and $a = 4150$ a.u., given by Mate et al. (1989) are used. The Hamaker constants for the liquid–tip and liquid–solid interactions, taken to be equal, $A_{int} = A_b = 0.03$ a.u., are estimated (with an accuracy of 20–30%) as the geometric mean of a typical metal–metal Hamaker constant (Israelachvili 1985:146) and the lubricant–lubricant constant. The lubricant–lubricant Hamaker constant is obtained from the surface tension of the lubricant using an empirical formula also given by Israelachvili (1985:156), where the surface tension coefficient is related to the energy of interfacial contact between two identical semi-infinite media.

$$\sigma = \frac{A_{lub-lub}}{24\pi D_0^2}, \tag{2.67}$$

where $D_0 = 3.12$ a.u. is a "universal" (empirical) interfacial contact separation (Israelachvili 1985:157).

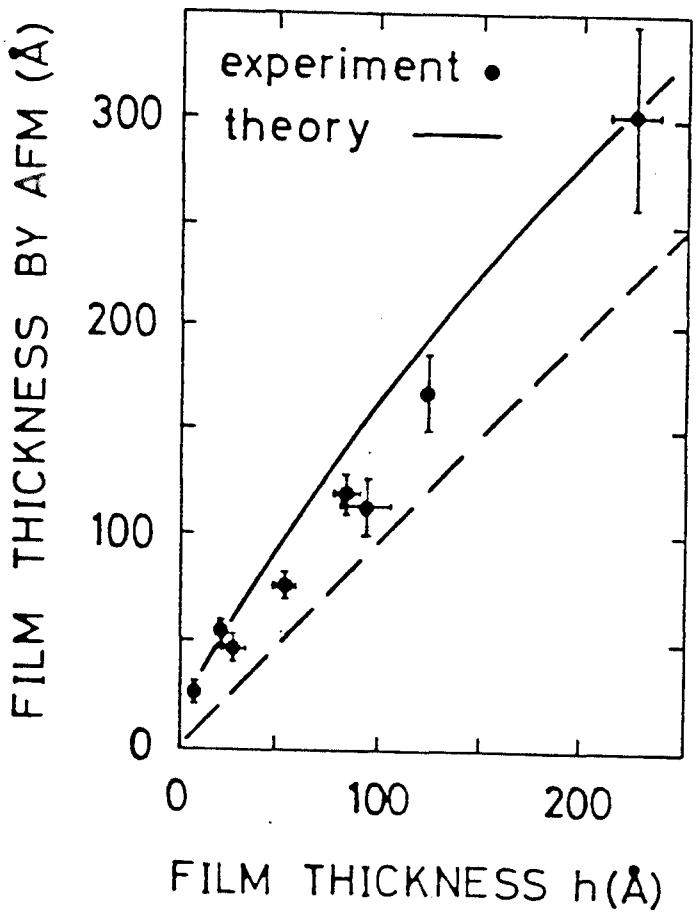

Figure 2.12. AFM thicknesses (experimental values and theoretical estimates) versus nominal (ellipsometric) thicknesses h. The dashed line corresponds to zero offset.

With these energies defined, the equilibrium equation (2.13) may be solved numerically using the same procedure as in the previous sections. The jump-to-contact, or minimal equilibrium distance R^* depends, for a given liquid, tip and substrate, only on the thickness of the film. This allows to compute a relation between ellipsometrical thickness and the AFM thickness.

Figure 2.12 shows: the thickness of the liquid film determined by AFM, and the thickness predicted by the present model, and defined as $R^* - a + h$; both plotted as a function of h, the nominal thickness of the unperturbed film (as measured by ellipsometry). There is reasonable agreement between the calculations and the experimental results, and the presence of an offset in both the theoretical and experimental AFM thicknesses is apparent. This offset indicates that the wetting of the tip occurs before the hypothetical contact between the tip and the unperturbed liquid surface would occur ($R^* - a$ is not zero). Furthermore, the offset increases with increasing thickness. The fact that R^* increases with h can be easily understood since, for larger h, the binding of the liquid to the solid substrate is weaker, and wetting of the tip occurs at larger tip–liquid distances. The agreement of the calculation with the experiment, however, should not be overstated, due to the lack of knowledge of accurate Hamaker constants. The results may be taken as an indication that bump instability contributes to the observed offset.

Other possible explanations for the offset (which have been mentioned before) are:

1. the presence of a film of liquid (whose thickness has recently been estimated by a hydrostatic formalism, Langlois (1991)) on the tip surface, due to previous wetting of the tip (Mate et al. 1989, 1991), or

2. the fact that the tails of the polymer molecules extending both off the film on the substrate and off the film possibly formed on the tip may intertwine (Mate et al. 1991).

The first effect could be incorporated into a hydrostatic model such as the present one, which should also consider the instability of the film on the tip. However, the second effect would not show such a clear dependence on the film thickness as the minimal distance R^* does. For a proper treatment of this effect on the calculated thickness offset, microscopic (molecular) models of the liquid films would be necessary. These microscopic models fall outside the scope of this work. In fact, the explanation in which the tails of lubricant molecules stick out from the main liquid under the attraction of the tip (Mate et al. 1989, 1991) may be seen as a molecular image of the swelling phenomenon, and suggests that, perhaps, the continuous description used here could be improved by considering a non-abrupt liquid–air interface.

2.6.3 Topography of the liquid–air interface

Description of the experiments

In another experiment described by Mate et al. (1989), a constant-force-gradient scan was used to get a topographical image of the liquid–air interface, to study the thickness distribution of a lubricant on a substrate. In the context of the theoretical work described in this chapter, the study of this case is interesting: the swelling of the liquid film in the vicinity of the tip, due to the attractive interaction, might distort the topographic image of the liquid–air interface.

The solid substrate, in the experiments by Mate et al. (1989), was a planar surface with cylindrical holes etched on it. These holes had a depth of 1 μm, a diameter of 2 μm, and

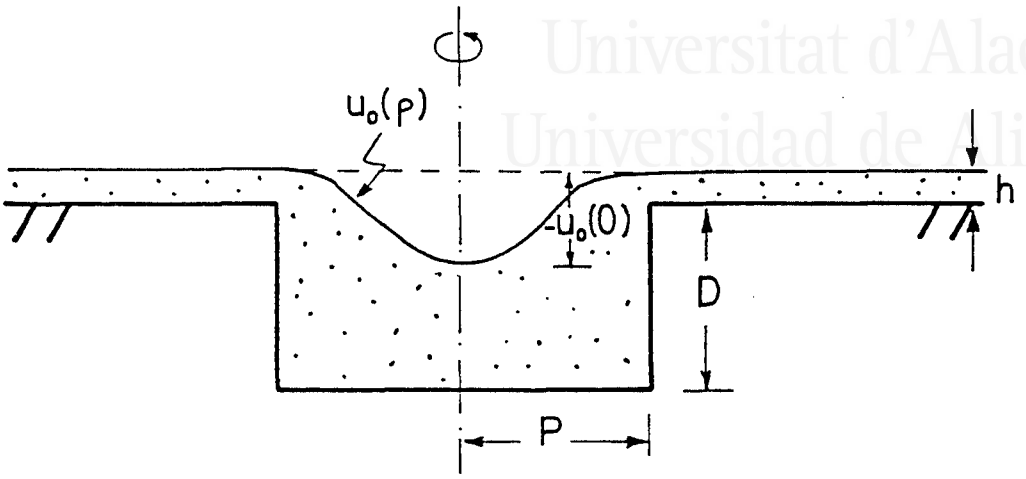

Figure 2.13. Filling of a cylindrical hole with lubricant.

were separated from each other by at least 8 μm (Philpott, Hussla and Coburn 1987). Films of lubricant of various thicknesses (5–100 nm) were deposited on these substrates.

One interesting result of the experimental study is an image of how the holes are filled with lubricant, and of the meniscus that forms inside them (see Figure 2.13). Two parameters, the radius of curvature of the meniscus and the depth of the depression at the symmetry axis of the hole, may be used to characterize the filling of the pores.

For a film of thickness 50 Å, the depth of the depression was measured to be around 0.4 μm, and the radius of curvature was 1.9 μm. For thicker films the radius of curvature was of course larger.

Theoretical calculations

A question arises when attempting to analyse the topographical measurements of Mate et al. (1989), that is, whether the surface is attracted towards the tip to such an extent that the topographical image is appreciably distorted with respect to the unperturbed topography of the liquid–air interface.

Indeed, one expects that, far from the holes, where the liquid is thinner and more tightly bound to the solid substrate, the height of the bump induced by the tip may be smaller than inside the holes, where the liquid is deeper and more loosely bound. A large difference of bump heights would affect the imaging: the holes would appear more filled than they really are.

A series of calculations have been done, the results of which suggest that this effect does not seriously affect the imaging for films as thin as 100 Å. For thinner films, the numerical solution of the appropriate differential equation becomes much more involved. The procedure devised to obtain the theoretical estimate of the distortion effect consists of the following steps:

1. Solve numerically the complete differential equation for the meridian curve of the liquid–air interface around a cylindrical hole, without the presence of the tip. In contrast to all systems studied so far, the binding potential in this case depends not only on z but also on ρ.

2. Compute the new meridian curve when a tip is held at a certain height above the liquid, at the symmetry axis of the hole. (Only predictions for this position of the tip will be given, in order to make use of the static formulation developed along this chapter, which is restricted to axisymmetrical situations). The height should be chosen to be a typical constant-force-gradient scan height.

3. Calculate the gradient of the force felt by the tip at that height by numerical differentiation of the potential energy (including the tip–substrate potential energy) with respect to tip height R. This involves three complete integrations of the differential equation for three different heights R, and the corresponding simultaneous numerical integrations of the total potential energy.

4. Look, by trial and error and numerical differentiation, for a tip height above the planar area of the solid substrate (outside the hole) that yields the same force gradient (including the corresponding bump). This also involves three complete calculations of the total potential energy per try.

5. Compare the height of the tip above the unperturbed (no-tip) level of the liquid–air interface, in the hole and outside the hole, that correspond to the same gradient.

The magnitude of the difference between the two heights that correspond to the same force gradient gives an indication of the vertical accuracy of the topographical image obtained using a constant-force-gradient AFM scan.

One of the first problems encountered in the process described above was the modelling of the binding potential around the hole. Integration of the non-retarded van der Waals interaction energy, eq. (2.64), does not seem to be possible in a closed form for this geometry. However, the results of a numerical integration (also reported by Papadopoulos and Kuo 1990) may be interpreted in terms of plane-wall contributions. A volume element of the liquid that fills the hole (of depth D and radius P, see figure 2.13) is only appreciably bound to the substrate when it is close to it. When this happens, the liquid element sees the substrate either as a plane wall of solid or as a corner of solid defined by two half-planes.

The van der Waals binding potential energy of a unit volume of liquid towards a plane wall of substrate material is, according to eq. (2.66),

$$v_p(x) = -\frac{A_b}{6\pi x^3}\Theta(x), \tag{2.68}$$

where x is the distance to the interface, and the Heaviside step function $\Theta(x)$ has been included to switch the plane-wall binding potential off when x is negative. This is a good approximation to the binding potential when the liquid element is (a) near the center of the bottom of the hole, (b) near the sides of the hole but far from the bottom or the top of it, or (c) far from the hole, above the planar area of the substrate.

When the liquid element is near one of the two corners (the one formed between the bottom and the side of the hole or the one formed between the side of the hole and the

external plane), the potential will have a transition value between two plane-wall potentials. This will be achieved using a smooth switching function, the complementary logistic function,

$$f_{c,\kappa}(t) = \frac{1}{1+e^{\kappa t}}. \tag{2.69}$$

where κ is a parameter that determines the smoothness of the switching. The function has a limiting value of one for large negative t, a value of 0.5 for $t = 0$ and a limiting value of zero for large positive t.

The outer plane only contributes when the liquid element is outside the hole, and its contribution must decrease from the full wall-plane value as the liquid element approaches the center of the hole. This decrease is more sudden when the liquid element is very near to the surface. The contribution of the outer plane may be then written as

$$v_b^{plane} = f_{c,\kappa}\left(\frac{P-\rho}{z+h}\right) v_p(z+h). \tag{2.70}$$

The side wall of the hole contributes only when ρ is smaller than the radius of the hole P. Its contribution goes from almost the full plane-wall value, deep inside the hole, to zero, when the liquid element is high above the hole. The switching function is set up so that the decrease is more abrupt if the liquid element is very near to the side wall. Accordingly,

$$v_b^{side} = f_{c,\kappa}\left(\frac{z+h}{P-\rho}\right) v_p(P-\rho). \tag{2.71}$$

Finally, the contribution of the bottom is chosen so that it goes from almost the full plane-wall value, when $\rho = 0$, to half of it when $\rho = P$. Then,

$$v_b^{bottom} = f_{c,\kappa}\left(\frac{\rho-P}{z+D+h}\right) v_p(z+D+h), \tag{2.72}$$

The total binding potential, for any value of z and ρ, is then

$$v_b(z,\rho) = v_b^{plane} + v_b^{bottom} + v_b^{side}. \tag{2.73}$$

The parameter κ in the switching functions was fitted to the numerical integration results and its optimum value was found to be around 3.0. The approximations that have just been described are satisfactory when the value of the binding potential are comparable to $v_b(0,\infty) = v_p(h) = -A_b/6\pi h^3$, the binding potential at the surface of the film very far from the hole.

With this analytical approximation for the binding potential, one may compute the equilibrium shape of the liquid–air interface by numerical integration. I have found, however, serious numerical problems when I have tried to apply the numerical methods to very thin films, mainly due to the abrupt changes of the slope of the meridian curve as it follows the shape of the hole. In fact, the thinnest film I have been able to treat had a thickness of 170 a.u. (= 90 Å.).

The results of the calculation of the depression at the center of the hole, $-u_0(0)$, (step 1 of the procedure described in pag. 36) are shown in table 2.2. The dimensions of the hole ($P = D = 1.9 \cdot 10^4$ a.u. = 1μm) correspond to those given by Mate et al. (1989). As can be seen, the liquid fills the hole completely for film thicknesses that are one order of magnitude smaller than the size of the hole. But as the film becomes thinner, the liquid

Table 2.2. Depression of the liquid surface at the center of the cylindrical hole on a metallic substrate, $-u_0(0)$, for different film thicknesses h. Dimensions of the hole: radius, $P = 1\mu\text{m} = 1.9 \cdot 10^4$ a.u., depth $D = 1\mu\text{m} = 1.9 \cdot 10^4$ a.u.; liquid–substrate Hamaker constant, A=0.03 a.u.

h (a.u.)	$-u_0(0)$ (a.u.)
3400	1.5
1000	39
470	190
425	240
400	270
300	520
240	940
200	1470
190	1690
180	1990
170	2300

starts to abandon the hole (as it was independently shown by the experiments of Philpott et al. 1987) by adjusting itself to the walls, due to the increasing importance of the adhesion of the lubricant film to the substrate.

The next steps (2 and 3 in pag. 36) involve including the tip at a typical scan distance ($\approx$ 200 a.u.), then finding the equilibrium shape of the liquid–air interface, and computing the force gradient by numerical differentiation of the total potential energy. The potential energy of the tip in the field of the lubricant-filled hole has to include four contributions: the surface energy of the liquid–air interface, the binding energy of the liquid, the tip–liquid interaction energy, and the tip–substrate interaction energy. To compute the force gradient with respect to tip height, one may neglect all the constant contributions to the energy and focus only on the ones that vary with tip height.

The tip–substrate contribution to the potential energy may be computed analytically, by dividing the volume of the substrate in two parts: a "flat" (a semi-infinite solid limited by a plane surface) at the bottom and a "ring" of solid material sitting on top of it (see Figure 2.14).

The tip–liquid contribution may also be divided in two parts: the first one will be a "cylinder" of liquid inside the hole, with the same radius P as that of the hole, and limited between the plane defined by the bottom of the hole and a parallel plane ($z = \tilde{u}(0)$) that contains the point where the liquid–air interface intersects the symmetry axis (the point of maximum depression). The second part will be the rest of the liquid (see Figure 2.14). For this second part, the integration is done only from $\rho = 0$ to $\rho = 2P$ (the z integration may be done analytically here). The potential energy of the "cylinder" in the field of the tip may also be written as a combination of "ring"- and "flat"-type contribution to potential energies, as will be shown later.

The potential energy of a sphere in front of a flat surface that limits a semi-infinite medium (see, for instance, Papadopoulos and Kuo 1990, eq. (14)) is

$$V_{flat}(x) = -\frac{A}{6}\left[\ln\left(\frac{x+a}{x-a}\right) + \frac{2ax}{x^2-a^2}\right], \tag{2.74}$$

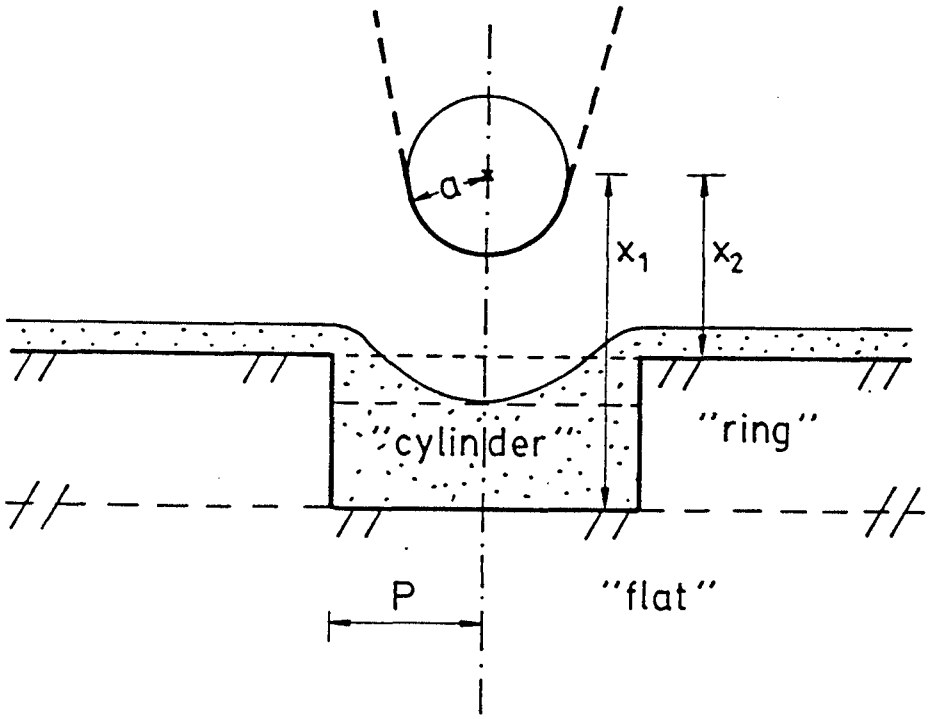

Figure 2.14. Partition of the liquid and substrate volumes for the calculation of tip–liquid and tip–substrate potential energies.

where x is the distance between the center of the sphere and the surface, a is the radius of the sphere, and A is the Hamaker constant for the pair of interacting media. For the tip–substrate interaction, a typical metal–metal value has been used, $A = 0.089$ a.u. (Israelachvili 1985:146).

The potential energy of a sphere of radius a in front of a laterally infinite ring of solid, delimited by two planes at distances x_1 and x_2 and of internal radius P (see Figure 2.14) is, by straightforward volume integration,

$$V_{ring}(x_1, x_2) = -\frac{a^3 A}{3\,(P^2 - a^2)^{3/2}} \left(\arctan \zeta_2 - \arctan \zeta_1 + \frac{\zeta_2}{\zeta_2^2 + 1} - \frac{\zeta_1}{\zeta_1^2 + 1} \right), \qquad (2.75)$$

where

$$\zeta_i = \frac{x_i}{\sqrt{P^2 - a^2}}. \qquad (2.76)$$

This analytical expression holds only for the case that the center of the sphere is on the symmetry axis of the "ring" (Papadopoulos and Kuo (1990) discuss the case as a model of colloid–pore interaction but do not provide any analytical expression for the potential energy). Eq. (2.75) is valid even for negative values of x_1, this is, when the sphere is inside the ring. The van der Waals interaction energy of a sphere and the cylinder "missing" from the "ring" is then

$$V_{cylinder}(x_1, x_2) = V_{flat}(x_1) - V_{flat}(x_2) - V_{ring}(x_1, x_2). \qquad (2.77)$$

The surface-tension energy of the film may be easily computed by numerical integration in ρ.

The binding energy of the liquid, V_b, will be computed with respect to the binding energy of the hypothetical case in which the liquid has a planar liquid–air interface and fills the hole completely (which is not the equilibrium situation). In fact, it will be minus the binding energy of the liquid that would abandon the vicinity of the hole if the starting point were a planar liquid–air interface corresponding to the $z = 0$ plane (see Figure 2.14). The binding energy integration may be done numerically, using the piecewise approximation for the liquid–substrate potential energy, eq. (2.73)

Using the procedure that has just been described, it is possible to compute the force gradient felt by the tip when it is held at a certain height above the liquid, at the symmetry axis of the hole, by performing three different calculations of the total potential energy at three different heights and by using a parabolic approximation to the second derivative of the total potential energy with respect to tip height.

The force gradient felt by the tip when it is held above the planar areas of the surface (step 4 in pag. 36) is easier to compute: the contribution of the bump to the surface-tension energy, and binding and tip–liquid interaction energies is computed numerically, and the contribution of the rest of the liquid film and the substrate may be easily computed using suitable combinations of the formula for the sphere in front of a "flat" (a semi-infinite body limited by a plane), eq. (2.74). The potential energy corresponding to a "layer" or "slab" of material limited by two horizontal planes is the difference between the "flat"-type potential energy for the upper plane and the "flat"-type potential energy for the lower plane. The results obtained in this way show that different film thicknesses yield different force gradients at a given distance R, and that most of the diference is due to the difference in bump size, rather than to the different thickness of the medium with smaller Hamaker constant, that is to say, the liquid.

Table 2.3. Computed differences in tip–unperturbed surface distances at the center of the hole (d_{hole}) and outside it (d_{plane}), for different film thicknesses h, using a given force gradient for the scan. The "error" is the difference $d_{hole} - d_{plane}$, relative to the unperturbed depression at the center of the hole, $-u_0(0)$. All quantities, except the error, are given in atomic units.

h	Force grad.	d_{plane}	d_{hole}	$-u_0(0)$	Error
425	$-1.3\cdot10^{-5}$	189	196	240	3%
300	$-1.0\cdot10^{-5}$	189	201	520	2%
200	$-9.0\cdot10^{-5}$	191	215	1470	2%

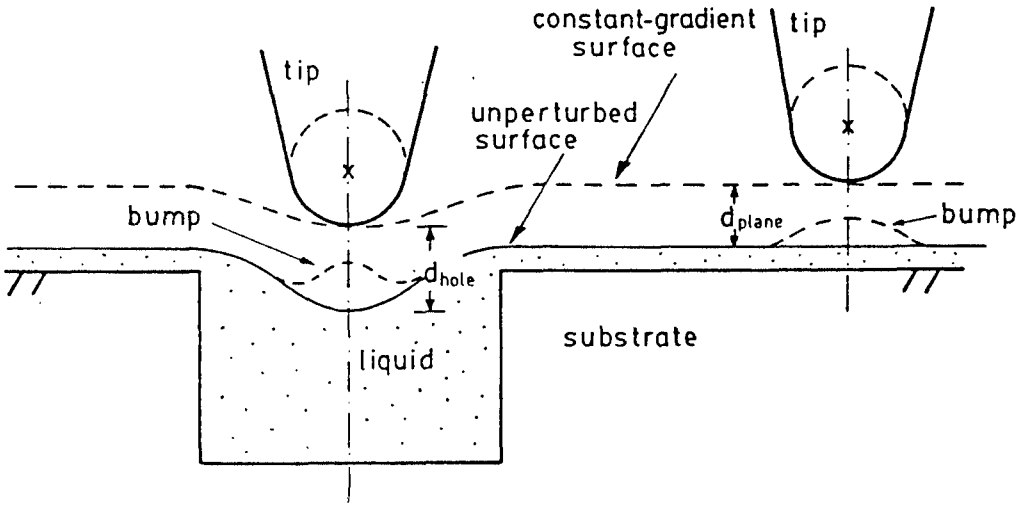

Figure 2.15. The distance between the tip and the original liquid–air interface in a constant-force-gradient AFM run.

Table 2.3 shows some results for the force gradient. For a given film thickness and a given force gradient (see Figure 2.15) the distance between the surface of the tip and what would be the unperturbed surface of the liquid, $d = R - a - u_0(0)$, is computed for two different situations: when the tip is over an area of the sample far away from the holes (d_{plane}), and when the tip is at the symmetry axis of the cylindrical hole (d_{hole}). If these two distances were equal, the constant-force-gradient scan would give the correct depth of the depression at the center of the hole, since the vertical distance travelled by the tip would be exactly the depth of the depression.

The interpretation of the difference between d_{hole} and d_{plane} is the following: in a constant-force-gradient experiment, when the tip scans the center of the hole, it does not fly exactly at the distance d_{plane} at which it flies above the planar areas of the sample, but a little bit higher (d_{hole}). This is mainly because the bump induced by the tip on the liquid surface is higher inside the hole. However, the results show that the difference in tip–surface distance is negligible compared to the depression at the center of the hole, so the difference in absolute tip height R is very similar to the depth of the depression.

In this way, these calculations give an indication of the usefulness of atomic-force microscopy to obtain topographical images of liquid–air interfaces. Furthermore, the model is ready to be applied in other circumstances of interest, which may correspond to different values of the participating parameters (hole size, material constants, etc.).

The hole-filling calculation in the absence of the tip provides, in addition, a detailed model for the physisorption of gases in substrate pores. A related work for an oblique corner in a substrate has recently been published (Cheng and Cole 1990).

Chapter 3

Linear dynamics of the interaction of a particle with the surface of an ideal liquid

3.1 Description of the physical situation

In this chapter, I will analyse the dynamical response of a system such as the one described in Chapter 1, this is, a laterally infinite, bound liquid body, when a particle, external to the liquid, and acting on it, is in motion (see Figure 3.1). The liquid will be set in motion by the particle: each volume element of the liquid will experience, in addition to the force due to the binding field, a time-dependent force due to the particle. The study of the response of the liquid is necessary to describe processes of energy transfer between the particle and the liquid. The response will be modelled by a generalized linear response function, relating the particle–liquid interaction energy at the surface and the amplitude of the surface waves excited by this interaction. The liquid will be a laterally infinite body of liquid of constant depth h, which may be taken to be infinity to include the limiting case of a semi-infinite liquid.

This chapter will only deal with small perturbations of the liquid. This allows the use linear approximations which are very closely related to the ones that were used in section 2.3, to solve the equation of motion of the ideal fluid (Euler's equation), from which the response function of the liquid surface will be derived. The general response function will be applied to various dynamical particle–liquid systems. Some of these systems are related to previous theoretical work (stopping of electrons flying parallel to the surface of a semi-infinite liquid bound by gravity: Gras-Martí and Ritchie, 1985) or to experimental situations (excitation of ripples on the surface of a lubricant film by a tip during atomic-force microscopy analysis: Mate, Lorenz and Novotny 1989). This chapter will only deal with ideal liquids, when the effects of viscosity may be neglected. This approximation will also help to set bounds to the behaviour of viscous liquids, which will be studied with more detail in Chapter 4.

3.2 The motion of the perturbed liquid

In this section, the approximations that linearize the dynamics of the particle–liquid system will be described, and Euler's equation (the equation of motion for ideal liquids) will be solved

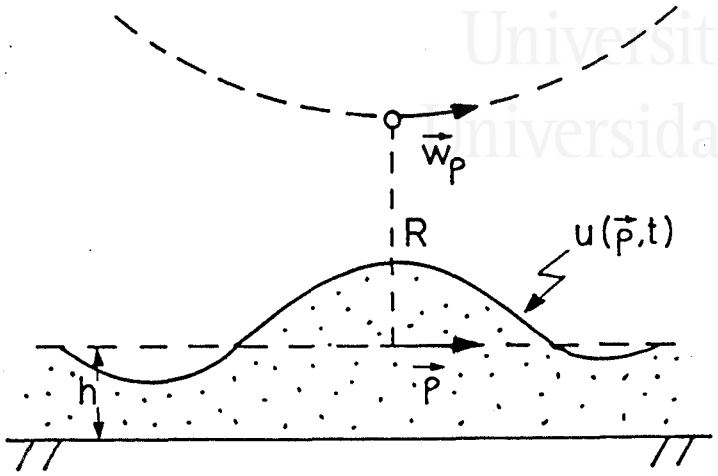

Figure 3.1. Sketch of the dynamical system described in this chapter.

in order to obtain the dispersion relation of the surface waves and the response function of the liquid surface.

3.2.1 Description of the approximations

Approximations used in the static case

To make a linear treatment of the system possible, it is necessary to make some approximations regarding the magnitude of the perturbation induced by the moving particle. Some of them were already introduced in section 2.3. Here, they will be adapted to the dynamical treatment, where Cartesian coordinates will be used for convenience.

Let $\vec{X}$ represent the position of the particle, (x_p, y_p, R). Surface displacements $u(\vec{\rho})$ will be assumed to be small compared with the particle–surface distance, R, as in eq. (2.16):

$$u(\vec{\rho}) \ll R. \tag{3.1}$$

In addition, the surface will be assumed to be very smooth (displacements will be small compared to typical wavelengths), as in eq. (2.17):

$$(\nabla u(\rho))^2 \ll 1. \tag{3.2}$$

For sufficiently small displacements, the linearization of the binding potential in the vicinity of the reference plane, eq. (2.18), holds true.

In addition to the linearizing approximations, the binding potential will be taken to independent of $\vec{\rho}$, the vector that defines the horizontal position of a liquid element: $\vec{\rho} = (x, y)$. This happens when the liquid is bound by gravity or by attraction towards a planar substrate, and is equivalent to approximation (2.15) in section 2.3:

$$v_b(z, \vec{\rho}) = v_b(z). \tag{3.3}$$

With this assumption, the response of the liquid to an external perturbation is translationally invariant with respect to $\vec{\rho}$.

These approximations will be used to obtain simple forms of the binding and interaction potentials, as well as to simplify the inclusion of surface tension.

Approximations that linearize Euler's equation

Euler's equation, the equation of motion for ideal liquids, may be written, in the case of an incompressible liquid (Landau and Lifshitz 1987:3, Feynman 1964:I-40-4), as

$$\rho_0 \left(\frac{\partial \vec{w}}{\partial t} + (\vec{w} \cdot \nabla)\vec{w} \right) = -\nabla p - \nabla v_{int} - \nabla v_b, \tag{3.4}$$

where $\vec{w}$ is the velocity of the liquid at a given position in space, ρ_0 its density, and p is the pressure at that position. The presence of a nonlinear term, $(\vec{w} \cdot \nabla)\vec{w}$, is evident. In addition to the approximations that have just been described to linearize the potentials, Euler's equation itself can be linearized. In the cases in which I am interested, there is room for an approximation that neglects this nonlinear term as compared to $\partial \vec{w}/\partial t$. Suppose that the flow in the liquid is an oscillatory one, and A is the amplitude of the motion, τ its period and λ its wavelength. In this case, $\partial \vec{w}/\partial t$ is of the order of A/τ^2, and $(\vec{w}\cdot\nabla)\vec{w}$ is of the order of $(A/\tau)^2/\lambda$. The approximation considered here is therefore equivalent to having waves whose length λ is large compared to their amplitude A (see Landau and Lifshitz 1987:31, 16). This is consistent with the approximation (3.2), for the surface waves. With this approximation, the equation of motion may be written as

$$\rho_0 \frac{\partial \vec{w}}{\partial t} = -\nabla p - \nabla v_{int} - \nabla v_b. \tag{3.5}$$

The liquid is assumed to be incompressible, and so, the equation of continuity (or mass balance) may be written (Landau and Lifshitz 1987:17) as

$$\nabla \vec{w} = 0. \tag{3.6}$$

The motion of a liquid executing small oscillations (such that $(\vec{w} \cdot \nabla)\vec{w} \ll \partial \vec{w}/\partial t$), may be assumed to be irrotational (Landau and Lifshitz 1987:16):

$$\nabla \times \vec{w} = 0. \tag{3.7}$$

This last property of the flow allows to define a *velocity potential* Φ such that

$$\vec{w} = \nabla \Phi, \tag{3.8}$$

and the linearized equation of motion may be rewritten as

$$\rho_0 \frac{\partial \Phi}{\partial t} = -(p + v_{int} + v_b). \tag{3.9}$$

3.2.2 Solution of Euler's equation at the surface: the response function

Euler's equation at the surface

Now, the approximations given above will be used to derive a response function of the liquid surface. The balance of normal forces at a surface for which approximation (3.2) holds may be written as (Landau and Lifshitz 1987:239)

$$p_0 - p = \sigma \left(\frac{\partial^2 u}{\partial x^2} + \frac{\partial^2 u}{\partial y^2} \right), \tag{3.10}$$

where p_0 is the external pressure and p the internal one. Now, consider the linearized form of the binding potential energy, eq. (2.18). According to the approximation given in eq. (3.1), the interaction potential at the surface does not depend on z; furthermore, its dependence of the position of the particle may be embedded into a time dependence:

$$v_{int} = v_{int}(\vec{\rho}, t). \tag{3.11}$$

With these approximations referring to p, v_b and v_{int}, eq. (3.9) may be rewritten *at the surface* as:

$$\rho_0 \frac{\partial \Phi}{\partial t} = \sigma \left(\frac{\partial^2 u}{\partial x^2} + \frac{\partial^2 u}{\partial y^2} \right) - Gu - v_{int}(\rho, t), \tag{3.12}$$

where Φ has been redefined by adding to it the coordinate-independent term $(p_0 + v_b(0))t/\rho_0$. Then, if the equality $\partial u/\partial t = \partial \Phi/\partial z$ is used, and the time derivative of eq. (3.12) is taken, the equation of motion for the surface reads:

$$\rho_0 \frac{\partial^2 \Phi}{\partial t^2} = \sigma \frac{\partial}{\partial z} \left(\frac{\partial^2 \Phi}{\partial x^2} + \frac{\partial^2 \Phi}{\partial y^2} \right) - G \frac{\partial \Phi}{\partial z} - \frac{\partial v_{int}(\rho, t)}{\partial t}. \tag{3.13}$$

Dispersion relation

To solve the equation of motion of the surface, the Fourier transform technique is used. Fourier transforms will be used extensively in this and the following chapter, and the notation that will be used is introduced here. Let H be a function that depends on $\vec{\rho}$, t, and other variables, $H(\vec{\rho}, t, \cdots)$. The two transforms of H that will be used are:

$$H_{\vec{k}}(t, \cdots) = \frac{1}{2\pi} \int d^2\vec{\rho}\, e^{-i\vec{k}\cdot\vec{\rho}}\, H(\vec{\rho}, t, \cdots) \tag{3.14}$$

and

$$H_{\vec{k},\omega}(\cdots) = \frac{1}{(2\pi)^{1/2}} \int_{-\infty}^{\infty} dt\, e^{i\omega t}\, H_{\vec{k}}(t, \cdots). \tag{3.15}$$

The 2π's are thus symmetrically distributed between the direct and the inverse transforms.

First, one needs to solve for the z dependence of Φ. The continuity equation, (3.6), may be rewritten in terms of the velocity potential as

$$\nabla^2 \Phi = 0, \tag{3.16}$$

which, in Fourier components, is

$$\frac{\partial^2 \Phi_{\vec{k},\omega}(z)}{\partial z^2} = k^2 \Phi_{\vec{k},\omega}(z). \tag{3.17}$$

From this equation, and the condition that the z component of the velocity is zero at the bottom of the liquid, $z = -h$ (for example, at the liquid–substrate boundary), one gets

$$\Phi_{\vec{k},\omega}(z) = \tilde{\Phi}_{\vec{k},\omega} \cosh[k(z+h)]. \tag{3.18}$$

By substituting the Fourier expansions for Φ and v_{int} into eq. (3.13), a relation for the flow of the liquid as a response to the external potential v_{int} is obtained:

$$\tilde{\Phi}_{\vec{k},\omega} = \frac{1}{\omega_k^2 - \omega^2 - 2i\omega\gamma_k} \frac{i\omega v^{int}_{\vec{k},\omega}}{\rho_0 \cosh(kh)}. \tag{3.19}$$

In this equation, the resonant frequencies of a mode of wavenumber k, $\pm\omega_k$, are defined by

$$\omega_k^2 = \frac{1}{\rho_0}\left(\sigma k^3 + Gk\right)\tanh(kh), \tag{3.20}$$

the *dispersion relation* of the surface waves (which are called *ripples* or *ripple* waves): the oscillation frequencies of mode $\vec{k}$ in the absence of the external perturbation v_{int} are $\pm\omega_k$. It is interesting to note here that, for this dispersion relation, there is always a minimum phase velocity $w_{min} = \min(\omega_k/k)$ for a certain $k = k_{min}$. In eq. (3.19), an infinitesimal damping $-i\gamma_k$ (with $\gamma_k > 0$) has been added to the resonant frequencies $\pm\omega_k$ to ensure that the response of the liquid is retarded and causality is preserved.

The response function of the liquid surface

Taking into account that, at the surface (using $u \simeq 0$),

$$\frac{\partial}{\partial t}u(\rho,t) = \frac{\partial}{\partial z}\Phi(\rho,0,t), \tag{3.21}$$

and expanding the instantaneous surface shape $u(\rho,t)$ in Fourier components $u_{\vec{k},\omega}$, eq. (3.19) may be written as a *response equation* that gives the amplitude of surface waves as a function of the perturbation:

$$u_{\vec{k},\omega} = R^0_{k,\omega} v^{int}_{\vec{k},\omega}, \tag{3.22}$$

where

$$R^0_{k,\omega} = -\frac{1}{\rho_0}\frac{k\tanh(kh)}{\omega_k^2 - \omega^2 - 2i\omega\gamma_k} \tag{3.23}$$

is the *response function* of the ideal liquid. This function will be used in the following sections to describe the response of the surface of an ideal liquid body to the perturbations induced by a particle that is in motion outside it.

3.3 Response of the ideal-liquid surface to external perturbations

3.3.1 Case 1: A particle executing small oscillations along the z axis

The potential generated by a particle situated at a height R on the surface, when surface displacements are small compared to this height, eq. (3.1), is, according to (2.5):

$$v_{int}(R,\rho) = \frac{-B}{(\rho^2 + R^2 - a^2)^m}. \tag{3.24}$$

Now, suppose that the particle is oscillating along the z axis with a frequency W,

$$R = R_0 + C\cos(Wt), \tag{3.25}$$

where R is the instantaneous height, C is the amplitude of the motion, and R_0 is the average height of the particle. One has, then, for $C \ll R_0$,

$$v_{int}(R,\rho) \simeq v_{int}(R_0,\rho) + \left.\frac{\partial v_{int}(R,\rho)}{\partial R}\right|_{R_0} C\cos(Wt). \tag{3.26}$$

The first (static) term will give rise to a bump on the surface (exactly the one calculated and discussed in Chapter 2, eq. (2.26)), whereas the second (oscillatory) term will cause the liquid surface to oscillate around this bump. The application of the linear response formalism discussed in the previous section requires the Fourier transform of the interaction potential (which, due to cylindrical symmetry, depends only on the modulus of $\vec{k}$):

$$v^{int}_{k,\omega} = v^{int,sta}_{k,\omega} + v^{int,osc}_{k,\omega}, \tag{3.27}$$

where

$$v^{int,sta}_{k,\omega} = (2\pi)^{1/2}\delta(\omega)\frac{-B}{(m-1)!}\left(\frac{k}{2\tilde{R}_0}\right)^{m-1} K_{m-1}(k\tilde{R}_0), \tag{3.28}$$

and

$$v^{int,osc}_{k,\omega} = (2\pi)^{1/2}\left[\delta(\omega - W) + \delta(\omega + W)\right]\frac{BCR_0}{(m-1)!}\left(\frac{k}{2\tilde{R}_0}\right)^{m} K_m(k\tilde{R}_0), \tag{3.29}$$

with $\tilde{R}_0^2 = R_0^2 - a^2$ and δ the Dirac delta.

Now, the response of an ideal liquid body of depth h will be considered. The response equation is given by eq. (3.22) and (3.23). There, all $\vec{k}$'s may be substituted by k's due to the symmetry of the system. Transforming back to ρ, t, one gets a sum of two components of the perturbation. The static one, as expected, is just the linearized static bump that has been computed in the statics part of this work (see eq. (2.26)),

$$u^{sta}(\rho) = \frac{B}{\sigma(m-1)!}\left(\frac{1}{2\tilde{R}_0^2}\right)^{m-1}\int_0^\infty ds\, s^m \frac{J_0(s\rho/\tilde{R}_0)K_{m-1}(s)}{s^2 + 2\tilde{R}_0^2/\xi^2}, \tag{3.30}$$

whereas the dynamic part may be written (taking $\gamma_k \to 0$, and using $\lim_{\epsilon\to 0+}(x+i\epsilon)^{-1} = \mathrm{PV}(x^{-1}) - i\pi\delta(x)$, where PV denotes a principal-value integration) in the following way:

$$u^{osc}(\rho,t) = U(\rho)\cos(Wt + \phi(\rho)), \tag{3.31}$$

i.e., as an oscillation whose amplitude is

$$U(\rho) = \frac{2BCR_0}{(m-1)!\rho_0}\left(\frac{1}{2\tilde{R}_0}\right)^m \sqrt{I_c^2(\rho) + I_s^2(\rho)}, \tag{3.32}$$

where

$$I_c(\rho) = \int_0^\infty dk\, k^{m+2} J_0(k\rho) K_m(k\tilde{R}_0)\tanh(kh)\,\mathrm{PV}\left(\frac{1}{W^2 - \omega_k^2}\right) \tag{3.33}$$

and

$$I_s(\rho) = k_W^{m+2} J_0(k_W\rho) K_m(k_W\tilde{R}_0)\frac{\pi}{2D(k_W)}, \tag{3.34}$$

where k_W is the value of k that satisfies $\omega_k = W$ and

$$D(k) = \frac{d}{dk}\omega_k^2. \tag{3.35}$$

The oscillation of the liquid is out of phase with respect to the particle by an angle

$$\phi(\rho) = \arctan\left(\frac{I_s(\rho)}{I_c(\rho)}\right). \tag{3.36}$$

This angle is always smaller than $-\pi$ at $\rho = 0$: in the case $\phi(0) = -\pi$ the liquid follows the particle exactly in opposition. This is because the interaction potential is attractive: if the particle approaches the liquid, its surface rises; if the particle moves away from the liquid, its surface lowers.

An interesting limiting behaviour occurs when the oscillation frequency approaches zero. In this case, $I_s(\rho)$ is very small, and it may be shown that

$$\lim_{W\to 0} U(\rho) = C\frac{\partial u^{sta}(\rho)}{\partial R_0}. \tag{3.37}$$

The phase at the origin, $\phi(0)$, is then $-\pi$: the liquid surface is following, in opposition exactly, the motion of the particle.

For slightly higher frequencies, the liquid will lag behind by a certain phase, slightly smaller than $-\pi$. As the frequency increases, the amplitudes will get smaller and the phase will go from $-\pi$ to -2π (the high-frequency limit), where the amplitude will tend to zero.

Calculations have been performed where a metal sphere (a model of an AFM tip, see section 2.6) is forced to oscillate over liquid helium films of different thicknesses. For this case, $m = 3$, a is the radius of the sphere, and $B = 4a^3A_{int}/3\pi$ (see eq. (2.65)). The Hamaker constant for the metal–liquid helium interaction ($A = 3.8 \cdot 10^{-3}$ a.u.) was estimated from the surface tension of liquid helium and a typical metal–metal Hamaker constant using an approach that has already been described in Section 2.6. The radius of the metal sphere is 4200 a.u. in the calculations. The same Hamaker constant was used to model the adhesion of the liquid film to the solid substrate: The corresponding value of G is $A_b/2\pi h^4$, where h is the thickness of the film.

The principal value integration was performed by subtracting from the integrand a function having a pole of the same strength (residue) at k_W, but of zero integral. This yielded a regular function that was integrated numerically.

The values of $U(0)/C$ (the ratio of the amplitude of the liquid oscillation at $\rho = 0$ to the amplitude of the oscillation of the tip) and $\phi(0)$ were computed for different frequencies, for three different film thicknesses. Figure 3.2 shows the amplitude ratios, and Figure 3.3 shows the phase at the origin, both as a function of frequency. Frequencies are in atomic units (1 a.u. $= 4.13 \cdot 10^{16}$ s^{-1}). A typical AFM tip oscillation frequency would be 10^5 s^{-1} $\sim 2 \cdot 10^{-12}$ atomic units. Figures 3.2 and 3.3 show that, for small frequencies, the ratio $U(0)/C$ is rather constant and the phase angle is close to $-\pi$. The tip was held at $R = 4500$ a.u., this is, at a separation $d = R - a = 300$ Å from the originally unperturbed surface. An interesting result is the presence, in the amplitude ratio, of a small maximum (shoulder) before the amplitude starts to decrease as at higher frequencies. The shoulder appears at increasing frequencies for decreasing film thicknesses. In fact, it is easy to show that the maximum occurs at a frequency W such that the corresponding wavevector k_W scales as the inverse capillary constant for the

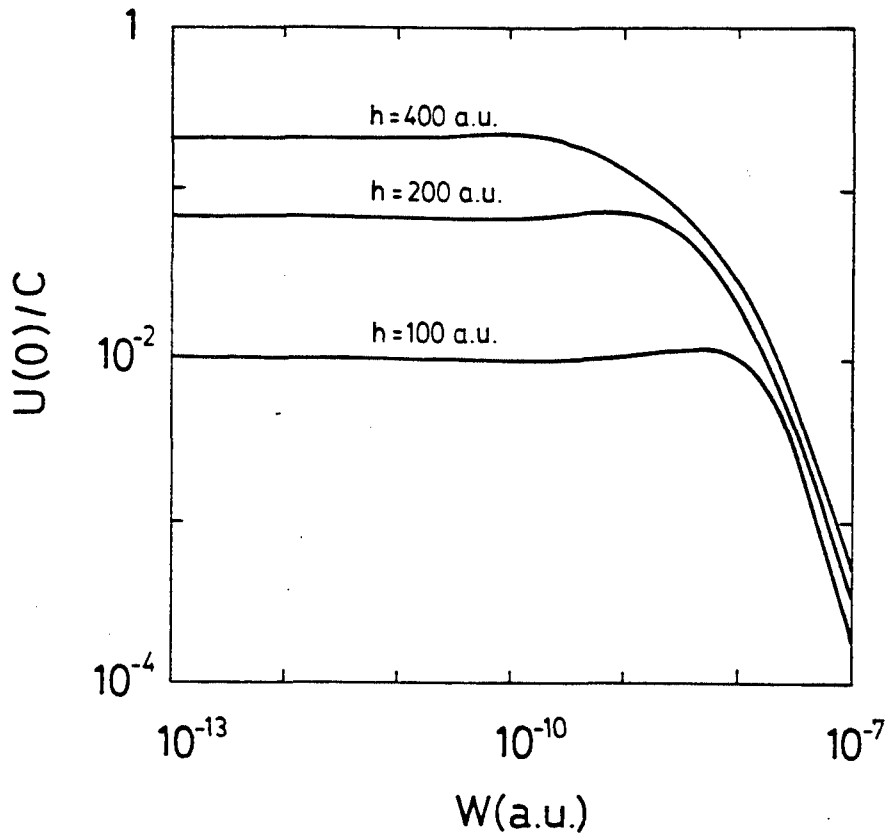

Figure 3.2. Ratio of oscillation amplitudes (liquid/particle) at the origin, $U(0)/C$, versus tip oscillation frequency W, for liquid helium films of different thicknesses h on a metal substrate (for $R = 4500$ a.u., $a = 4200$ a.u.).

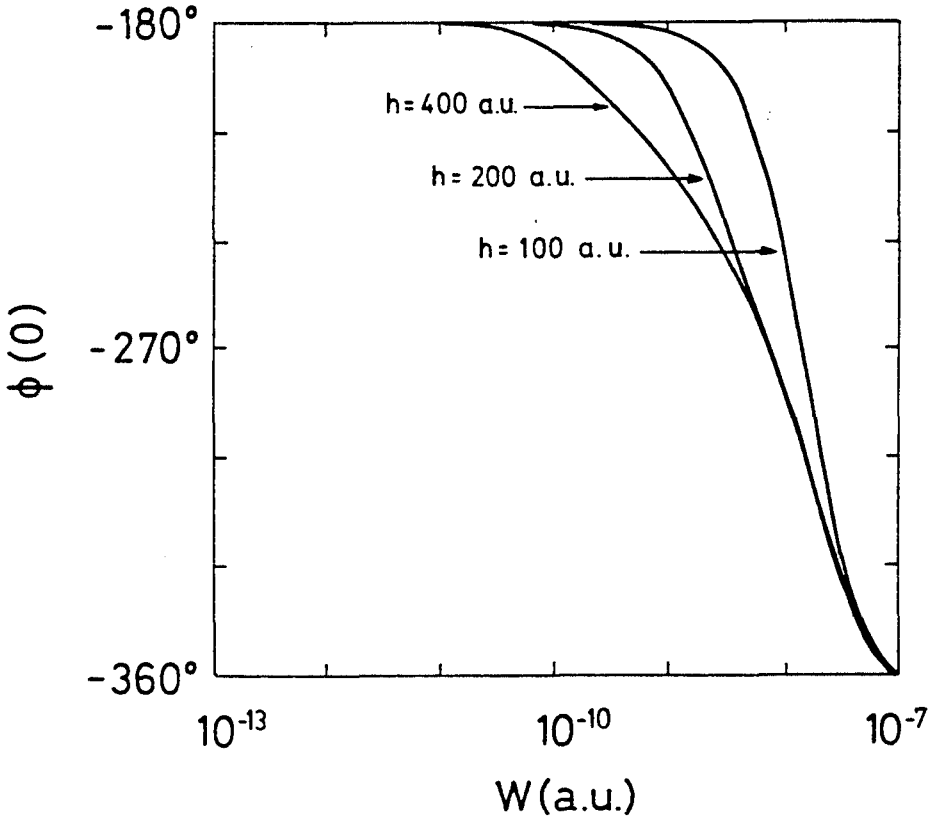

Figure 3.3. Phase of the oscillation of the liquid at the origin $\phi(0)$ (degrees), versus tip oscillation frequency W for liquid helium films of different thicknesses h on a metal substrate (for $R = 4500$ a.u., $a = 4200$ a.u.).

film, ξ^{-1} (for these films, $\xi = 2h^2\sqrt{\pi\sigma/A_b}$). The capillary constant is related to the lateral size (width) of the bump on the liquid surface. The shoulder is then the result of a size effect: ripples whose wavelength matches the width of the bump are excited more easily.

It is also interesting to note the small amplitude of the oscillations that a tip may induce on a liquid film of this nature, even at relatively short distances. This has important implications for the atomic force microscopy of liquid films. The films studied by Mate et al. (1989) consist of a very viscous fluid, a perfluoropolyether (PFPE). The amplitude of the oscillation at the operating frequency W and distance R of the experiment has been computed in the way that has been described in the preceding paragraphs, assuming an ideal behaviour for the ripple waves. At a frequency of 150 s^{-1} (a value that corresponds to the low-frequency limit) and a tip–liquid separation $R - a$ of 106 Å (R = 4400 a.u, a = 4200 a.u.), the results are the following: for a thickness of 100 a.u., the amplitude ratio $U(0)/C$ is 0.026 and the height of the tip-induced bump is 3.3 a.u.; for 200 a.u., the ratio is 0.086 and the height, 7.4 a.u.; and for 400 a.u., the ratio is 0.17 and the height, 15 a.u.. These results for the amplitude ratio overestimate the result that would have been obtained if the viscosity of the liquid had been taken into account (the response of viscous liquids will be studied in Chapter 4). According to the results in the present subsection, and for a typical tip oscillation amplitude of 1 Å, the oscillation amplitudes of the liquid would have subatomic dimensions and be very small compared to bump heights. A conclusion that may be drawn from these results is that the effect of the excitation of ripples by the AFM tip may be neglected in the constant-force-gradient experiments performed by Mate et al. (1989).

3.3.2 Case 2: Stopping of a particle flying parallel to the surface of an ideal liquid

When a particle is moving external to the surface of an ideal liquid, it may transfer some of its energy to the liquid via excitation of ripples. In this section, classical dynamics will be used to compute the energy loss per unit path of a particle that flies parallel to the surface of the liquid. The results will be then applied to the case of an electron flying over a semi-infinite non-polar liquid. This case was studied, using a quantum formalism, by Gras-Martí and Ritchie (1985): the ripples were quantized as bosons and many-body techniques were used to calculate the energy loss. As will be shown, their results may be obtained with the classical formalism developed here.

To obtain the energy loss of the particle per unit path, the force on the particle, due to the *wake* induced by the particle on the liquid surface, will be computed. The energy loss per unit path will then be

$$-\frac{dE}{ds} = -\frac{1}{w_p}\vec{w}_p \cdot \vec{F}^{\parallel}, \tag{3.38}$$

where $\vec{w}_p = (w_p^x, w_p^y, 0)$ is the (constant) velocity of the particle (see figure (3.1), and $\vec{F}^{\parallel} = (F_x, F_y, 0)$ is the component of the force on the particle, parallel to the reference plane, due to the excitation of the surface. To compute the force on the particle the contribution of each volume element of the liquid, $\vec{f}^{\parallel}$ has to be obtained first. For this, one has to differentiate v_{int}, the potential energy of interaction between the particle and a unit volume of the liquid wake, eq. (3.24),

$$v_{int}(\vec{\rho}, t) = \frac{-B}{\left[(\vec{\rho} - \vec{\rho}_p)^2 + \tilde{R}^2\right]^m} \tag{3.39}$$

where $\vec{\rho}_p = \vec{w}_p t$ and $\tilde{R} = \sqrt{R^2 - a^2}$ define the instantaneous position of the particle in motion. The force on the particle due to a unit volume of liquid is then

$$\vec{f}^{\parallel}(\vec{\rho}, t) = -\left(\vec{e}_x \frac{\partial}{\partial x_p} + \vec{e}_y \frac{\partial}{\partial y_p}\right) v_{int}(\vec{\rho}, t) \tag{3.40}$$

where $\vec{e}_x$ and $\vec{e}_y$ are unit vectors along the coordinate axes, or

$$\vec{f}^{\parallel}(\vec{\rho}, t) = \left(\vec{e}_x \frac{\partial}{\partial x} + \vec{e}_y \frac{\partial}{\partial y}\right) v_{int}(\vec{\rho}, t). \tag{3.41}$$

The total parallel force on the particle, due to the wake, may be written as

$$\vec{F}^{\parallel} = \int d^2\vec{\rho}\, \vec{f}^{\parallel}(\vec{\rho}, t)\, u(\vec{\rho}, t), \tag{3.42}$$

or, using eq. (3.41), and changing to Fourier space,

$$\vec{F}^{\parallel} = \int d^2\vec{k}\, i\vec{k}\, v_{\vec{k}}^{int}(t)\, u_{-\vec{k}}(t), \tag{3.43}$$

where $v_{\vec{k}}^{int}(t)$ may be easily computed from eq. (3.39) to give

$$v_{\vec{k}}^{int}(t) = \tilde{v}_k e^{-i\vec{k}\cdot\vec{w}_p t} \tag{3.44}$$

with

$$\tilde{v}_k = \frac{-B}{(m-1)!}\left(\frac{k}{2\tilde{R}}\right)^{m-1} K_{m-1}(k\tilde{R}). \tag{3.45}$$

On the other hand, the Fourier transform of the surface displacement is related to the Fourier transform of the interaction potential through the response equation (3.22). To compute the force on the particle, eq. (3.43), one only has to obtain the $\vec{k}$-Fourier transform of the surface displacement, which may be easily computed from the response equation:

$$u_{\vec{k}}(t) = R^0_{k,\vec{k}\cdot\vec{w}_p}\, \tilde{v}_k\, e^{-i\vec{k}\cdot\vec{w}_p}, \tag{3.46}$$

and substitute it, together with eq. (3.44), into eq. (3.43). Further substitution of this result for $\vec{F}^{\parallel}$ into eq. (3.38) yields

$$-\frac{dE}{ds} = \frac{i}{w_p}\int d^2\vec{k}\,(\vec{k}\cdot\vec{w}_p)\,\tilde{v}_k^2\, R^0_{k,\vec{k}\cdot\vec{w}_p}. \tag{3.47}$$

The response function $R^0_{k,\omega}$, eq. (3.23), for the ideal liquid surface contains the positive infinitesimal γ_k. In the limit $\gamma_k \to 0$ it may be written as

$$R^0_{k,\omega} = \frac{k}{\rho_0}\left[\mathrm{PV}\left(\frac{1}{\omega^2 - \omega_k^2}\right) - i\pi[\delta(\omega - \omega_k) + \delta(\omega + \omega_k)].\right] \tag{3.48}$$

When substituting this response function in eq. (3.47), the principal part vanishes due to the symmetry of the integrand. After transforming to polar coordinates, azimuthal integration (ϕ) yields the following general formula for the energy loss:

$$-\frac{dE}{ds} = \frac{2\pi}{\rho_0 (w_p)^2}\int_0^\infty dk\, k\, \tanh(kh)\, \tilde{v}_k^2\, \frac{\Theta\left(1 - (\frac{w_k}{kw_p})^2\right)}{\sqrt{1 - (\frac{w_k}{kw_p})^2}}, \tag{3.49}$$

where $\Theta(x)$ is the Heaviside step function. It is interesting to note here that, in the case that the velocity of the particle is less than the minimum phase velocity of the surface waves, w_{min}, the energy loss will be zero: the particle does not transfer any of its energy to the liquid.

Another interesting feature of the dependence of the energy loss on the velocity of the particle is the fact that, at $w_p = w_{min}$, there is a discontinuity in the energy loss. The value of dE/ds to the right of that point may be computed by taking the limit,

$$\lim_{w_p \to w_{min}^+} \left(-\frac{dE}{ds}\right) = \frac{2\pi}{\rho_0 w_{min}^2} k_{min} \tanh(k_{min}h) \tilde{v}_{k_{min}}^2 I, \tag{3.50}$$

where

$$I = \lim_{w_p \to w_{min}^+} \int_{k^{(-)}}^{k^{(+)}} \frac{dk}{\sqrt{1 - (\frac{\omega_k}{k w_p})^2}} \tag{3.51}$$

and $k^{(-)}$ and $k^{(+)}$ (with $k^{(-)} < k^{(+)}$) are the solutions of $w_p = \omega_k/k$. Expanding, for w_p approaching w_{min}, ω_k/k around the minimum,

$$\frac{\omega_k}{k} = w_{min} + \beta(k - k_{min})^2, \tag{3.52}$$

with

$$\beta = \frac{1}{2}\frac{d^2}{dk^2}\frac{\omega_k}{k}\bigg|_{k=k_{min}}, \tag{3.53}$$

the integral, eq. (3.51), reduces to

$$I = \sqrt{\frac{w_{min}}{2\beta}} \int_{k^{(-)}}^{k^{(+)}} \frac{dk}{\sqrt{(k^{(+)} - k)(k - k^{(-)})}}, \tag{3.54}$$

where the integral is independent of the limits and has the value π. The energy loss at the threshold is then

$$\lim_{w_p \to w_{min}^+} \left(-\frac{dE}{ds}\right) = \frac{\pi^2}{\rho_0} \sqrt{\frac{2}{\beta w_{min}^3}} k_{min} \tanh(k_{min}h) \tilde{v}_{k_{min}}^2. \tag{3.55}$$

Stopping of a particle that flies parallel to the surface of a semi-infinite liquid bound by gravity

Now, the results of the previous treatment will be applied to the case of a particle that flies parallel to a semi-infinite liquid bound by gravity ($G = nMg = \rho_0 g$). This is a generalization of the case that was studied, using a quantum formalism, by Gras-Martí and Ritchie (1985), namely, the case of a travelling electron.

When the liquid has infinite depth ($h \to \infty$), the dispersion relation simplifies, and so does the energy loss integral: the $\tanh(kh)$ terms are equal to unity. Substituting eq. (3.45) into the general expression for the energy loss, eq. (3.49), one gets

$$-\frac{dE}{ds} = \frac{\pi B^2}{\rho_0 w_p [(m-1)!]^2 2^{2m-3} \tilde{R}^{4m-2}} D_m(b, r_0), \tag{3.56}$$

with

$$D_m(b, r_0) = \int_{x^-}^{x^+} dx\, x^{2m-1} \frac{K_{m-1}^2(x)}{\sqrt{1 - \frac{x}{b}\left[1 + r_0^2/x^2\right]}}, \tag{3.57}$$

where $b = \rho_0 (w_p)^2 \tilde{R}/\sigma$, $r_0^2 = \tilde{R}^2 \rho_0 g/\sigma$ are dimensionless parameters, and

$$x^{(\pm)} = \frac{1}{2}(b \pm \sqrt{b^2 - 4r_0^2}). \tag{3.58}$$

The ratio between the velocity of the particle and the minimal velocity may be expressed in terms of the dimensionless parameters as follows:

$$w_p/w_{min} = \sqrt{\frac{b}{2r_0}}. \tag{3.59}$$

The particular case in which the particle is an electron was studied by Gras-Martí and Ritchie in 1985. In this case, $m = 2$, $a = 0$ ($\tilde{R} = R$), and $B = C = -n\alpha Q^2/2$. Eq. (25) in Gras-Martí and Ritchie (1985) is obtained by neglecting gravity in eq. (3.56). This shows that the classical and the quantum treatments of this problem are equivalent, which confirms the classical nature of the energy loss.

One may define four different regimes of energy loss, depending on the velocity, or the related parameter b:

1. The interval near the threshold where $b > 2r_0$ but they are still comparable;
2. the interval where $b \gg 2r_0$ but $b \ll 1$;
3. the interval where $b \approx 1$; and
4. the interval where $b \gg 1$.

Note that, for liquid helium, $r_0/\tilde{R} \sim 10^{-7}$ a.u., $b/R \sim 10^8 w_p^2$ a.u., and $w_{min} = 4.5 \cdot 10^{-8}$ a.u.

For velocities in interval 1, slightly larger than the threshold velocity, w_{min}, the integral has to be solved numerically: b and r_0 have comparable values and so, the limits depend strongly on the velocity.

For velocities in interval 2, $x^+ \approx b$ and $x^- \approx 0$. In addition, one may use the small-argument approximation for the Bessel function (Olver 1965, eq. (9.6.9))

$$z^j K_j(z) \approx (j-1)!2^{j-1}. \tag{3.60}$$

With these approximations, the dimensionless integral D_j may be evaluated in closed form:

$$D_m = \frac{4}{3}[(m-2)!2^{m-2}]^2 b^2, \tag{3.61}$$

and the expression for the energy loss per unit path is

$$-\frac{dE}{ds} = \frac{2\pi B^2 \rho_0 (w_p)^2}{3\sigma^2 (m-1)^2 \tilde{R}^{4m-4}}. \tag{3.62}$$

This expression shows a simple quadratic dependence on the velocity of the particle.

For velocities in interval 3, the maximum of the energy loss is reached. Due to the fact that neither the square root nor the Bessel function in the integrand of D_m may be easily approximated, an analytical expression is not available for this range of velocities.

And finally, for higher velocities (interval 4), the Bessel function may not be easily approximated, but the square root in the denominator of D_m may be approximated by unity (it will only be different from unity when $u \approx b$, where the Bessel function will be exponentially small, making the integrand vanish altogether). The dimensionless integral D_m (using eq. (11.3.31) in Olver 1965) is then independent of b:

$$D_m = \frac{[(m-1)!2^{m-1}]^2}{2(2m-1)}, \tag{3.63}$$

and the value of the energy loss has the typical high-velocity behaviour (it decreases as w_p^{-2}):

$$-\frac{dE}{ds} = \frac{\pi B^2}{\rho_0 (w_p)^2 (2m-1)\tilde{R}^{4m-2}}. \tag{3.64}$$

This high velocity result may be interpreted in terms of the *impulse* approximation. The momentum P that the particle transfers to an element of liquid is equal to the mutual force F times the time τ during which the force has an appreciable value. The time τ is proportional to a certain distance D related to the range of the force divided by the particle velocity w_p, this is, $\tau = D/w_p$. The liquid element moves, as a consequence of the interaction, but too slowly for the particle to detect it: the velocity of the liquid element is small compared to the particle velocity. This is why the force F does not vary during the time period τ. The total energy transferred to the liquid element is $P^2/2M$ where M is the mass of the liquid element. This explains why, for high velocities, the energy loss has $\rho_0 w_p^2$ in the denominator. The absence of terms referring to surface tension or gravity (shape terms) in the eq. (3.64) arises from the fact that liquid displacements are negligible during the time of interaction.

The low-velocity (increasing) regime (interval 2) and the high-velocity (decreasing) regime (interval 4) may be brought to intersection in order to get an approximate expression for the maximum energy loss and the corresponding velocity. The resulting expressions are:

$$w_{max} \approx \left[\frac{3(m-1)^2}{2(2m-1)}\right]^{1/4} \sqrt{\frac{\sigma}{\rho_0 \tilde{R}}} \tag{3.65}$$

$$-\left(\frac{dE}{ds}\right)_{max} \approx \left[\frac{2}{3(2m-1)(m-1)^2}\right]^{1/2} \frac{\pi B^2}{\sigma \tilde{R}^{4m-3}}. \tag{3.66}$$

The maximum energy loss occurs when the velocity w_p of the particle is of the order of the phase velocity ω_k/k of waves having a wavenumber $k = 1/\tilde{R}$. In other words, the energy transfer from the particle to the liquid is maximum when the waves having a phase velocity around w_p have a wavelength of the order of the (reduced) particle–surface distance.

Figures 3.4 and 3.5 show full numerical integration results for the energy loss per unit path of an electron ($m = 2$, $B = -n\alpha e^2/2$, $a = 0$) and a helium atom ($m = 3$, $B = n\Lambda$, $a = 0$) respectively. The existence of the squared-velocity and inverse-squared-velocity regimes (intervals 2 and 4) discussed in the previous paragraphs is clear from the double logarithmic representation. In these straight-line parts of curves, the analytical approximations hold. The position of the maximum of the energy loss and its value coincides, within much less than

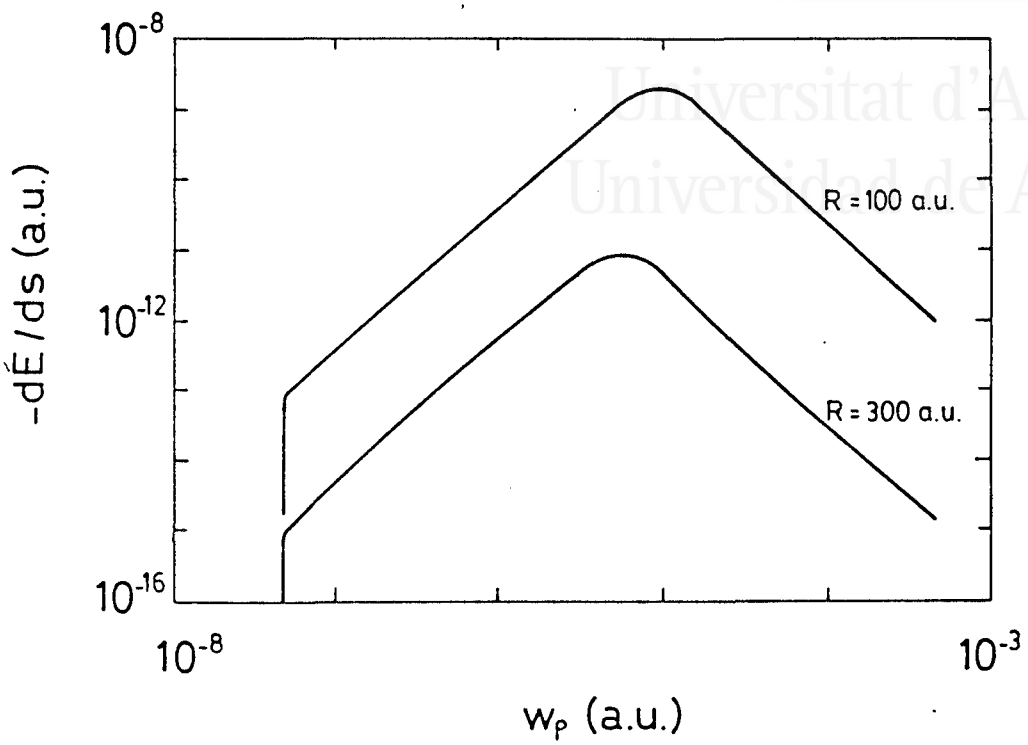

Figure 3.4. Energy loss per unit path of an electron flying parallel to the surface of a semiinfinite body of liquid helium, at two different heights, $R = 100$ and $R = 300$ a.u., as a function of particle velocity.

an order of magnitude, with the analytical approximations, eqs. (3.65) and (3.66). Overall, energy losses are very small. For example, for an electron flying at $R = 100$ a.u. over the surface of liquid helium, w_{max} corresponds to an energy of ≈ 3 meV, and the corresponding $(dE/ds)_{max}$ is $\approx 10^{-4}$ meV/Å.

Volver al índice/Tornar a l'índex

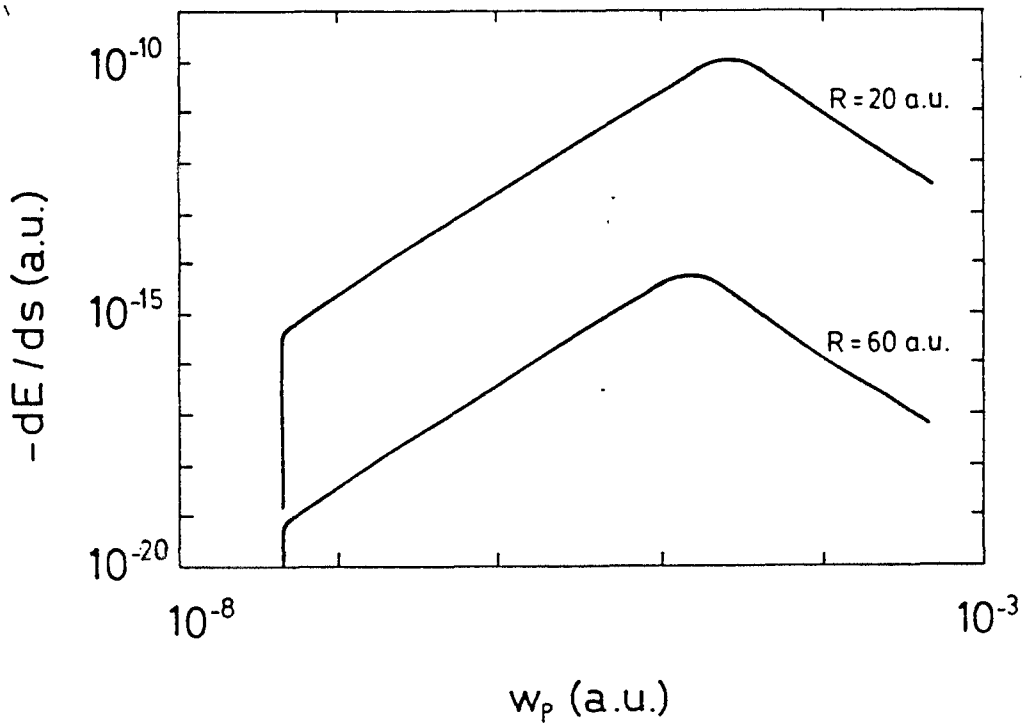

Figure 3.5. Energy loss per unit path of a helium atom flying parallel to the surface of a semiinfinite body of liquid helium, at two different heights, $R = 20$ and $R = 60$ a.u., as a function of particle velocity.

Chapter 4

Linear dynamics of the interaction of a particle with the surface of a semi-infinite viscous liquid

4.1 The response function of the surface

In the previous chapter, the function that describes the response of an ideal liquid to an external perturbation has been obtained. In the study of the dynamics of a real liquid, it is necessary to take into account the effect of the viscosity on the flow of the liquid.

Now, the objective is to study the flow in a semi-infinite, incompressible, viscous liquid subject to an external perturbation. The method of solution used here is based on the one given in Landau and Lifshitz (1987:94). All the linear approximations that were made in section 3.2.1 to obtain the response function of an ideal liquid will also be made here. The equation of motion for viscous liquids, called the Navier-Stokes equation, may be written, in the case of incompressible liquids, as

$$\rho_0 \left(\frac{\partial \vec{w}}{\partial t} + (\vec{w} \cdot \nabla)\vec{w} \right) = -\nabla(p + v_b + v_{int}) + \eta \nabla^2 \vec{w}. \tag{4.1}$$

where η is the dynamical viscosity of the liquid. All the linear approximations that were made in section 3.2.1 to obtain the response function of an ideal liquid will also be made here. Then, taking the curl of both sides of the Navier-Stokes equation (4.1), (which cancels the pressure and potential-energy terms), one gets the equation

$$\frac{\partial}{\partial t}(\nabla \times \vec{w}) = -\nu \nabla^2 (\nabla \times \vec{w}), \tag{4.2}$$

where $\nu = \eta/\rho_0$ is the kinematic viscosity. To solve this equation, the Fourier transform technique will be employed. For the three components of $\vec{w}_{\vec{k},\omega}(z)$, the symbols $w^x_{\vec{k},\omega}(z)$, $w^y_{\vec{k},\omega}(z)$ and $w^z_{\vec{k},\omega}(z)$ will be used.

The equations of motion in Fourier space are then

$$\left(\frac{\partial^2}{\partial z^2} - \mu^2 \right) \left(\frac{\partial w^y_{\vec{k},\omega}}{\partial z} - i k_y w^z_{\vec{k},\omega} \right) = 0, \tag{4.3}$$

$$\left(\frac{\partial^2}{\partial z^2}-\mu^2\right)\left(\frac{\partial w^x_{\vec{k},\omega}}{\partial z}-ik_x w^z_{\vec{k},\omega}\right)=0, \tag{4.4}$$

$$\left(\frac{\partial^2}{\partial z^2}-\mu^2\right)\left(k_y w^x_{\vec{k},\omega}-k_x w^y_{\vec{k},\omega}\right)=0. \tag{4.5}$$

In addition to these equations one has to use the continuity equation, $\nabla\cdot\vec{w}=0$, or

$$ik_x w^x_{\vec{k},\omega}+ik_y w^y_{\vec{k},\omega}-\frac{\partial w^z_{\vec{k},\omega}}{\partial z}=0. \tag{4.6}$$

In eqs. (4.3-4.5),

$$\mu^2=k^2-\frac{i\omega}{\nu}. \tag{4.7}$$

The general solution of this set of equations (4.3-4.6) may be shown to be a superposition of longitudinal (marked $\|$) and transverse (marked $\perp$) waves. Later it will be shown that the transverse solution is cancelled by the application of surface boundary conditions. In the case of the semi-infinite liquid, the first boundary condition, this is, that the waves have to vanish when $z\to-\infty$, may be applied immediately (the semi-infinite liquid occupies the $z<0$ half-space). The longitudinal solution of the Navier-Stokes equation is then

$$w^{x,\|}_{\vec{k},\omega} = k_x\left(Ae^{kz}+Be^{\mu z}\right) \tag{4.8}$$

$$w^{y,\|}_{\vec{k},\omega} = k_y\left(Ae^{kz}+Be^{\mu z}\right) \tag{4.9}$$

$$w^{z,\|}_{\vec{k},\omega} = -ik\left(Ae^{kz}+\frac{k}{\mu}Be^{\mu z}\right) \tag{4.10}$$

and the transverse solution is

$$w^{x,\perp}_{\vec{k},\omega} = -k_y Ee^{\mu z} \tag{4.11}$$

$$w^{y,\perp}_{\vec{k},\omega} = k_x Ee^{\mu z} \tag{4.12}$$

$$w^{z,\perp}_{\vec{k},\omega} = 0 \tag{4.13}$$

where μ has been chosen such that $\mathrm{Re}(\mu)>0$. A, B and E are constants that will be determined by applying the boundary conditions at the surface.

Substituting this general solution into the Navier-Stokes equuation (4.1), the expression for the Fourier transform of the pressure is easily obtained:

$$p_{\vec{k},\omega}=\omega\rho_0 Ae^{kz}-v^{int}_{\vec{k},\omega}-v^{b}_{\vec{k},\omega}. \tag{4.14}$$

It is convenient here to use the linearized form of the binding potential $v_b(z)=v_b(0)+Gz$. Now, to calculate A, B and E, the boundary conditions for a free surface will be applied (Landau and Lifshitz 1987:48), this is,

$$\sum_j \sigma_{ij}n_j=0, \tag{4.15}$$

where

$$\sigma_{ij}=-p\delta_{ij}+\eta\left(\frac{\partial w_i}{\partial x_j}+\frac{\partial w_j}{\partial x_i}\right) \tag{4.16}$$

and n_j is the j-th component of the normal vector at the surface and x_i and x_j may be any of (x, y, z).

In the case considered here, where one may, as an approximation, assume that the surface is parallel to the $z = 0$ plane, the conditions (4.15) may be written as

$$\sigma_{zz} = \sigma_{xz} = \sigma_{yz} = 0 \tag{4.17}$$

at $z = u$. To apply the first boundary condition, $\sigma_{zz} = 0$, one takes the time derivative of this condition, and then substitutes $z = 0$ (since u is a small displacement). One gets

$$\left(\omega^2 - \omega_k^2 + 2i\nu k^2\omega\right) A - \left(\omega_k^2 \frac{k}{\mu} - 2i\nu k^2\omega\right) B = \omega \frac{v^{int}_{\vec{k},\omega}}{\rho_0}, \tag{4.18}$$

where ω_k, given in eq. (3.20), defines the dispersion relation for an *ideal* liquid; here, its value when the liquid is semi-infinite ($h \to \infty$) is used. The second and third conditions of eq. (4.17) may be directly applied (no differentiation with respect to time is needed). The resulting equations read:

$$2k\mu A + (k^2 + \mu^2)B = \frac{k_y}{k_x}\mu^2 E, \tag{4.19}$$

and

$$2k\mu A + (k^2 + \mu^2)B = -\frac{k_x}{k_y}\mu^2 E. \tag{4.20}$$

The last two equations have equal left-hand sides. Then, it is clear that $E = 0$, this is, transverse waves (eqs. (4.11-4.13)) cannot exist if the surface is free.

The z component of the velocity at the surface is just the time derivative of the surface displacement u. In Fourier space,

$$-i\omega u_{\vec{k},\omega} = v^z_{\vec{k},\omega}(0). \tag{4.21}$$

This equation may be combined with the equations corresponding to the boundary conditions to eliminate A and B. This yields the response equation of the viscous liquid, which reads

$$u_{\vec{k},\omega} = R_{k,\omega} v^{int}_{\vec{k},\omega}, \tag{4.22}$$

where

$$R_{k,\omega} = \frac{k}{\rho_0} \frac{1}{\frac{\mu^2+k^2}{\mu^2-k^2}\omega^2 - \omega_k^2 + \frac{\mu-k}{\mu+k} 2i\nu k^2\omega} \tag{4.23}$$

is the function describing the response of the surface of a semi-infinite viscous liquid to a weak external perturbation. It may be used in much a similar manner as the response function for the surface of an ideal liquid was used in the previous chapter, eq. (3.23). The denominator of the response function, equated to zero, gives the dispersion relation for the ripple waves on that surface. It may be cast into the form

$$\nu^2 k^4 \left[-\left(2 - \frac{i\omega}{\nu k^2}\right)^2 + 4\sqrt{1 - \frac{i\omega}{\nu k^2}} \right] = \omega_k^2, \tag{4.24}$$

which is a generalization (to include surface tension) of the dispersion relation given by Landau and Lifshitz (1987:94) for gravity waves on a semi-infinite liquid. When the viscosity is small, one may use an approximation that is first-order in viscosity, and eq. (4.24) becomes:

$$\omega^2 + 4i\nu k^2 \omega = \omega_k^2. \tag{4.25}$$

The first-order approximation to the complex dispersion relation is then

$$\omega^{\pm} = \pm\omega_k - 2i\nu k^2, \tag{4.26}$$

which agrees with the small-viscosity result described by Landau and Lifshitz (1987:93). This approximation is valid for viscous liquids at sufficiently low wavenumbers.

In the limiting case when the viscosity approaches zero, $R_{k,\omega}$ approaches the response function for the surface of an ideal semi-infinite liquid, $R^0_{k,\omega}$, eq. (3.23). The positive infinitesimal that was introduced there appears here naturally as a result of taking the limit $\nu \to 0^+$:

$$R^0_{k,\omega} = \frac{k}{\rho_0} \frac{1}{\omega^2 - \omega_k^2 + 2i\gamma_k \omega}, \tag{4.27}$$

with $\gamma_k = 2\nu k^2 \to 0^+$.

4.2 The dispersion relation of viscous ripples

In the previous section, the dispersion relation of surface waves on the surface of a semi-infinite viscous liquid, eq. (4.24), has been obtained. This relation is well known, and has been shown to be valid even at very high frequencies (for a recent experimental work, see Sakai, Tanaka and Takagi 1990).

In this section, I report a scaling and iterative process that provides an easy way to obtain, according to eq. (4.24), the complex frequency for each k, and provides a simple way to decide, for a given k, if the ripples are underdamped or overdamped. I have not been able to locate this simple treatment in the literature.

The dispersion relation, eq. (4.24), may be written as

$$\chi = \frac{1}{2}\left[1 + \left(a_k^2 + \chi^2\right)^2\right], \tag{4.28}$$

where

$$\chi = 1 - \frac{i\omega}{2\nu k^2}, \tag{4.29}$$

and

$$a_k = \frac{\omega_k}{2\nu k^2}. \tag{4.30}$$

We are only interested in the two solutions with a negative $\mathrm{Im}(\omega)$; in other words, those that are damped. If the motion is underdamped for a certain k, χ will be a complex number; if it is overdamped, χ will be a real number.

By studying the behaviour of eq. (4.28) it has been found that, for values of a_k below 0.38125194..., χ has two positive real solutions corresponding to overdamped motion. Only the solution with the smallest damping is of interest. It has also been found that it may always be bracketed between $\chi = 1$ and $\chi = 0.73278561...$ (the last is the value of χ at the point of critical damping). A bisection algorithm easily finds the solution.

The underdamped solutions are such that $\mathrm{Re}(\chi)$ is always bracketed between 0 and 1 (this is to say, the damping is always smaller than the first order approximation $2\nu k^2$). By a straightforward manipulation of the complex equation in χ, eq. (4.28), it has been found that a bisection algorithm may be applied to the following equation in $x = \mathrm{Re}(\chi)$:

$$x = \frac{1}{2}\left[1 + \frac{1}{4x^2} - 4x^2\left(x^2 + a^2 - \frac{1}{2x}\right)\right]. \tag{4.31}$$

After x has been found, $y = \mathrm{Im}(\chi)$ may be computed as

$$y = -\sqrt{a^2 + x^2 - \frac{1}{2x}}. \tag{4.32}$$

Figure 4.1 shows the results for the viscous dispersion relation ($\mathrm{Re}(\omega)$, $-\mathrm{Im}(\omega)$) for water at 20°C ($\rho_0 = 163$ a.u., $\sigma = 4.67 \cdot 10^{-5}$ a.u., $\nu = 8.690 \cdot 10^{-3}$ a.u.; $g = 1.085 \cdot 10^{-22}$ a.u.), compared to the ideal frequency ω_k and the damping in the first-order approximation, $2\nu k^2$. For small values of k, $\mathrm{Re}(\omega)$ is almost indistinguishable from the ideal resonance frequency ω_k; however, the damping $-\mathrm{Im}(\omega)$, starts to deviate appreciably from the low-viscosity approximation $2\nu k^2$ for small k.

Figure 4.2 shows a detail of the high-k area. One may easily see that, for high k, both the real frequency $\mathrm{Re}(\omega)$ and the damping $-\mathrm{Im}(\omega)$ deviate clearly from the ideal and first-order approximations. At a certain critical k ($\approx 6.5 \cdot 10^{-3}$ a.u.) the real frequency goes to zero and the damping $-\mathrm{Im}(\omega)$ shows a change of behaviour. This is the point of critical damping. Water is a liquid of moderate viscosity, and one has to go to very high k (very short wavelengths, of the order of 500 Å) to find critical damping. However, the highest frequency measurements reported so far (Sakai et al. 1990) only reach $4 \cdot 10^7$ s^{-1} (approx. 10^{-9} a.u., corresponding to a wavelength of $\approx 10\mu$m). As these authors show, the agreement of the theoretical expression for the dispersion relation (identical to the one derived here, eq. (4.24)) with their experimental results is remarkable.

The k corresponding to critical damping for liquid helium at 1.7 K (a liquid of very low viscosity, $\nu = 7.82 \cdot 10^{-5}$ a.u.), is 2.7 a.u., which corresponds to a wavelength of atomic dimensions, where the continuous-medium approximation made here is questionable. This means that, in cases where such small wavelengths do not occur, liquid helium may be studied using the first-order approximations (ω_k and $2\nu k^2$). Later on it will be shown how, for some cases, one may even neglect the viscous behaviour and treat liquid helium as an ideal liquid. For a high-viscosity liquid, such as the lubricant used by Mate et al. (1989) in their atomic-force microscopy experiments, ($\rho_0 = 331$ a.u., $\sigma = 1.35 \cdot 10^{-5}$ a.u., $\nu \approx 9$ a.u.), the overdamped regime is already reached at very low k ($\approx 10^{-8}$ a.u., corresponding to a wavelength of ≈ 1 cm!); this means that most of the ripples will be strongly overdamped, and these ripples will have little effect in AFM measurements, since oscillations of the surface will be virtually absent.

4.3 Case study: excitation of ripples on the surface of a viscous liquid with an oscillating metal tip

This section will describe a calculation of the amplitude and phase of oscillations induced by a metal sphere (a model of an AFM tip) on the surface of a semi-infinite viscous liquid. This will model the behaviour of a very thick, loosely bound liquid film in AFM. The results will

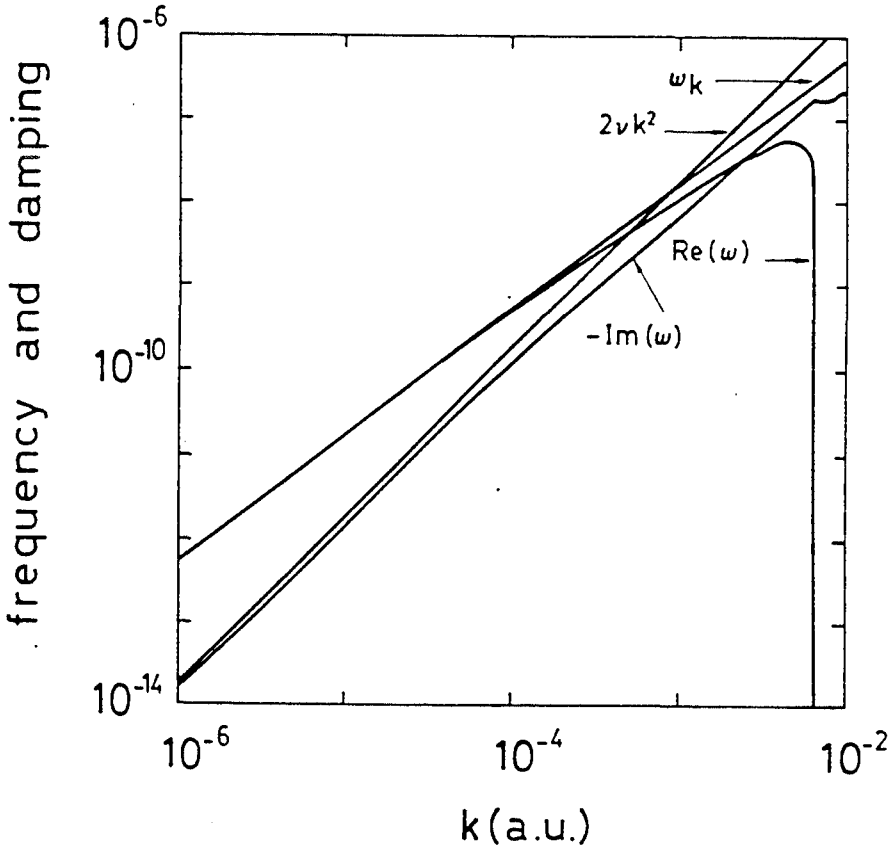

Figure 4.1. The dispersion relation for liquid water. Comparison of exact results (Re(ω), $-$Im(ω)) with the corresponding approximations (ω_k, $2\nu k^2$).

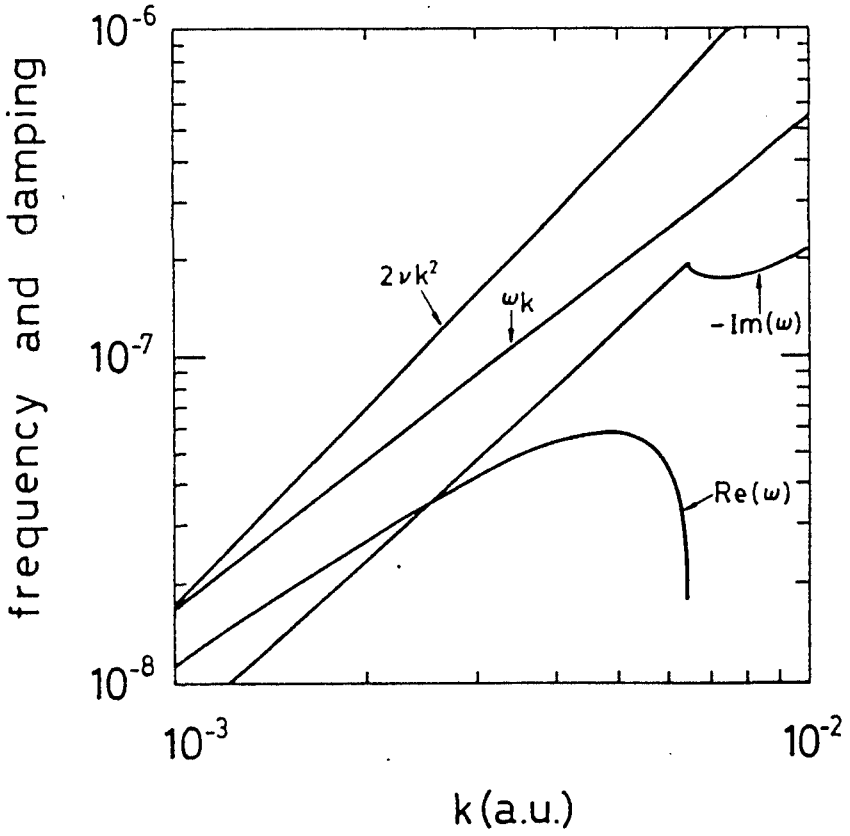

Figure 4.2. The dispersion relation for liquid water. Comparison of exact results ($\mathrm{Re}(\omega)$, $-\mathrm{Im}(\omega)$) with the corresponding approximations (ω_k, $2\nu k^2$). Detail of the high-k area of Figure 4.1.

Table 4.1. Data used to compute the excitation of ripples on the surface of semi-infinite liquids (Donnelly 1989; Weast 1982, Anderson and Cohen 1989, Mate et al. 1989; Israelachvili 1985:137,154,156). All data are given in atomic units.

Quantity	*He*	*Water*	*Fomblin Y/R*
Density, ρ_0	22.8	163	311*
Surface tension, σ	$2.25 \cdot 10^{-7}$	$4.67 \cdot 10^{-5}$	$1.35 \cdot 10^{-5}$
Metal-liq. Hamaker constant A	$3.8 \cdot 10^{-3}$	$2.7 \cdot 10^{-2}$	$3.0 \cdot 10^{-2}$
Kinematic viscosity, ν	$7.82 \cdot 10^{-5}$	$8.69 \cdot 10^{-3}$	9.05*

* C.M. Mate, private communication.

be compared with results for hypothetical ideal liquids with the same density and surface tension, to study the effect of viscosity.

The physical model and the mathematical treatment are the same as in subsection 3.3.1, where the excitation of ripples on an ideal liquid was studied: the only difference is that the response function of the surface of a viscous semi-infinite liquid substitutes the response function of an ideal liquid film that was used there. The static part of the surface perturbation has the same form in both cases (it is, obviously, independent of the viscous behaviour of the liquid). The new general form of the oscillating part of the perturbation, which replaces eq. (3.32) is:

$$U(\rho) = \frac{2BCR_0}{(m-1)!}\left(\frac{1}{2\tilde{R}_0}\right)^m \sqrt{J_c^2(\rho) + J_s^2(\rho)}, \tag{4.33}$$

where

$$J_c(\rho) = \int_0^\infty dk\, k^{m+1}\, J_0(k\rho)\, K_m(k\tilde{R}_0)\, \mathrm{Re}(R_{k,\omega}) \tag{4.34}$$

and

$$J_s(\rho) = \int_0^\infty dk\, k^{m+1}\, J_0(k\rho)\, K_m(k\tilde{R}_0)\, \mathrm{Im}(R_{k,\omega}). \tag{4.35}$$

The oscillation of the liquid is out of phase with respect to the particle by an angle

$$\phi(\rho) = -\arctan\left(\frac{J_s(\rho)}{J_c(\rho)}\right). \tag{4.36}$$

One may expect that viscous amplitudes will be smaller than their ideal counterparts, and that the phase will be smaller for viscous liquids than for ideal liquids.

To perform the calculations, the same situation as in subsection 3.3.1 is assumed: a metal tip of radius $a = 4200$ a.u. is held at a height R over the surface of the liquid, and forced to oscillate at a given frequency W. For this case, $m = 2$, $B = 4a^3A_{int}/3\pi$ and $G = dg$. The response of the following liquids is studied: liquid helium at 1.7 K, liquid water at 20^0C, and a lubricant (Fomblin Y/R, a perfluoropolyether) at room temperature. The data for these three liquids, which have been given in different parts of the text, are collected in Table 4.1.

The calculations have been made for a range of frequencies (extending up to the 10^{10} s^{-1} range) which is much wider than the range of frequencies that may be mechanically available to a tip, only to illustrate the limiting behaviour of the liquid at high frequencies.

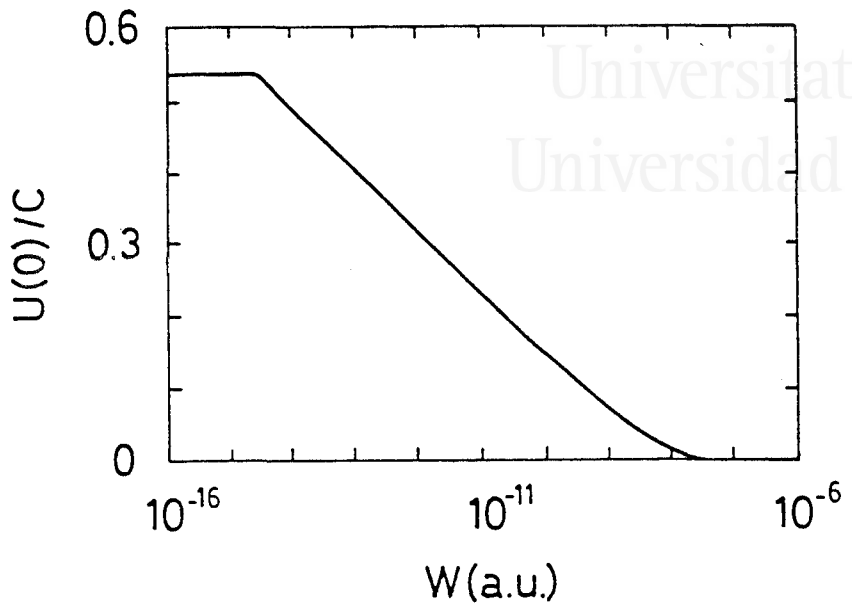

Figure 4.3. Amplitude ratio (liquid/tip) at the origin, $U(0)/C$, versus excitation frequency W for ripples induced by an oscillating metal tip on the surface of liquid helium ($R = 4600$ a.u.).

Liquid helium

The tip height used for these calculations is $R = 4600$ a.u. For this case, only one curve will be given for the liquid/tip amplitude ratio $U(0)/C$ and one for the phase $\phi(0)$. This is because in the range of frequencies covered the results of the viscous model are almost indistinguishable from the results obtained using the ideal model. The amplitude ratio (liquid/tip) at the origin is shown in Figure 4.3 and the phase at the origin is shown in Figure 4.4 (note the similarity between the present results for a semi-infinite liquid and the results for films shown in figures 3.2 and 3.3). As can be seen from these figures, at low frequencies the liquid follows the tip almost exactly in opposition of phase, and the amplitude ratio is almost constant. For higher frequencies, the amplitude ratio decays very slowly with frequency, going from the low-frequency value to a almost zero over seven decades. The transition between the low-frequency (constant amplitude ratio) regime to the high-frequency (decreasing amplitude ratio) occurs at a frequency of $\approx 2 \cdot 10^{-15}$ a.u., which corresponds to a wavelength of the order of the capillary constant ξ (≈ 0.7 mm); in fact, this is where a small maximum appeared for ideal films, as shown in subsection 3.3.1, figure 3.2; here, however, it is too small to be perceived. The phase of the liquid motion deviates only very slowly from -180^0 over the mechanically available frequency range, but in the 10^7 s^{-1} range (10^9 a.u. range), where the amplitude ratio is already very small, there is a sudden drop towards a value of -360^0.

Liquid water at 20^{0}C

In this case the height of the tip is $R = 4500$ a.u. Results for the amplitude ratio at the origin and the phase at the origin are shown in Figures 4.5 and 4.6. There is a very small difference

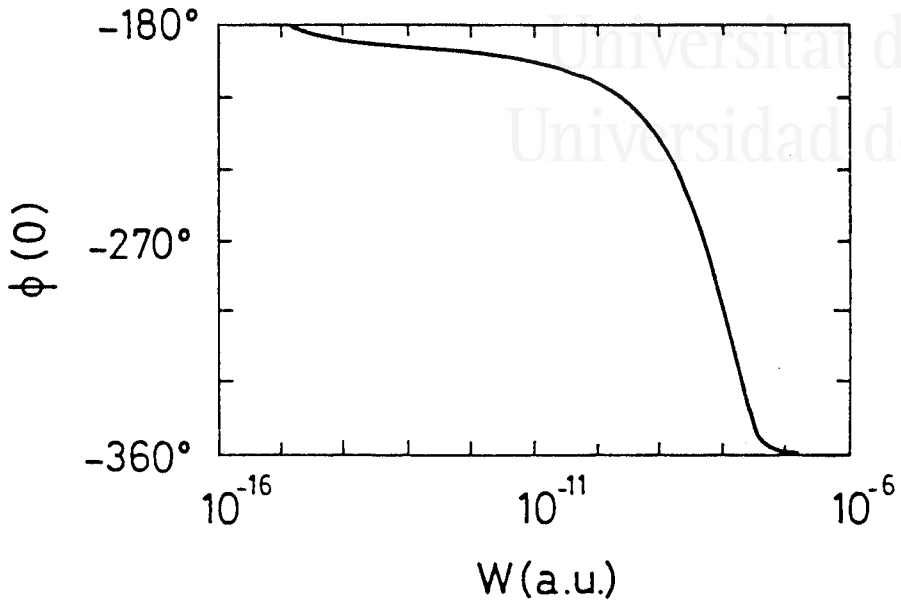

Figure 4.4. Relative phase at the origin versus excitation frequency for ripples induced by an oscillating metal tip on the surface of liquid helium ($R = 4600$ a.u.).

between the viscous and the ideal results, only for high frequencies. Both the amplitude ratio and the phase show a behaviour which is very similar to that of liquid helium: a gradual fall of the amplitude ratio after the low-frequency regime, and a sudden drop of the phase in the 10^7 s^{-1} range. Water is a liquid of medium viscosity, but, as indicated by the results in these graphs, under the tip it behaves almost as an ideal liquid.

Fomblin Y/R

This is a high-viscosity liquid, which belongs to a family of commonly used lubricants (for example, in vacuum systems). The viscosity of Fomblin Y/R is three orders of magnitude higher than that of water; therefore, one might expect a marked change of the response. Figures 4.7 and 4.8 show the results obtained for the amplitude ratio at the origin and the phase at the origin, using a tip height of $R = 4500$ a.u.. As expected, the ideal and viscous results are very different for this liquid.

As was also advanced in subsection 3.3.1, the amplitude ratio for the viscous liquid (Figure 4.7) is always lower than the ideal amplitude ratio. The fall of the ratio in the viscous case is faster than in the ideal one; it is such that the viscous liquid response is negligible in the 10^6 s^{-1} (10^{-11} a.u) range. This will also be true for liquid films with finite depth h, although I still have not extended the viscous response function to this case to get a quantitative assessment of the effect of viscosity on the excitation of ripples on a liquid film. However, as it was shown in subsection 3.3.1, the ideal amplitudes for films are already very small. This allows me to conclude that a modelling of the behaviour of a lubricant film under the AFM tip may be done without considering the effect of ripples, as it has been done in the statics

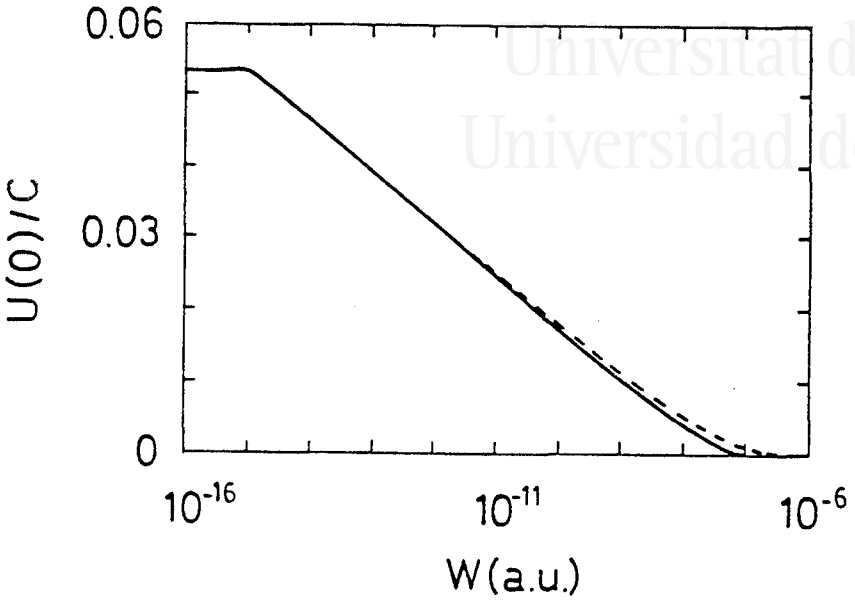

Figure 4.5. Amplitude ratio at the origin versus excitation frequency for ripples induced by an oscillating metal tip on the surface of water (R = 4500 a.u.): solid line, viscous liquid; dashed line, ideal liquid.

part, Chapter 2 of this work.

The difference between the results of the viscous and the ideal treatment is especially marked for the phase (Figure 4.8). For low frequencies, the viscous phase is more negative than the ideal one; however, in the 10^{10} s^{-1} (10^{-10} a.u.) range, it reaches a wide plateau where the phase is approx. -270^0. The plateau of the viscous phase intersects the ideal result as it drops towards -360^0. This behaviour may be explained if one recalls by which angle ϕ a forced, damped harmonic oscillator is out of phase with respect to the excitation force. Take a single oscillating mass attached to a spring. Let m be the oscillating mass, K the constant of the spring, D a viscous damping coefficient, F the amplitude of the force, and W its frequency. The equation of motion is

$$m\ddot{x} + D\dot{x} + Kx = F\cos(Wt). \tag{4.37}$$

It is easy to show that the oscillator is out of phase with respect to the force by an angle

$$\phi = -\arctan\left(\frac{\gamma W}{W^2 - \omega_0}\right). \tag{4.38}$$

where $\gamma = D/m$ and $\omega_0 = \sqrt{K/m}$.

When such an oscillator is strongly overdamped ($\gamma \gg \omega_0$), it may be shown that, for a wide range of frequencies around its natural frequency ω_0, the phase is very close to -90^0 or -270^0, depending on the sign of F. This is indeed what happens in the case of Fomblin Y/R. At high frequencies, the surface modes that are excited by the tip have a wavelength k such that they are strongly overdamped; the collective phase is then very near to -270^0 .

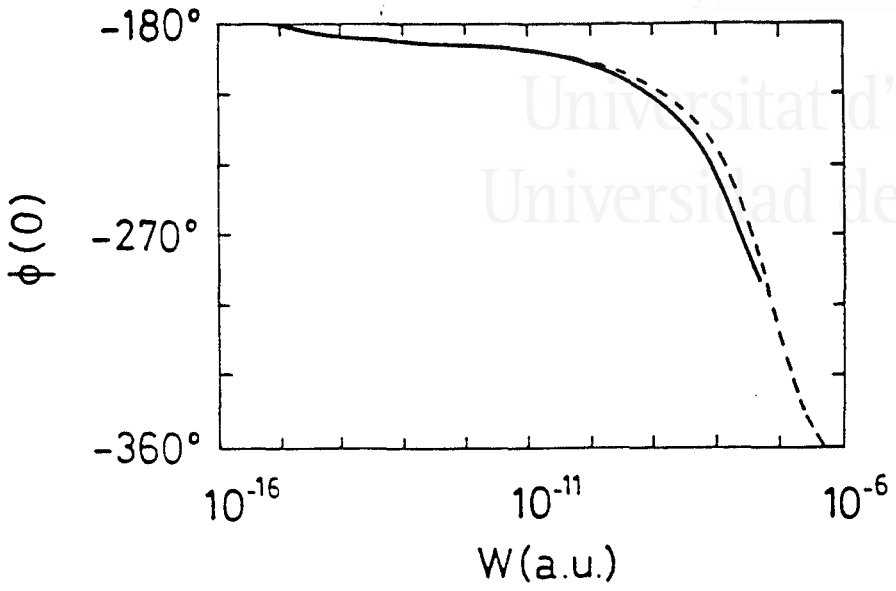

Figure 4.6. Relative phase at the origin versus excitation frequency for ripples induced by an oscillating metal tip on the surface of water ($R = 4500$ a.u.): solid line, viscous result; dashed line, ideal result.

The results of this section show that the behaviour of a liquid under an oscillating tip may be approximated by an ideal behaviour unless it is a very viscous liquid. They also confirm the expectation that the ideal result for the amplitude ratio is always an upper bound for the result obtained when viscosity is taken into account.

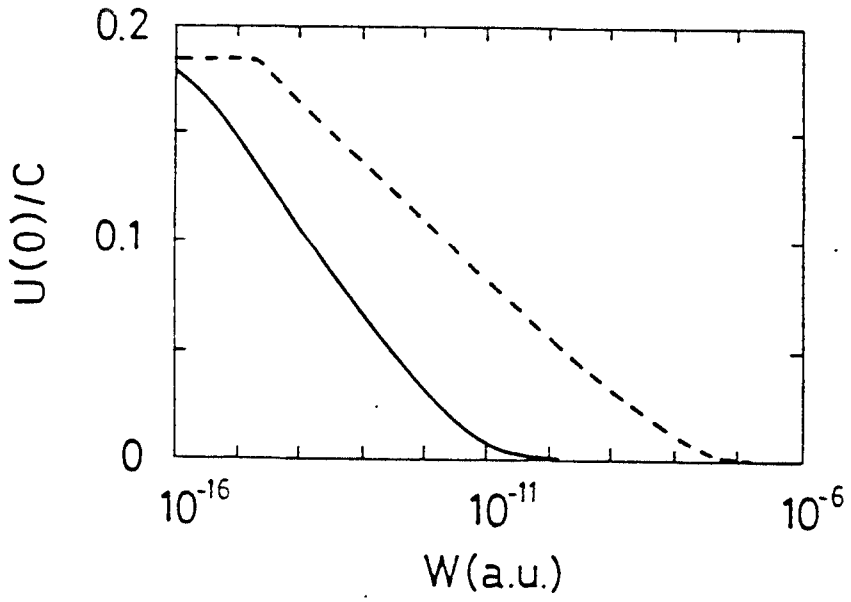

Figure 4.7. Amplitude ratio at the origin versus excitation frequency for ripples induced by an oscillating metal tip on the surface of Fomblin Y/R (R = 4500 a.u.): solid line, viscous liquid; dashed line, ideal liquid.

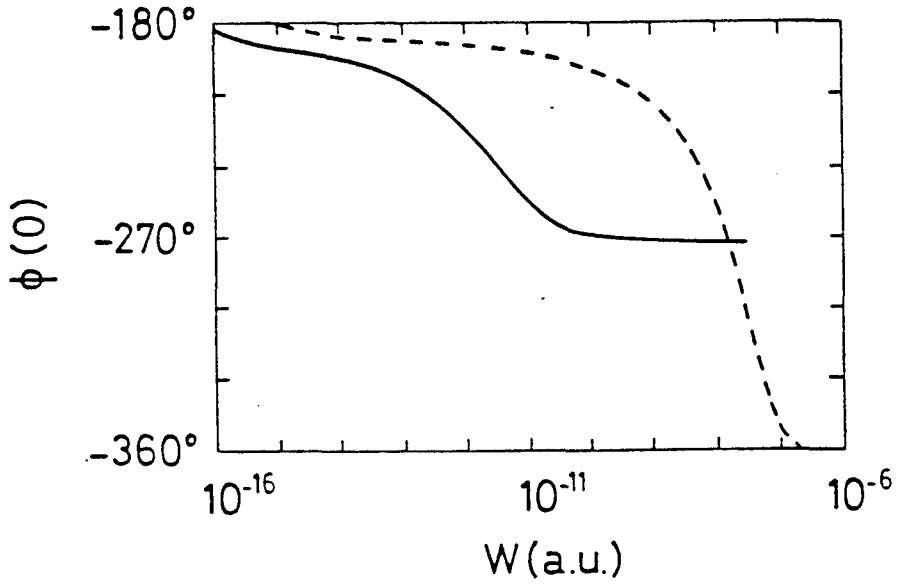

Figure 4.8. Relative phase at the origin versus excitation frequency for ripples induced by an oscillating metal tip on the surface of Fomblin Y/R (R = 4500 a.u.): solid line, viscous liquid; dashed line, ideal liquid.

Chapter 5

Summary and future directions

5.1 Summary

This thesis describes a theoretical study of the interaction of a continuous liquid with a microscopic or macroscopic particle located outside it. Classical mechanics have been used to study several aspects of both the statics and the dynamics of this system.

When a particle is held at a certain distance above a liquid surface, the attractive interaction between the particle and the liquid (which may be, for instance, of electrostatic or van der Waals nature), causes a swelling of the liquid surface in the vicinity of the particle. In Chapter 2, this static situation has been studied: the perturbed shape of the liquid surface as well as the potential energy of the system have been calculated numerically as well as using various approximation schemes, and compared with previous quantum many-body results of Gras-Martí and Ritchie (1985); the agreement of the classical results of this thesis with their results confirms the classical nature of the phenomenon.

The calculation of the gradient of the force on the particle, by differentiation of the total potential energy of the system, has been used to assess and confirm the validity of the atomic-force microscopy determination (Mate et al. 1989) of the shape of the liquid–air interface when a lubricant is spread on a solid substrate. This experimental determination was done by scanning a metal tip over the surface while keeping constant the gradient of the force on it, to get a topographical image of the liquid–air interface.

It has also been found that there is a minimal particle-liquid distance such that, if the particle approaches the liquid further, the surface becomes unstable and the liquid *jumps* to incorporate the particle. The study of this instability point, which has also been described for solid surfaces (Landman et al. 1989; Pethica and Sutton 1988), has been applied to analyse the use of the atomic-force microscope (Mate et al. 1989) as a tool to determine the thickness of thin lubricant films on a planar solid substrate. In these experiments, the thickness was determined by moving the tip vertically towards the liquid film and measuring the diference in tip height between the position in which wetting of the tip occurs and the position where the tip knocks the solid substrate. The results presented in this work explains the systematic difference between these measurements and optical (ellipsometrical) measurements; part of the difference may be due to the fact that the liquid film becomes unstable before tip–liquid contact occurs.

In Chapter 3 the dynamics of the surface of an ideal liquid when the external particle is in motion has been described. First, the linear response function of the surface has been

obtained using classical hydrodynamics, and then this response function is used to study two different configurations. The first one is the excitation of ripples on the liquid surface by a particle that oscillates perpendicularly to the surface; the effect of this phenomenon on the atomic-force microscopy measurements of Mate et al. (1989) is estimated to be very small, even when the viscosity of the film is not taken into account. The second situation is the stopping, due to the excitation of ripples, of a particle that flies parallel to the surface. The quantum many-body results of Gras-Martí and Ritchie (1985) for an electron and the surface of liquid helium are reproduced, and, in addition, the dependence of the energy loss as a function of particle velocity is studied in detail.

In Chapter 4 the dynamical response of the surface of a semi-infinite viscous fluid has been studied. The excitation of ripples by a particle that oscillates perpendicularly to the surface is studied, and the influence of viscosity is studied for liquid helium (a liquid of very low viscosity), water (a liquid of medium viscosity) and for the highly viscous lubricant used by Mate et al. (1989), Fomblin Y/R. The results show that viscosity may be neglected except in the last case. As expected, the amplitude of the rippling oscillation of real liquids is always overestimated by the calculations in which viscosity is neglected.

5.2 Future directions

In this thesis, liquid films have been studied using hydrostatic and hydrodynamic formalisms that assume a continuous liquid where molecular structure is of no importance. However, some of the films have thicknesses that are comparable to the size of the molecular constituents, and there, concepts such as viscosity, surface tension, and the Hamaker constant, may have to be replaced by a model in which the molecular features of the liquid would play a basic role. Mate et al. (1989, 1991) have performed some experiments in which the role of conformation of the lubricant molecules appears to be relevant.

For films thicker than a few hundreds of ånsgtröms, continous hydrodynamics and hydrostatics are still applicable. The theory for the dynamic response of a viscous liquid, described in Chapter 4 can be extended to include the case of a liquid of finite depth, as well as to different geometries (non-planar and rough substrates) that are of technological interest.

When performing atomic-force experiments, the tip that probes the film may also be covered by a thin film of liquid due to previous immersion. The interaction of the two liquid films, their stability when they come near to each other, as well as the formation of the film on the tip, arising from the contact situation have just begun to be studied (Langlois 1991) and deserve a more complete statical and dynamical analysis.

Some other aspects of the dynamics of the system formed by the oscillating tip and the liquid film, which may be explored with the tools developed in the present theoretical approach, are the energy transfer from the oscillating tip to the liquid film and the possible detection of resonances at characteristic frequencies (subsection 3.3.1), a phenomenon that could be used to measure the thickness of the films.

A nonlinear theory for the dynamic response of liquid surfaces is still missing. It would be interesting to be able to step into the nonlinear dynamics of close encounters between particles and surfaces, especially to be able to set up a first-principles theory for the atom reflectivity of liquid helium surfaces, a field of considerable experimental and theoretical interest (Echenique and Pendry 1976a,b; Swanson and Edwards 1988; Goodman 1989; Martin, Bruinsma and Platzman 1989; Berkhout et al. 1989). The current theories for these phenomena use empirical

ingredients (Swanson and Edwards 1988) to get a better description of the experimental results. An appealing task, in view of the equivalence of classical and quantum results for some phenomena studied in this thesis, would be that of testing the performance of a classical formalism in explaining some aspects of atom reflectivity. So far, all theoretical treatments have used quantum many-body tools.

Another important application of the non-linear response theory to be developed would be the study of the effect of surface ripples on the *jump-to-contact* distance: the potential energy basin that binds the liquid surface seems to become more shallow as the particle approaches the liquid at the critical height; so shallow that at the critical distance, the potential energy is unable to bind the liquid. Surface oscillations superimposed on the equilibrium bump would help the liquid escape the potential energy basin at distances that could be appreciably longer than the jump-to-contact distance, with the result of a longer *wetting* distance.

Appendix A

Quantization of Ripple Waves

Ripple waves on the surface of an ideal, incompressible liquid may be quantized as a boson field, the quanta of which are called *ripplons*. Quantization is used so often that the word *ripplon* is sometimes used in entirely classical contexts (Sakai, Tanaka and Takagi 1990).

The interaction of electrons and small atoms with the surface of liquid helium has been treated in most cases using the ripplon formulation (Cole 1970, 1974; Echenique and Pendry 1976a,b; Gras-Martí and Ritchie 1985; Martin, Bruinsma and Platzman 1988; Swanson and Edwards 1988; Barberán, Garcia-Molina and Gras-Martí 1989; Tiesinga, Stoof and Verhaar 1990). In this thesis it has been shown that the statics of the interaction of a particle with a liquid surface and the excitation of ripple waves by particles whose trajectory is known may be treated without resorting to a quantum formalism.

This appendix shows how a classical Hamiltonian for the ripples on the surface of an ideal liquid of depth h may be easily obtained and then quantized by imposing boson commutation relations.

A.1 Potential energy

The axisymmetrical, linearized forms of the surface energy, eq. (2.33), and the binding energy, eq. (2.34), may be easily rewritten for a general surface profile, $u(\vec{\rho})$:

$$V_{st} = \frac{\sigma}{2}\int d^2\vec{\rho}\left[\left(\frac{\partial u}{\partial x}\right)^2 + \left(\frac{\partial u}{\partial y}\right)^2\right], \tag{A.1}$$

$$V_b = \frac{G}{2}\int d^2\vec{\rho}\, u^2(\vec{\rho}). \tag{A.2}$$

The surface profile may be expanded in normal-mode coordinates,

$$u(\vec{\rho}) = \frac{1}{\Omega^{1/2}}\sum_{\vec{k}} u_{\vec{k}} e^{i\vec{k}\cdot\vec{\rho}}, \tag{A.3}$$

where Ω is a normalization area.

Using this expansion, the surface and binding energies, eqs. (A.1) and (A.2), may be combined to obtain an expression of the potential energy of the surface in terms of the normal-mode coordinates:

$$V = V_{st} + V_b = \frac{1}{2}\sum_{\vec{k}}(G + \sigma k^2) u_{\vec{k}}\, u_{-\vec{k}}. \tag{A.4}$$

A.2 Kinetic energy

To obtain the kinetic energy of the liquid, the velocity potential ϕ, such that the velocity of the liquid is

$$\vec{w}(\vec{\rho},z) = \nabla\Phi(\vec{\rho},z), \tag{A.5}$$

will be used as the basic quantity (I will only consider the case of irrotational flow). The velocity potential may be expanded similarly to the surface profile:

$$\Phi(\vec{\rho},z) = \frac{1}{\Omega^{1/2}}\sum_{\vec{k}}\Phi_{\vec{k}}(z)e^{i\vec{k}\cdot\vec{\rho}}. \tag{A.6}$$

Applying the continuity equation, eq. (3.16), and the condition that the vertical component of the velocity of the liquid is zero at the bottom (for a liquid film of thickness h),

$$w_z(\vec{\rho},-h) = \frac{\partial}{\partial z}\Phi(\vec{\rho},z)|_{z=-h} = 0, \tag{A.7}$$

the velocity potential may be rewritten as

$$\Phi(\vec{\rho},z) = \frac{1}{\Omega^{1/2}}\sum_{\vec{k}}\tilde{\Phi}_{\vec{k}}\cosh[k(z+h)]e^{i\vec{k}\cdot\vec{\rho}}. \tag{A.8}$$

If this result is substituted in the equation of motion for the free surface, eq. (3.13) with $v_{int} = 0$, the time dependence of the velocity potential is obtained:

$$\tilde{\Phi}_{\vec{k}} = A_{\vec{k}}e^{i\omega_k t} + B_{\vec{k}}e^{-i\omega_k t}, \tag{A.9}$$

where ω_k is defined in eq. (3.20). The kinetic energy of the liquid,

$$T = \frac{\rho_0}{2}\int_{-h}^{0}dz\int d^2\vec{\rho}\,w^2(\vec{\rho},z), \tag{A.10}$$

may be integrated in a straightforward way to obtain

$$T = \frac{\rho_0}{4}\sum_{\vec{k}}\tilde{\Phi}_{\vec{k}}\tilde{\Phi}_{-\vec{k}}\,k\,\sinh^2(2kh). \tag{A.11}$$

Now it is necesary to relate the normal-mode components of the velocity potential to the time derivatives of the surface normal-mode coordinates. The time derivative of the surface displacement, eq. (A.3), is

$$\dot{u}(\vec{\rho}) = \frac{1}{\Omega^{1/2}}\sum_{\vec{k}}\dot{u}_{\vec{k}}e^{i\vec{k}\cdot\vec{\rho}}, \tag{A.12}$$

but also

$$\dot{u}(\vec{\rho}) = w_z(\vec{\rho},0) = \frac{1}{\Omega^{1/2}}\sum_{\vec{k}}\tilde{\Phi}_{\vec{k}}\,k\,\sinh(kh)\,e^{i\vec{k}\cdot\vec{\rho}}. \tag{A.13}$$

Identifying eqs. (A.12) and (A.13), one gets

$$\tilde{\Phi}_{\vec{k}} = \frac{\dot{u}_{\vec{k}}}{k\sinh(kh)}. \tag{A.14}$$

If this equation is substituted into the expression for the kinetic energy, eq. (A.11), the result is

$$T = \frac{\rho_0}{2}\sum_{\vec{k}}\frac{\dot{u}_{\vec{k}}\dot{u}_{-\vec{k}}}{k\tanh(kh)}. \tag{A.15}$$

A.3 The Hamiltonian

From the Lagrangian of the system (following Cole 1970),

$$L = T - V = \frac{1}{2}\sum_{\vec{k}}\left[\frac{\rho_0}{k\tanh(kh)}\dot{u}_{\vec{k}}\dot{u}_{-\vec{k}} - (G+\sigma k^2)u_{\vec{k}}u_{-\vec{k}}\right], \tag{A.16}$$

and the definition of canonical momentum,

$$p_{\vec{k}} = \frac{\partial L}{\partial \dot{u}_{\vec{k}}} = \frac{\rho_0 \dot{u}_{-\vec{k}}}{k\tanh(kh)}, \tag{A.17}$$

the Hamiltonian for the free rippling surface becomes

$$H^0 = \frac{1}{2}\sum_{\vec{k}}\left[\frac{k\tanh(kh)}{\rho_0}p_{\vec{k}}p_{-\vec{k}} + (G+\sigma k^2)u_{\vec{k}}u_{-\vec{k}}\right]. \tag{A.18}$$

This Hamiltonian may now be quantized by imposing the following boson commutation relations upon the operators $u_{\vec{k}}$ and $p_{\vec{k}}$:

$$[u_{\vec{k}}, p_{\vec{k}'}] = i\hbar\delta_{\vec{k},\vec{k}'}, \tag{A.19}$$

where $\delta_{a,b}$ is the Kronecker delta and $\hbar$ is Planck's constant divided by 2π. The operators $u_{\vec{k}}$ and $p_{\vec{k}}$ may be rewritten in terms of ripplon creation and annihilation operators $a^+_{\vec{k}}$ and $a_{\vec{k}}$ as follows:

$$u_{\vec{k}} = \left[\frac{\hbar k\tanh(kh)}{2\rho_0\omega_k}\right]^{1/2}(a^+_{-\vec{k}} + a_{\vec{k}}), \tag{A.20}$$

and

$$p_{\vec{k}} = \left[\frac{\hbar\rho_0\omega_k}{2k\tanh(kh)}\right]^{1/2}(a^+_{\vec{k}} - a_{-\vec{k}}). \tag{A.21}$$

After these transformations, the Hamiltonian takes the canonical form:

$$H^0 = \sum_{\vec{k}}\hbar\omega_k\left(a^+_{\vec{k}}a_{\vec{k}} + \frac{1}{2}\right) \tag{A.22}$$

A.4 The interaction potential as a perturbation Hamiltonian

The interaction potential ΔV between the particle and the deviation from planarity of the surface may be treated in the quantum formalism as a perturbation Hamiltonian, H^1. Rewriting the axisymmetrical form, eq. (2.37) to consider a general surface profile $u(\vec{\rho})$, and using the expansion (A.3), one gets

$$H^1 = \frac{2\pi}{\Omega^{1/2}}\sum_{\vec{k}}u_{\vec{k}}v^{int}_{\vec{k}}(\vec{\rho},\vec{R}), \tag{A.23}$$

where $v^{int}_{\vec{k}}(\vec{\rho},\vec{R})$ is the Fourier transform of the interaction potential between the particle and a unit volume of liquid located near the surface at $\vec{\rho}$, and $\vec{R}$ is the position of the particle.

Volver al índice/Tornar a l'índex

As an example, in the case that the particle is an electron held fixed over the surface of liquid He at a height R, eq. (2.43),

$$v_{int}(\vec{\rho}, \vec{R}) = -\frac{n\alpha e^2}{2(\rho^2 + R^2)^2}, \tag{A.24}$$

and taking $h \to \infty$, the expression for the perturbation Hamiltonian in eqs. (4-6) of Gras-Martí and Ritchie (1985) is reproduced.

Appendix B

Table of frequently used symbols

A	Hamaker constant (van der Waals interaction)
A_b	Hamaker constant for liquid-substrate interaction
A_{int}	Hamaker constant for particle-liquid interaction
a	particle-size-related parameter; particle radius
b	dimensionless parameter (energy loss): $\rho_0(w_p)^2\tilde{R}/\sigma$
B	general coefficient for particle-liquid interaction
C	amplitude of the oscillation of the particle
D	depth of cylindrical hole
dE/ds	energy loss of particle per unit path length
$f_{c,\kappa}(x)$	complementary logistic function, $(1+\exp(\kappa x))^{-1}$
g	gravity acceleration at the Earth's surface
G	dv_b/dz at the reference plane
h	liquid depth
$-h(\rho)$	function defining the shape of the bottom of the liquid
I_F	bump shape parameter in the scaled-shape approximation
$i_m(x)$	dimensionless function, defined in eq. (2.29).
$J_0(x)$	Bessel function of the first kind of order zero
$j_m(x)$	dimensionless function defined in eq. (2.42).
$K_m(x)$	modified Bessel function of the second kind of order m
k	modulus of $\vec{k}$
$\vec{k}$	wavevector, reciprocal of $\vec{\rho}$ in Fourier transforms
M	molecular (atomic) mass of the liquid
m	integer exponent for the particle-liquid interaction
n	number density of the liquid
p	pressure
P	radius of cylindrical hole
Q	charge of particle
R	height of particle over reference plane; particle-liquid distance

R_0	average value of R
r_0	dimensionless parameter (energy loss): $\tilde{R}^2\rho_0 g/\sigma$
R^*	minimum particle-liquid distance for stable equilibrium
$R_{k,\omega}$	response function for the surface of a semi-infinite viscous liquid
$R^0_{k,\omega}$	response function for the surface of an ideal liquid
$\tilde{R}$	"reduced" particle-surface distance, $\sqrt{R^2-a^2}$.
t	time; also, dimensionless dummy variable in integrals
U^*	maximum height for a stable bump on the liquid surface
$u(\rho)$	meridian curve for the perturbed liquid surface
$U(\rho)$	amplitude of the oscillation of the liquid surface
$\tilde{u}(\rho)$	equilibrium meridian curve for the liquid surface
$u_0(\rho)$	meridian curve for the unperturbed liquid surface
$\hat{v}$	potential energy of interaction between two unit volumes
V_b	binding potential energy
v_b	binding potential energy per unit volume of liquid
V_{int}	interaction (particle-liquid) potential energy
v_{int}	interaction (particle-liquid) potential energy per unit volume of liquid
$v_p(x)$	van der Waals potential of a unit volume of liquid in front of semiinfinite solid
V_{planar}	interaction (particle-liquid) potential energy due to the unperturbed planar surface
V_{st}	surface tension energy
V_{tot}	total potential energy
W	oscillation frequency of particle
$\vec{w}$	velocity of a liquid element
w_{min}	minimum phase velocity of ripple waves
w_p	modulus of $\vec{w}_p$
$\vec{w}_p$	velocity of particle
z	vertical position relative to the reference plane
α	atomic polarizability of the liquid
γ	Euler's gamma, 0.5772156...
γ_k	infinitesimal damping in ideal liquids
δ	Dirac delta
ΔV	potential energy of the particle-liquid system due to the bump
$\phi(\rho)$	phase of the oscillation of the liquid surface, relative to the particle
Φ	velocity potential in an ideal liquid
$\Theta(x)$	Heaviside step function
η	dynamic viscosity of liquid
Λ	atom-atom van der Waals coefficient

Volver al índice/Tornar a l'índex

ν	kinematic viscosity
ρ	distance to the symmetry axis
ρ_0	density of the liquid
$\vec{\rho}$	vector of horizontal position
σ	surface tension coefficient
ξ	generalized capillary constant, $\sqrt{2\sigma/G}$
ω	angular frequency
ω_k	angular frequency corresponding to wavevector k in an ideal liquid

Bibliography

Anderson, H.L. and Cohen, E.R. (1989) "General Part" in "A physicist's desk reference", H.L. Anderson, ed. (AIP, New York), p. 2-51.

Atkins, P.W. (1983) "Molecular quantum mechanics", 2nd. ed. (Oxford Univ. Press, Oxford).

Barberán, N., Garcia-Molina, R. and Gras-Martí, A. (1989) "Charged-particle interaction with liquids: ripplon excitations", *Phys. Rev.* **B40**, 10-19.

Berkhout, J.J., Luiten, O.J., Setija, I.D., Hijmans, T.W., Misuzaki, T. and Walraven, J.T.M. (1989) "Quantum reflection: focusing of hydrogen atoms with a concave mirror", *Phys. Rev. Lett.* **63**, 1689-1692.

Binnig, G. and Rohrer, H. (1982) "Scanning tunnelling microscopy", *Helv. Phys. Acta* **55**, 726.

Binnig, G., Quate, C.F. and Gerber, C. (1986) "Atomic force microscope", *Phys. Rev. Lett.* **56**, 930-933.

Boucher, E.A. and Jones, T.G. (1987) "Thermodynamic quantities involving Bessel functions for axisymmetric fluid bodies of low curvature in a gravitational field", *J. Colloid Interf. Sci.* **119**, 277-290.

Cheng, E. and Cole, M.W. (1990) "Physical adsorption near an oblique corner", *Phys. Rev.* **B41**, 9650-9653.

Cole, M.W. (1970) "Properties of image-potential induced surface states of insulators", *Phys. Rev.* **B2**, 4239-4252.

Cole, M.W. (1974) "Electronic surface states of liquid helium", *Rev. Mod. Phys.* **46**, 451-464.

Davis, P.J. and Polonsky, I. (1965) "Numerical interpolation, differentiation and integration" in "Handbook of mathematical functions", Abramowitz, M. and Stegun, I., eds. (Dover, New York), p. 875-924.

Donnelly, R.J. (1989) "Cryogenics", in "A physicist's desk reference", H.L. Anderson, ed. (AIP, New York), p. 114-130.

Echenique, P.M. and Pendry, J.B. (1976a) "Reflectivity of liquid ^{4}He surfaces to ^{4}He atoms", *Phys. Rev. Lett.* **37**, 561-563.

Echenique, P.M. and Pendry, J.B. (1976b) "Scattering of ^{4}He atoms from the surface of liquid ^{4}He at 30 mK", *J. Phys. C: Solid State Phys.* **9**, 3183-3191.

Feynman, R.P., Leighton, R.B. and Sands, M. (1964) "The Feynman lectures on Physics", 3 vols. (Addison-Wesley, Reading, Massachusetts).

Forcada, M.L., Arista, N.R., Gras-Martí, A., Urbassek, H.M. and Garcia-Molina, R. (1990) "Interaction between a charged or neutral particle and a semi-infinite non-polar dielectric liquid", submitted to *Phys. Rev.* **B**

Forcada, M.L., Arista, N.R., Gras-Martí, A., Urbassek, H.M. and Garcia-Molina, R. (1991) "Interaction of a charged particle with a semi-infinite, non-polar dielectric liquid" in "Proceedings of the NATO ASI on 'Interactions of charged particles with solids and surfaces"', A. Gras-Martí *et al.*, ed. (Plenum, New York, in press).

Forcada, M.L., Jakas, M.M. and Gras-Martí, A. (1991) "On liquid-film thickness measurements with the atomic-force microscope", accepted for publication in *J. Chem. Phys.*

Gianetta, R.W. and Ikezi, H. (1982) "Macroscopic structures on the electron-charged surface of liquid ^{4}He", *Surf. Sci.* **113**, 412-417.

Goodman, F.O. (1989) "Effective potentials for the scattering of hydrogen and helium atoms by the surface of liquid helium", *Surf. Sci.* **214**, 577-590.

Gras-Martí, A. and Ritchie, R.H. (1985) "Charged-particle excitation of ripplon fields", *Phys. Rev. B* **31**, 2649-2655.

Hamaker, H.C., (1937) "The London–van der Waals attraction between spherical particles", *Physica* **4**, 1058-1072.

Israelachvili, J.N. and Tabor, D. (1972a) "The measurement of van der Waals dispersion forces in the range 1.5 to 130 nm", *Proc. R. Soc. Lond.* **A331**, 19-38.

Israelachvili, J.N. and Tabor, D. (1972b) "The calculation of van der Waals dispersion forces between macroscopic bodies", *Proc. R. Soc. Lond.* **A331**, 39-55.

Israelachvili, J.N. (1985) "Intermolecular and surface forces (with applications to colloidal and biological systems)" (Academic, London).

Israelachvili, J.N. (1987) "Direct measurements of forces between surfaces in liquids at the molecular level", *Proc. Natl. Acad. Sci. USA* **84**, 4722-4724.

Landau, L.D. and Lifshitz, E.M. (1987) "Fluid Mechanics", 2nd. ed. (Pergamon, Oxford).

Landman, U., Luedtke, W.D., Burnham, N.A. and Colton, R.J. (1989) "Atomic mechanisms and dynamics of adhesion, nanoindentation and fracture", *Science* **248**, 454-461.

Langlois, W.L. (1991) "Hydrostatic investigation of the liquid bridge formed when the atomic-force microscope is used to measure the thickness of a liquid film" (IBM Report RJ 7960 (73229)), submitted to Surface Science.

Lehndorf, B. and Dransfeld, K. (1989) "Microwave absorption of electrons bound to films of liquid helium", *J. Phys. France* **50**, 2576-2586.

Leiderer, P., Ebner, W. and Shikin, V.B. (1982) "Macroscopic electron dimples on the surface of liquid helium", *Surf. Sci.* **113**, 405-411.

Luke, Y.L. (1965) "Integrals of Bessel Functions", in "Handbook of mathematical functions", Abramowitz, M. and Stegun, I., eds. (Dover, New York), p. 479-494.

Martin, T., Bruinsma, R. and Platzman, P.M. (1988) "Quantum reflection in the presence of dissipation", *Phys. Rev.* **B38**, 2257-2266.

Mate, C.M., Lorenz, M.R. and Novotny, V.J. (1989) "Atomic force microscopy of polymeric liquid films", *J. Chem. Phys.* **90**, 7550-7555.

Mate, C.M., Lorenz, M.R. and Novotny, V.J. (1990) "Determination of lubricant film thickness on a particulate disk surface by atomic force microscopy", *IEEE Trans. Magn.* **26**, 1225-1228.

Mate, C.M. and Novotny, V. (1991) "Molecular conformation and disjoining pressure of polymeric liquid films", to be published in *J. Chem. Phys.*

Mate, C.M. and Novotny, V.J. (1991) "Molecular conformation and disjoining pressure of polymeric liquid films" (courtesy preprint, submitted to *J. Chem. Phys.*).

Mel'nikov, V.I. and Meshkov, S.V. (1981) "Instability of a charged surface of liquid helium", *JETP Lett.* **33**, 211-214.

Mellor, C.J. and Vinen, W.F. (1990) "Experimental observation of crystallization and ripplon generation in a two-dimensional pool of helium ions", *Surf. Sci.* **229** 386-380.

Olver, F.W.J. (1965) "Bessel functions of integer order", in "Handbook of mathematical functions", Abramowitz, M. and Stegun, I., eds. (Dover, New York), p. 355-433.

Papadopoulos K.D. and Kuo, C.-C. (1990) "The van der Waals interaction between a colloid and a host pore", *Colloids and Surfaces* **46**, 115-125.

Pethica, J.B. and Sutton, A.P. (1988) "On the stability of a tip and flat at very small separations", *J. Vac. Sci. Technol.* **A6**, 2490-2494.

Philpott, M.R., Hussla, I. and Coburn, J.M. (1987) "Properties of polymeric liquid film lubricants adsorbed on patterned gold and silicon surfaces under high vacuum", in "Fluid film lubrication - Osborne Reynolds Centenary", Dowson, D., Taylor, C.M., Godet, M. and Berthe, D., eds. (Elsevier, Amsterdam); p. 333-335.

Pohl, H.A. (1978) "Dielectrophoresis: The behavior of neutral matter in nonuniform dielectric fields" (Cambridge Univ. Press, Cambridge).

Rossolenko, S.N. and Zhdanov, A.V. (1990) "Equilibrium shapes of liquid menisci subject to gravity force and surface tension", *J. Cryst. Growth* **104**, 8-13.

Rugar, D. and Hansma, P.K. (1990) "Atomic force microscopy", *Physics Today*, october issue, 23-30.

Sakai, K., Tanaka, H and Takagi, K. (1990) "Dispersion of thermal ripplon on free surfaces of pure liquids measured up to 6 MHz", *Jap. J. Appl. Phys.* **29**, L2247-L2249.

Shikin, V.B. and Monarkha, Yu.P. (1974) "On the interaction of surface electrons in liquid helium with oscillations of the vapor-liquid interface", *J. Low Temp. Phys.* **16**, 193-207.

Shikin, V.B. and Leiderer, P. (1981) "Many-electron holes on the surface of liquid helium", *JETP Lett.* **32**, 416-418.

Spruch, L. (1986) "Retarded, or Casimir, long-range potentials", *Physics Today*, november issue, 37-45.

Swanson, D.R. and Edwards, D.O. (1988) "Path integral theory of the scattering of ^{4}He atoms form the surface of liquid ^{4}He", *Phys. Rev.* **37**, 1539-1549.

Volver al índice/Tornar a l'índex

Tiesinga, E., Stoof, H.T.C. and Verhaar, B.J. (1990) "Reflection of hydrogen atoms from the surface of superfluid helium", *Phys. Rev.* **B41**, 8886-8890.

Weast, R.C., ed.: "CRC Handbook of Chemistry and Physics", 63rd. ed. (CRC, Boca Ratón, Florida).